27th International Applied
Geochemistry Symposium

Short Course No. 2

Application of Indicator Mineral Methods to Exploration

Beth McClenaghan & Dan Layton-Matthews

Course Organizers

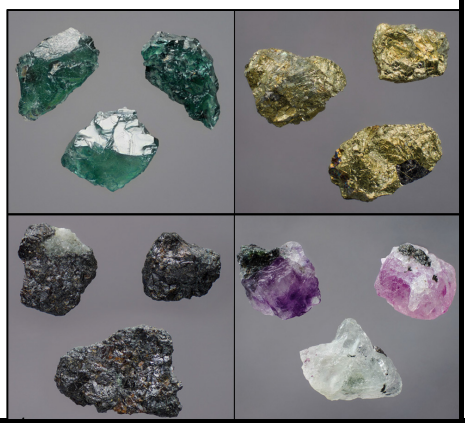

April 18th, 2015

Tucson AZ

Short Course 02

Application of Indicator Mineral Methods to Exploration

Convenors: M.B. McClenaghan & D. Layton-Matthews

April 18, 2015

WORKSHOP OVERVIEW

This one-day workshop builds on the success of the indicator mineral workshops held at the 24th, 25th, and 26th International Applied Geochemistry Symposia (IAGS). Indicator mineral methods can now be applied to exploration for a broad range of mineral deposit types. This workshop will review principles, methods, and developments in indicator mineral methods in mineral exploration around the world and consists of presentations by some of the most experienced practitioners in the field. Topics covered include indicator minerals for porphyry Cu, VMS, Sn-W-Mo, and REE, Ta-Nb deposits as well as mineral chemistry techniques.

Beth McClenaghan & Dan Layton-Matthews
April, 2015

Mineral chemistry: modern techniques and applications to exploration

D. Layton-Matthews[1*], C. Hamilton[2] & M.B. McClenaghan[3]

[1]Department of Geological Sciences, Queen's University, Kingston, Ontario, Canada K7L 3N6
[2]Systems for Research, #45, 155 Tycos Drive, Toronto, Ontario, Canada M6B 1W6
[3]Geological Survey of Canada, 601 Booth Street, Ottawa, Ontario, Canada K1A 0E8
**Corresponding author e-mail: dlayton@geol.queensu.ca*

It is likely that undiscovered ore reserves are currently buried under recently deposited sedimentary cover. As such, our capacity to see through the complexities of this cover and to perceive the nature of the underlying bedrock ore environment has become a fundamental aspect of modern mineral exploration and ore deposit science. To date, the recognition of buried mineral deposits has been aided by our ability to (1) predict indicator minerals in bedrock sources, (2) identify and separate indicator minerals from sedimentary cover, and (3) measure the unique chemical and isotopic composition of these indicator minerals.

A substantial amount of research has been devoted to chemical and physical dispersal of minerals and elements at the Earth's surface in the development of bedrock weathering and erosional footprints. The aerial and spatial extent of these footprint models has been partially limited by our incomplete understanding of the processes involved in mineral and chemical dispersal, but moreover, by the technological challenges of identifying and measuring subtle mineral and chemical changes in these footprint sediments. Within mineral deposit footprints, the examination of the physical dispersion of relatively large (>63 micron) and heavy (>2.85 g/cm^3) mineral concentrates (HMC) from bedrock sources during glaciation has met with great successes in the exploration for kimberlite (Thorleifson 1993; Ward *et al.* 1996; McClenaghan & Kjarsgaard 2001; McClenaghan 2002; McClenaghan *et al.* 2002), base metals (Sarala & Peuraniemi 2007; Kelley *et al.* 2010; Averill 2011; Eppinger *et al.* 2011; McClenaghan *et al.* 2011; McClenaghan *et al.* 2012a,c; McClenaghan & Peter 2013), and gold (Averill & Zimmerman 1984; Sauerbrei *et al.* 1987; Craw *et al.* 1999; Averill 2013) deposits. By using HMC and the mineral chemistry of these indicator minerals, which have been separated from sediments using complex and expensive techniques (e.g. sieved, tabling, heavy liquids, magnetic separation, and hand-picking), the recognition of the spatial extent of the mineral deposit footprint has increased from 100s of metres to 1000s of metres.

In this paper, we present an overview of the current methods and the applications of mineral chemistry using indicator minerals recovered from sedimentary cover. We also discuss new methods and instrumental developments, highlight current research on mineral chemistry, indicator minerals, and mineral exploration, and consider future research directions.

MINERAL IDENTIFICATION AND MINERAL CHEMISTRY

Indicator minerals, by definition, are minerals that have a physical or chemical characteristics that allow them to be readily recovered from stream, alluvial, glacial, or aeolian sediments or soils samples (McClenaghan *et al.* 2000; McClenaghan & Kjarsgaard 2001). Traditionally, the identification and separation of indicator minerals rely on the characteristics largely related to the minerals' chemistry, i.e., visual distinctiveness and moderate to high density.

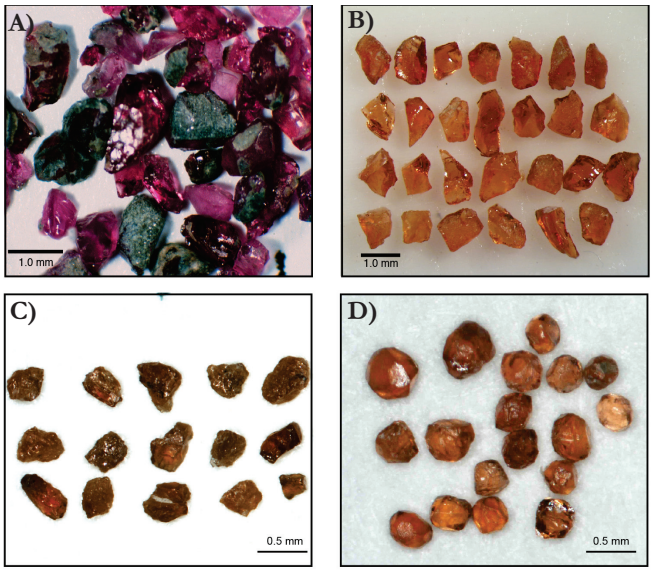

Fig. 1. Examples of colour and habit variation in indicator minerals using optical techniques (modified after McClenaghan & Kjarsgaard 2007; Hicken 2012). **A)** Purple -pyrope, some retaining kelyphite (dark). **B)** Orange eclogitic pyrope-almandine garnets. **C)** Staurolite in sample 09-MPB-006, 0.25–0.5 mm. **D)** Spessartine with deltoidal icositetrahedron habit in sample 09-MPB-031, 0.25–0.5 mm

Optical techniques

Indicator minerals are traditionally selected from samples after the samples have undergone heavy mineral separation (see McClenaghan *et al.* 2000b; McMartin & McClenaghan 2001; McClenaghan 2005). Indicator minerals are "picked" from concentrates during an optical examination under a stereoscopic microscope, a process that may require up to 3 hours per sample. A few tens to several thousand grains may be separated into vials based on colour (Fig. 1A,B) and mineral habit (Fig. 1C,D). The success of a laboratory to produce high-quality mineral concentrates and subsequent mineral picking using experienced technicians is the first critical step in any indicator mineral chemical study.

Electron-based techniques

Once indicator minerals have been recovered, they are commonly epoxy-mounted, polished, and carbon-coated for exam-

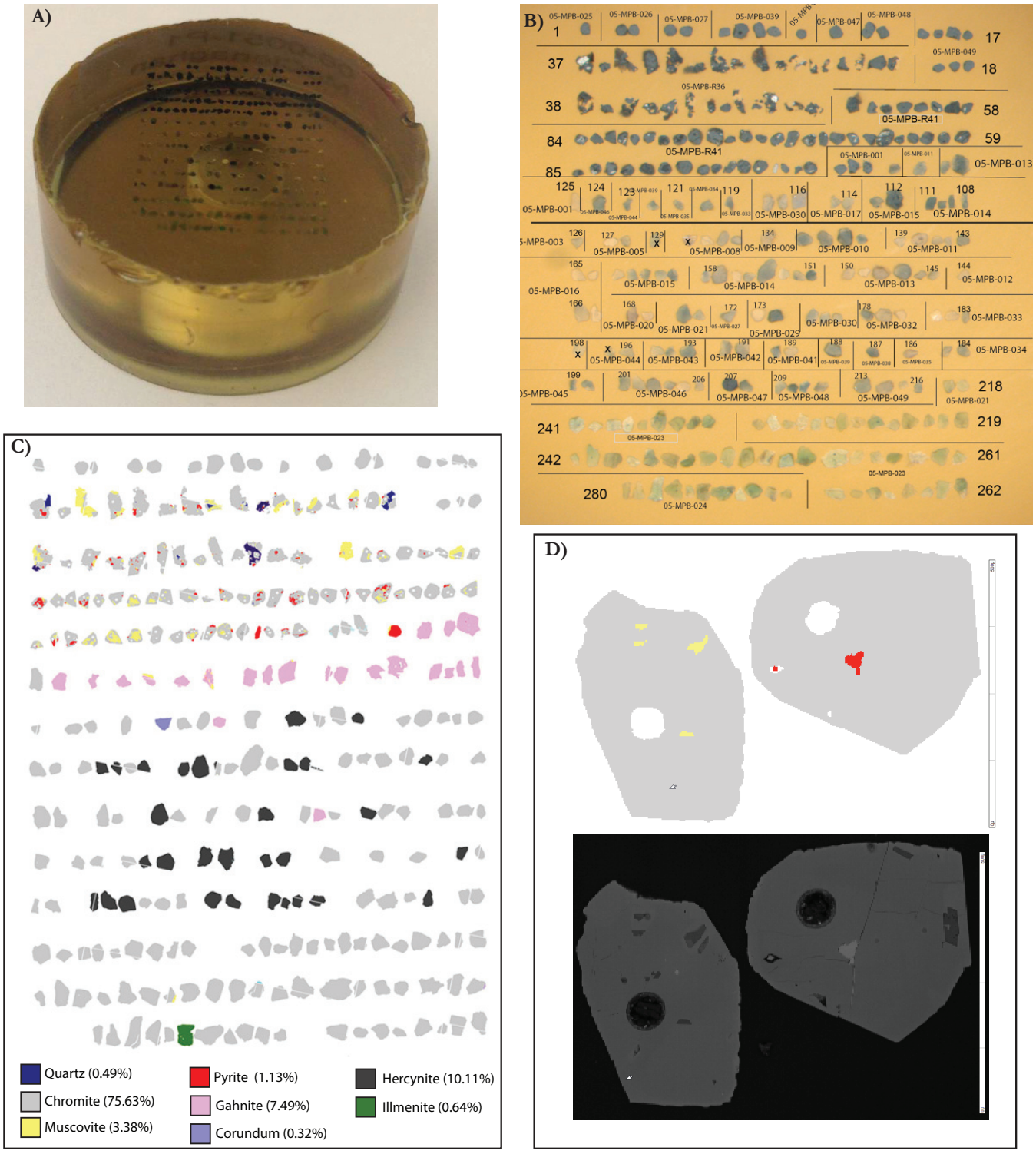

Fig. 2. Example of indicator mineral chemistry workflow from epoxy mount to laser ablation. **A)** Epoxy-mounted mineral grains after mineral separation. **B)** Optical stereo binocular photomicrograph. **C)** False colour processed Mineral Liberation Analysis (MLA) image. **D)** MLA image of chromite (upper) and corresponding BSE image (lower). Note the circular 50 micron laser ablations spots in each grain.

ination using micro-analytical techniques (Fig. 2A). Most mineral chemical investigation methods examine these indicator mineral mounts using an electron-based instrument. Traditionally, a scanning electron microscope (SEM) is used to examine the spatial distribution of backscatter secondary electrons (BSE), which is a reflection of differences in the average atomic number of an area of a grain. This is done in combination with energy dispersive spectrometry (EDS) in order to identify relative element concentrations within mineral phases and mineralogy.

The goals of using an SEM are to (1) confirm of mineralogy that has determined through mineral picking, (2) document mineral associations, (3) document mineral textures and morphology (shape, rounding, size, etc.), and (4) identify opti-

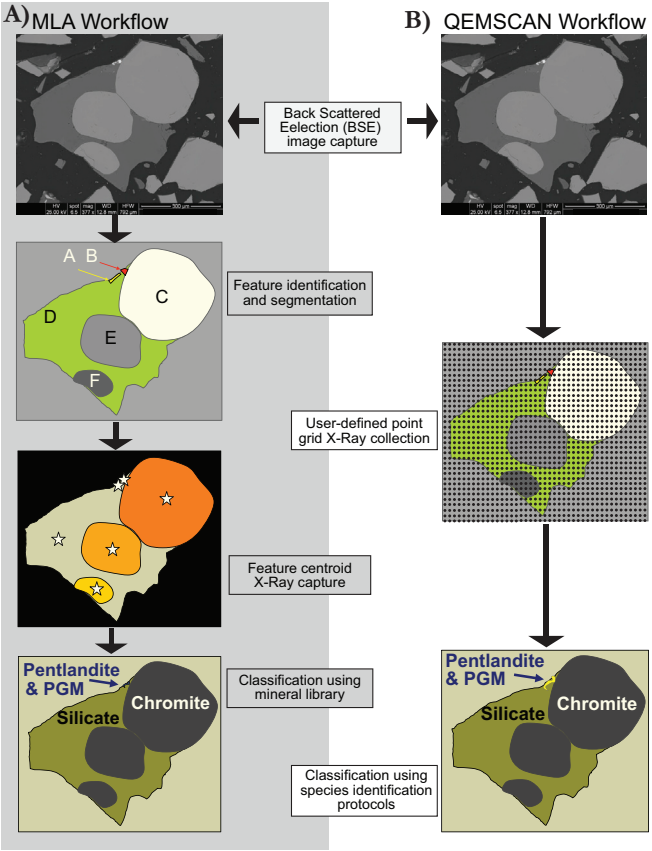

Fig. 3. Comparison of sample work-flow for automated mineralogy for **(A)** mineral liberation analysis and **(B)** QEMSCAN®.

mal mineral grains for further, more costly, mineral chemical characterization. The full characterization of a single epoxy mount with 200 to 500 grains can take 6 to 12 hours on a traditional SEM. Recent advances in automated scanning electron microscopy coupled with energy-dispersive X-ray spectroscopy (EDS) are transforming the analysis of mineral grain mounts. Time-consuming and qualitative mineral descriptions are now been replaced with fast, quantitative, and repeatable SEM analysis. These automated SEM methods provide confirmation of mineralogy, quantification of mineral textures and morphology, and reduces grain mount analysis time to 1 to 2 hours.

The most popular automated SEM supplier is FEI™; the company currently offers a tungsten-based or a field emission gun-based hardware that can be coupled with either Quantitative Evaluation of Minerals by SCANning electron microscopy (QEMSCAN®) or Mineral Liberation Analysis (MLA™) software. Mineral Liberation Analysis was initially developed for the mining industry by the University of Queensland, Australia (JKTech) (Burrows & Gu 2006; Gu *et al.* 2012); QEMSCAN® was developed for the mining industry by CSIRO, Australia (Butcher *et al.* 2000; Gottlieb *et al.* 2000; Pirrie *et al.* 2004; Pirrie & Rollinson 2009). However, both software packages are currently licensed and sold through FEI™ and their regional supply companies (e.g. Systems for Research, Canada).

MLA automated mineralogy is based on high-resolution BSE images, image analyses, and elemental chemistry from EDS. Collections of BSE images are combined to create a mosaic image of an epoxy grain mount (Fig. 3). Each BSE image is used to remove epoxy from the image, and centroid image analysis segments grains and minerals into individual particles. The MLA software then collects a full X-Ray spectrum (EDS) at the centre of each particle (Fig. 3). In post-collection processing, the full X-Ray spectrum is compared with a user-defined mineral EDS library and the BSE image to create a coherent data set, which includes a false-colour mineral map, modal mineralogy, grain size, mineral associations (occurrence and interlocking), particle properties (roundness, area, shape), and mineral liberation.

QEMSCAN® automated mineralogy is fundamentally different than MLA, in that is based on fast mineral identification using point analysis on a finely spaced grid. Similar to MLA, QEMSCAN® collects BSE images to create a mosaic image of an epoxy grain mount; however, during automated measurement, the system collects EDS spectra along a pre-defined grid (similar to modal counting using a petrographic microscope). QEMSCAN® uses the EDS spectra in combination with the BSE image data to determine areas of epoxy and areas of mineral, minimizing the collection of background data. On mineral phases, a low-count EDS spectrum is collected that allows for ultra-fast discrimination of most minerals. QEMSCAN® also differs from MLA in the way that mineralogy is determined. In MLA, minerals are identified through comparison of unknown EDS with a user-defined EDS database of known minerals. QEMSCAN® uses a built-in library of 72 elemental reference spectra are used to build a composite elemental spectra that is then used in conjunction with user-defined Species Identification Protocols (SIP) to identify discrete minerals. In addition to output data similar to MLA, QEMSCAN® produces elemental maps in addition to mineral maps.

MLA- or QEMSCAN®-generated BSE and false-colour images of a mineral concentrate have many advantages over traditional optical microscopy (Hartner *et al.* 2011; Gu *et al.* 2012; Sylvester 2012): 1) measurement of compositional data, 2) measurement of thousands of points per sample mount, 3) repeatable and quantitative measurements, 4) fully automated work-folk, 5) faster processing time, 6) less training required, 7) modal mineralogy calculated assay data, 8) micron-scale resolution, and 9) better determination of analysis points for texturally difficult (i.e. polymineralic) grains and for choosing grains for in situ chemical or isotopic analyses.

The occurrence and modal quantification of distinct HMC in till is of great importance in the definition of till dispersion trains in many ore exploration programs (i.e. gold); however, many HMC mounts are further characterized for individual mineral chemistry. Many HMC studies ((McClenaghan 2002b; Morris *et al.* 2002; Lehtonen *et al.* 2005 and references therein) have used the occurrence of HMC in bedrock sources coupled with the major and minor element chemistry to identify the provenance and fertility of the HMC.

The quantification of major elements can be obtained quickly for many elements from EDS software using a SEM with detection limits between 2000 and 10,000 ppm (Z>4). However, because EDS requires that individual X-Ray spectra be separated from other X-Ray spectra in a mineral analysis, some X-Ray energies cannot be separated from background radiation (high detection limit) or from X-Ray spectra of other elements (i.e. peak overlap). Most modern EDS detectors have an energy resolution of 130 to 160 eV (Full Width Half Max). For example, the quantitative analysis of molybdenite (MoS_2)

by EDS is not possible because the Mo L alpha line is at 2.2930 keV and overlaps with the S K alpha line at 2.3070 keV.

More commonly, indicator minerals are analyzed for major and minor elements using electron probe microanalyzer (EPMA). In principle, a EPMA is very similar to a SEM, as the electron source and focusing column are nearly identical. However, an EPMA and SEM collect X-Ray data differently. Both instruments collect chemical spectra using an EDS detector, but on a EPMA, spectra are also collected using wavelength dispersive spectroscopy (WDS). During the collection of WDS, spectra are separated by the mechanical diffraction of X-Rays into wavelengths that are individually measured by a detector. Most modern EPMA have up to 5 wavelength dispersive spectrometers, which allows the simultaneous measurement of five elements. EDS and WDS each have advantages and disadvantages. EDS can quickly collect a full X-Ray spectrum in 10s of seconds; whereas WDS is time consuming, requiring the movement of a diffraction crystal to measure each individual element. Much of the spectral interference encountered during EDS can be eliminated by the high-energy resolution of WDS (~10 eV). The biggest disadvantage of both EDS and WDS systems are the detection limits (~0.1 and 0.01%, respectively) for most elements in the characterization of mineral chemistry.

Mass spectrometry-based techniques

The use of laser ablation inductively coupled plasma mass spectrometry (LA-ICP-MS) for characterization of mineral chemistry has grown since its first application to geological media (Hale *et al.* 1984; Jackson *et al.* 1992). Conceptually the application of laser ablation for mineral chemical and isotopic analyses is a straightforward, albeit destructive, technique. A short-pulsed (femto- to nanosecond) laser ablates a small volume (~8000 um^3) of a mineral sample over a period of 10s of seconds. During ablation the mineral is converted into vapour and aerosol components. This material is then continually transferred in an Ar or He carrier gas to be ionized in an inductively coupled plasma and mass analyzed in either a quadrupole or magnetic-sector mass spectrometer.

There are several instrument parameters that must be optimized to measure element and isotopic compositions of a mineral by LA-ICP-MS (Arevalo *et al.* 2010; Rogers *et al.* 2010; Koch & Gunther 2011); these include (1) laser pit size, (2) laser wavelength, (3) laser pulse-rate, (4) mass spectrometer, (5) matrix-match standards, and (6) curve calibration. Most laser ablation instruments are capable of adjusting the laser beam size from 1–2 to 300 microns, however, most analyses are completed at ~30 microns. If a laser pit is too small then not enough material is ablated to create a suitable signal in the mass spectrometer. If a laser pit is too large, the mass spectrometer detector may become saturated or go beyond the element calibration curve.

Numerous studies have examined the analyses of geological media using variable laser wavelengths (Motelica-Hieno & Donard 2001; Guillong *et al.* 2005; Jochum *et al.* 2007; Gaboardi & Humayun 2009) and laser pulse-rates (Poitrasson *et al.* 2003; Gonzalez *et al.* 2007; Horn 2008; Saetveit *et al.* 2008; Glaus *et al.* 2010), and collectively using similar laser energies. There is consensus that shorter wavelengths and higher laser pulse rates produce superior data that require fewer corrections for elemental and isotopic bias. In mineral analysis, a shorter wavelength laser (i.e. 193 nm vs 213 nm) produces a flat-bottomed and sharp-walled ablation pit. The higher pulse rate (i.e. femtosecond vs nanosecond) of the mineral, the less thermal heating occurs with a lower abundance of secondary condensates (Gunther & Heinrich 1999; Gunther *et al.* 2000; Poitrasson *et al.* 2003; Hirata *et al.* 2004).

Ultimately, the ability of LA-ICP-MS to measure low-concentration elemental and isotopic data is a function of the mass spectrometer paired with the laser ablation system. There are three options for inductively coupled plasma mass spectrometers for use in laser ablation: 1) quadrapole, 2) high-resolution single collector, and 3) high-resolution multi-collector.

By far the most common mass spectrometer used in laser ablation studies of mineral chemistry is the quadrapole mass analyzer. These instruments filter ions created in the plasma by mass and charge (m/z) as they travel to the detector using variable DC voltages on four parallel stainless steel rods. By adjusting the DC voltage on the quadrupoles, the transient ions created in laser ablation can be filtered and analyzed for most of the periodic table in milliseconds (Hill 2007).

In high-resolution mass spectrometers, ions created in laser ablation and in the inductively coupled plasma are passed along a curved flight path through magnetic and electrical fields to disperse ions according to their momentum and translational energy (Willard 1988). By adjusting the magnetic and electrostatic fields, the transient ions arriving at the detector(s) can be varied on the basis of mass. Because of this geometry, the mass resolution of these instruments is superior to that of quadrupole instruments (e.g. ~10,000 versus ~600, respectively). As such, fractions of mass unit can be effectively separated during analysis, allowing for separation of polyatomic interferences (Hill 2007).

For effective ion transmission through both the magnetic and electrical sectors, ions are accelerated at much higher energies than in quadrapole instruments (e.g. 10 kV versus 10 eV, respectively). As such, less ion scattering is created and lower detection limits are observed using high-resolution instruments. For many mineral chemical applications, a high-resolution mass spectrometer commonly has only one detector. However, in applications where isotopic ratios are measured, high-resolution instruments commonly have several detectors (known as multi-collector). These instruments can measure individual isotopes (i.e. ^{204}Pb, ^{206}Pb, ^{207}Pb, ^{208}Pb) simultaneously, without adjustment of the magnetic or electric sectors, which yields superior isotopic ratios.

Quadrapole and high-resolution mass spectrometers each have advantages and disadvantages in mineral chemical analyses using laser ablation. In quadrapole instruments, a wide range of elements (i.e. m/z) can be analyzed very quickly, compared to magnetic and electrical field sector instruments. In high-resolution instruments, the magnetic sector must be adjusted and allowed to stabilize before analyzing of the next mass range (Giessmann & Greb 1994; Jakubowski *et al.* 1998). Given the transient nature of laser ablation analysis, a quadrapole instrument is much better suited for mineral analyses with varied element mass (i.e. rare earth elements, U, Pb). When there are narrow mass differences (<30%), very small laser ablation pits (<10 microns) or isotopic ratios are needed, for which high-resolution mass spectrometers offer vastly superior precision and detection limits.

Multi-element trace element analysis by LA-ICP-MS has not been universally adopted for mineral analysis because there is a

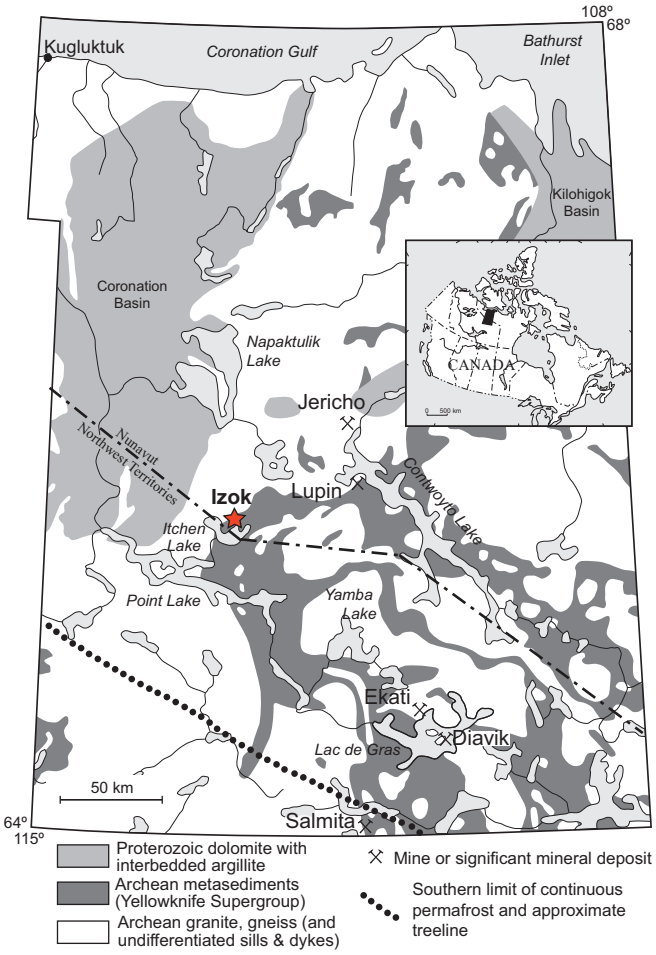

Fig. 4. Location map of the Izok Lake mineralization, Nunavut, Canada (modified after (Dredge *et al.* 1999; Hicken 2012; Hicken *et al.* 2013).

lack of suitable reference materials with similar matrix compositions. Furthermore, there has been a limited effort to find or create matrix-matched standards with variable concentrations of trace elements (i.e. 10, 100, 500 ppm), which is necessary to create standard calibration curves and element quantification. Recently there have been several geological glasses that have been created from rock powder standards (Jochum *et al.* 2000, 2006, 2012; Jochum & Nohl 2008) or by the doping of rock powder standards at variable concentrations (Guillong *et al.* 2005; Jochum *et al.* 2005; Kaiyun *et al.* 2013). The use of these standards in conjunction with EPMA data now allows the reliable quantification of many trace elements in minerals using LA-ICP-MS.

APPLICATIONS IN INDICATOR MINERAL STUDIES

During this workshop, several recent examples will outline the use of mineral chemistry in indicator mineral studies illustrating the methods described above. Due to brevity of an extended abstract, only one case study will be presented.

In exploration for volcanogenic massive sulphide (VMS) deposits in northern Canada, an indicator mineral survey was completed around the Izok Lake mineralization (Fig. 4) occurrence in Nunavut, Canada (McClenaghan *et al.* 2012b,c; McClenaghan *et al.* 2012c; McClenaghan 2013; Paulen *et al.* 2013). Ice-flow mapping in this area shows that glacial trajectories have undergone clockwise rotation from southwest to northwest, in a series of discrete ice-flow phases rather than as a continuous ice-flow change (Kerr *et al.* 1995; Dredge *et al.* 2003; Paulen *et al.* 2013). An early southwest ice-flow was followed by strong west- to west-northwest-trending flow. Surface morphology and ice-flow indicators (e.g. striations) within the Izok Lake area reflect this dominant northwest phase (Paulen *et al.* 2013).

Field documentation of ice-flow in the Izok Lake area, led to till sampling up- and down-ice (Fig. 5). Both bedrock and till

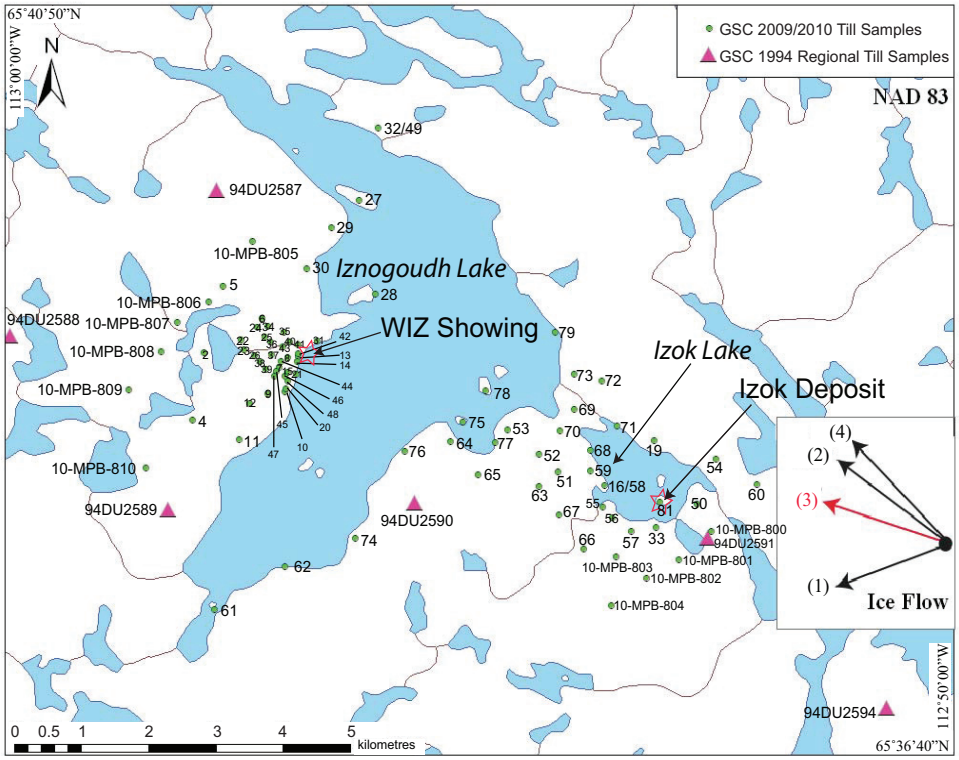

Fig. 5. Locations of till samples (green dots) 1994 Geological Survey of Canada regional samples (pink triangle) and bedrock mineralization (red star) near the Izok Lake deposit (Hicken 2012; Hicken *et al.* 2013).

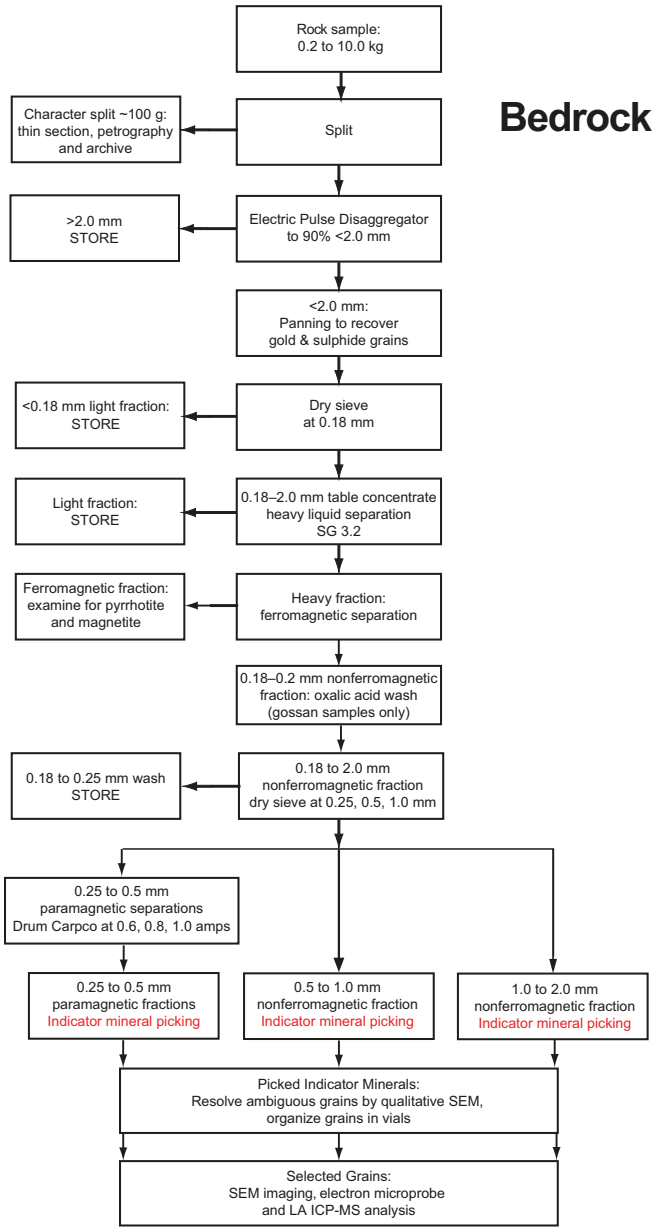

Fig. 6. Flow-sheet outlining the sample processing and picking procedure for bedrock samples processed from the Izok Lake deposit area (Hicken 2012).

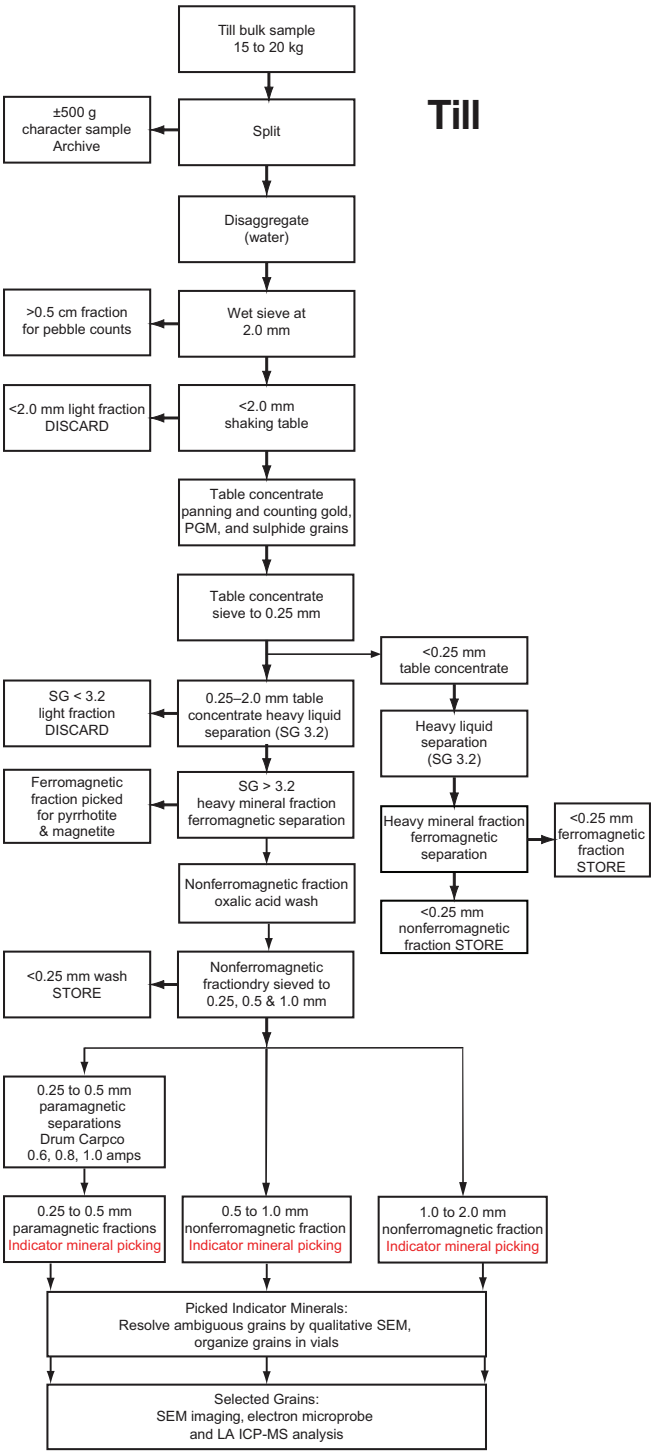

Fig. 7. Flow-sheet outlining the sample processing and picking procedure for till samples processed from the Izok Lake deposit area (Hicken 2012).

Table 1. Comparison of sizes (mm) of key indicator minerals observed in polished thin sections, heavy mineral concentrates, and pan concentrates.

Mineral	**Size Range in Polished Thin Section** (mm)	**Size Range in Heavy Mineral Concentrate** (mm)	**Size Range in Pan Concentrate** (μm)
Pyrite	0.1-6	0.25-1.0	25-200
Chalcopyrite	0.1-5	0.25-1.0	15-200
Sphalerite	0.2-5	0.25-1.0	15-100
Galena	0.01-0.6	0.25-0.50	15-100
Gahnite	0.2-3.0	0.25-1.0	n/a
Staurolite	0.2-1.3	0.25-0.50	n/a
Axinite	0.4-2.0	0.25-0.50	n/a

samples were processed for geochemistry, HMC mineral counts, and HMC mineral chemistry (Figs. 6, 7). The 0.25–0.5, 0.5–1.0, and 1.0–2.0 mm non-ferromagnetic fractions of the bedrock and till samples were examined using optical techniques (Fig. 8). Representative thin sections were made, in addition to mineral grain mounts based on indicator minerals counted/selected during optical examination (Table 1). Thin sections and grain mounts were examined using MLA-ESEM (Figs. 9, 10) to quantify modal mineralogy, mineral associations,

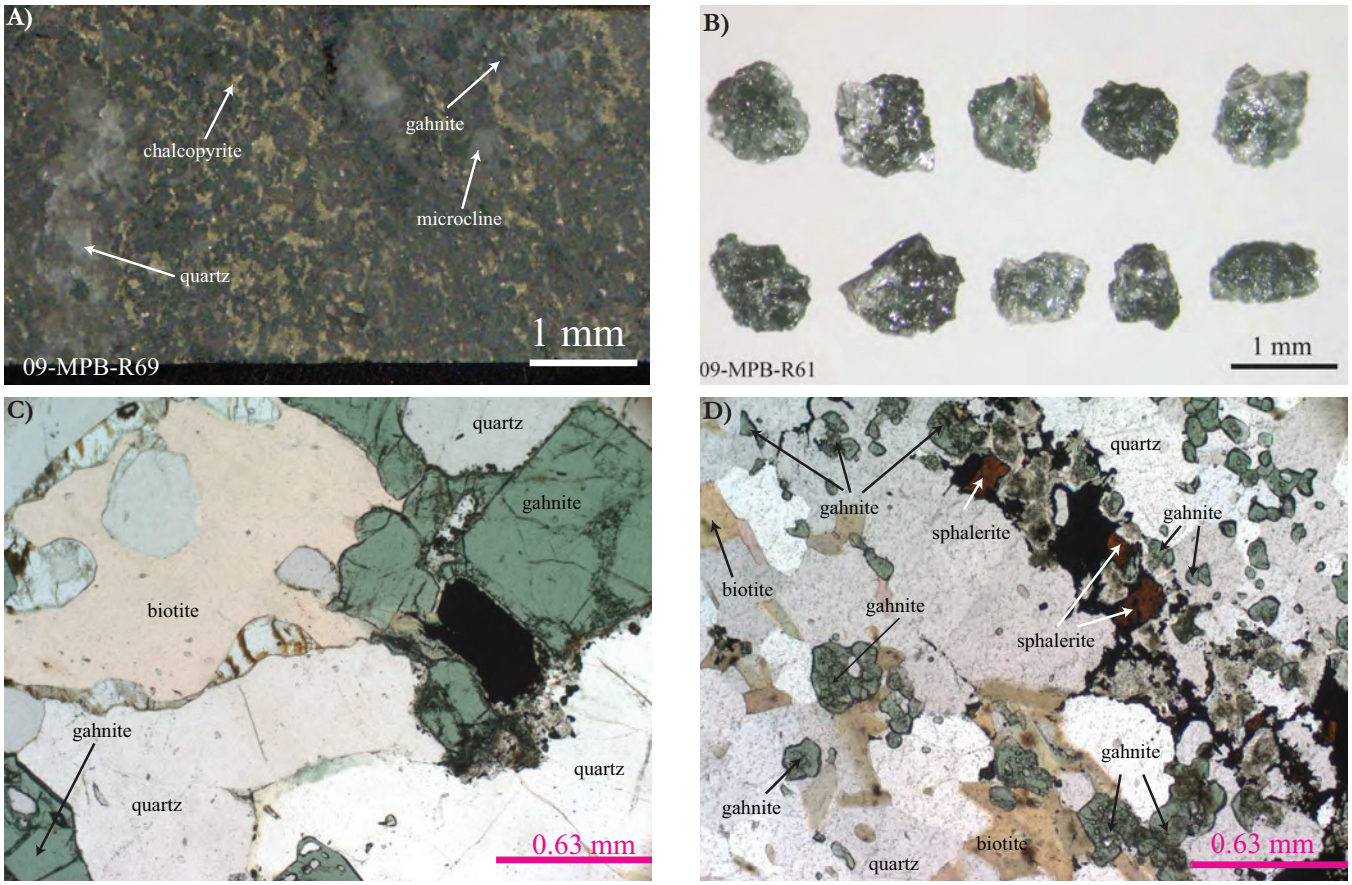

Fig. 8. Gahnite in **(A)** polished slab of drill core (sample 09-MPB-R69); **(B)** grains from a heavy mineral concentrate (sample 09-MPB-R61); **(C)** polished thin section (sample 09-MPB-R37); and **(D)** polished thin section (sample 09-MPB-R41B).

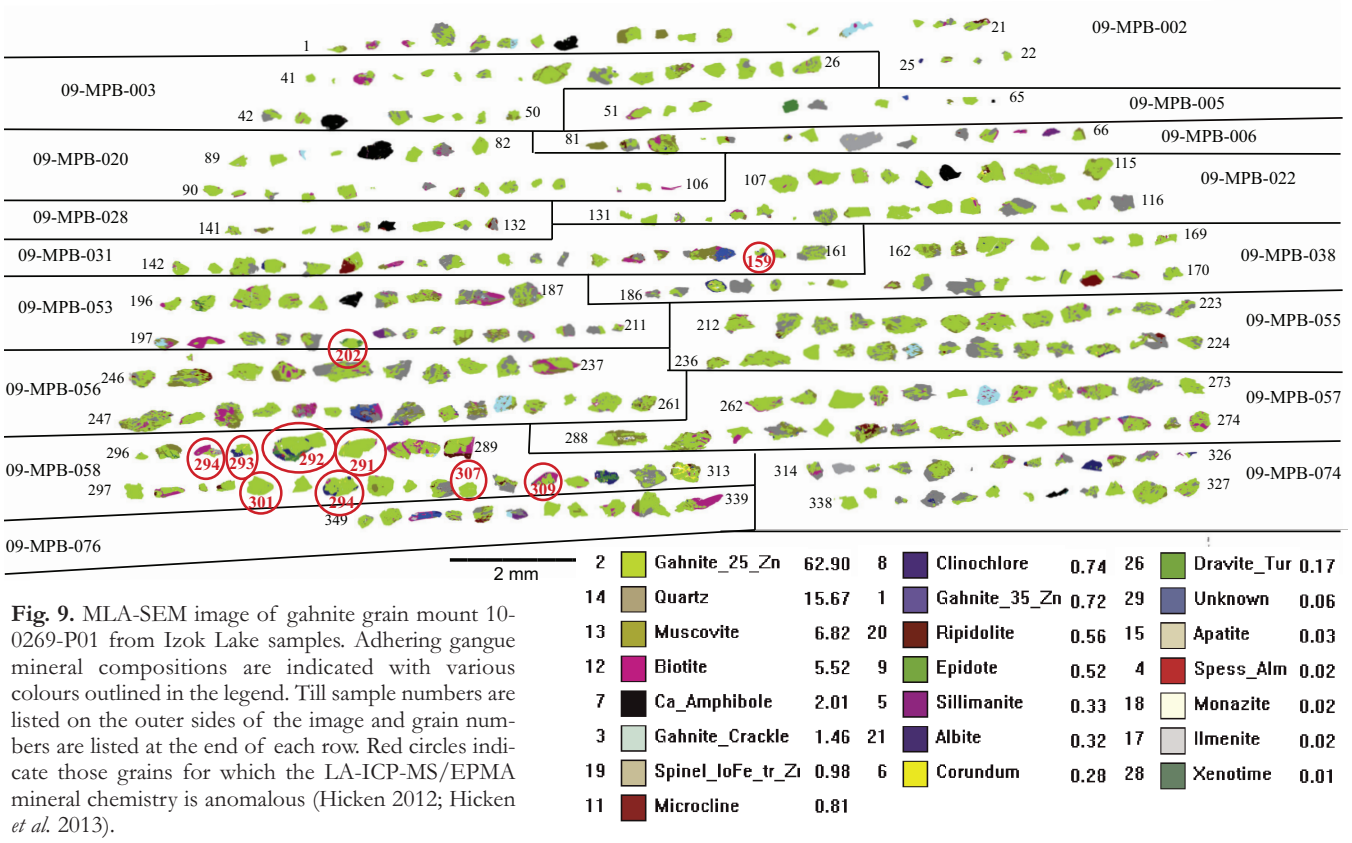

Fig. 9. MLA-SEM image of gahnite grain mount 10-0269-P01 from Izok Lake samples. Adhering gangue mineral compositions are indicated with various colours outlined in the legend. Till sample numbers are listed on the outer sides of the image and grain numbers are listed at the end of each row. Red circles indicate those grains for which the LA-ICP-MS/EPMA mineral chemistry is anomalous (Hicken 2012; Hicken *et al.* 2013).

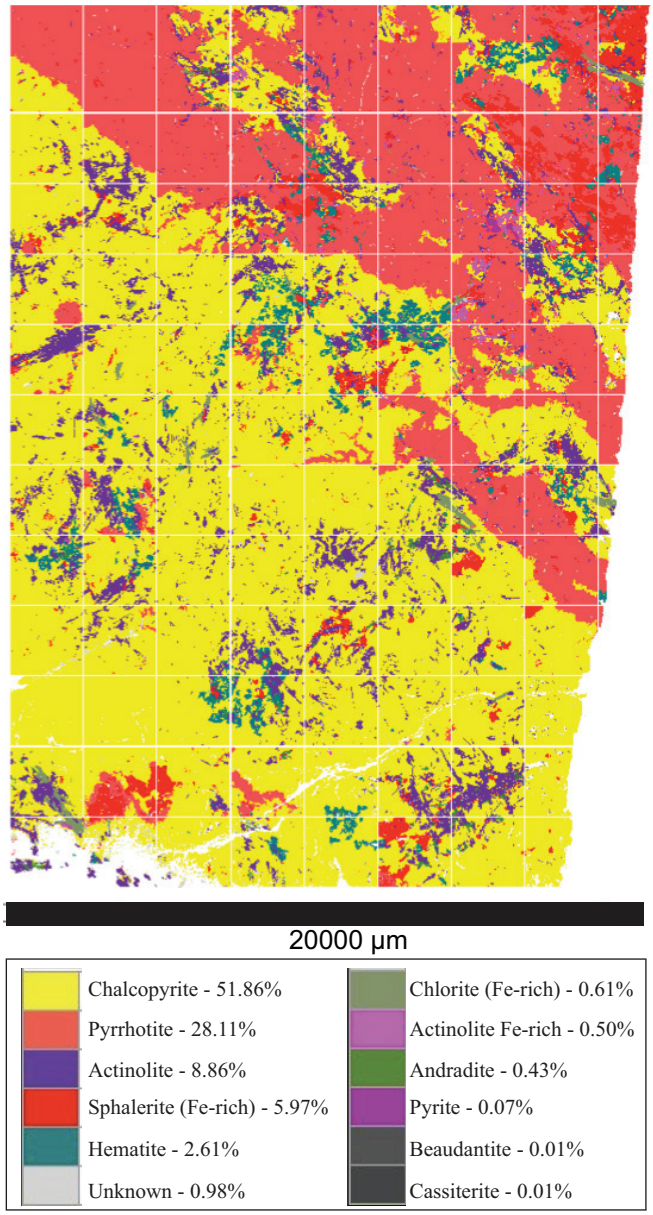

Fig. 10. MLA image of 09-MPB-R60 (massive sulphide) from Izok Lake showing percentages of chalcopyrite, pyrrhotite, actinolite, sphalerite, hematite/magnetite, and trace minerals (Hicken 2012).

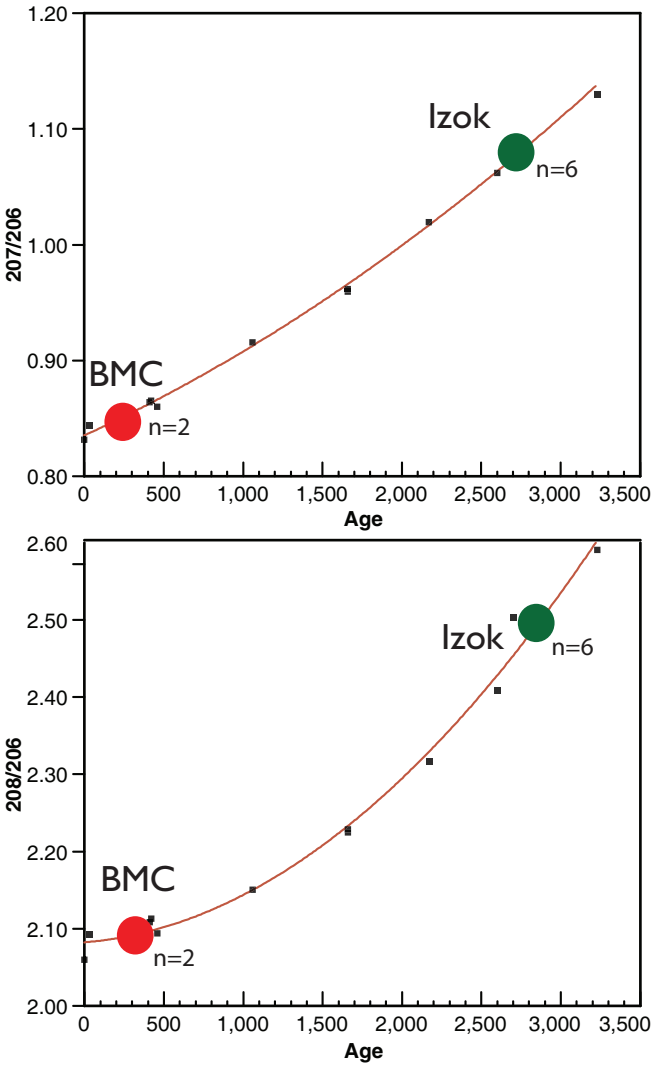

Fig. 11. LA-ICP-MS quadrupole Pb isotopic ratios for gahnite. **A)** $^{207}Pb/^{206}Pb$ age relations for Izok Lake (green circles) and Halfmile Lake (Bathurst Mining Camp, New Brunswick: red circles); **B)** $^{208}Pb/^{206}Pb$ age relations for Izok Lake (green circles) and Halfmile Lake (Bathurst Mining Camp, New Brunswick: red circles). Red line is an approximation of terrestrial lead isotopic evolution (Stacey & Kramers 1975). High-precision U/Pb ages for Halfmile Lake is 465 Ma (van Staal *et al.* 2003), for is Izok Lake is 2623 ± 20 Ma (Mortensen *et al.* 1988), and for Izok Lake is 2680.5 +7/-3 Ma (J. Gebert, unpub. 1995).

grain shape, and grain size. EPMA was completed on a selection of indicator minerals and LA-ICP-MS was conducted on a subset of gahnite grains (>50 microns) for trace element and Pb/Pb dating (Fig. 11).

FUTURE DIRECTIONS IN MINERAL CHEMISTRY

Need for novel methods

The identification of discrete indicator minerals in till has greatly influenced mineral exploration. There are well established methods for separation and identification of minerals in HMC. Indicator mineral chemistry has been used to identify bedrock sources and assess their fertility. The question then becomes, "Why do we need new techniques in the application of mineral chemistry to HMC?"

Successful mineral exploration using sediments and HMC requires a high degree of specialization. This type of work requires a person with not only a background in bedrock geology and ore deposits, but also a person with training in sample collection and preparation, mineralogy, analytical chemistry, and quaternary geology. Current exploration models use a team approach, where each individual contributes their own area of expertise. At present, mineral separation methods have been well established for size-fractions larger than 0.063 mm, but these methods are slow, expensive, and require a highly qualified mineralogist.

New HMC and mineral chemical methods are currently being developed to include a greater number of deposit types (e.g. volcanogenic massive sulphides, uranium, Ni-Cu-PGE, rare earth elements), to utilize the smaller size (i.e. <0.063 mm) and less dense fractions (i.e. <2.85 g/cm^3) of samples, and

incorporate new, faster, and more accessible analytical instruments (i.e. hyperspectral, MLA express). Development of these new methods will decrease the need for extensive specialized training, decrease the time and cost of HMC characterization, extend the spatial footprint of dispersion trains (i.e. smaller and farther), and ultimately lead to the identification of new indicator minerals in uncharacterized mineralized systems.

REFERENCES

Arevalo, R., Bellucci, J. & McDonough, W.F. 2010. GGR Biennial review: Advances in laser ablation and solution ICP-MS from 2008 to 2009 with particular emphasis on sensitivity enhancements, mitigation of fractionation effects and exploration of new applications. *Geostandards and Geoanalytical Research*, **34**, 327–341.

Averill, S.A. 2011. Viable indicator minerals in surficial sediments for two major base metal deposit types; Ni-Cu-PGE and porphyry Cu. *Geochemistry Exploration, Environment, Analysis*, **11**, 279–291.

Averill, S.A. 2013. Discovery and delineation of the Rainy River gold deposit using glacially dispersed gold grains sampled by deep overburden drilling; a 20 year odyssey. *In:* Paulen, R.C. & McClenaghan, M.B. (eds.) *New Frontiers for Exploration in Glaciated Terrain*. Geological Survey of Canada, Open File **7374**, 37–46.

Averill, S.A. & Zimmerman, J.R. 1984. The riddle resolved; the discovery of the Partridge gold zone using sonic drilling in glacial overburden of Waddy Lake, Saskatchewan. *CIM Bulletin*, **77**, 88.

Burrows, D. & Gu, Y. 2006. JKMRC mineral liberation analyser – a modern tool for ore characterisation and plant optimization. *In:* Proceedings Metallurgical Plant Design and Operating Strategies 2006. Australasian Institute of Mining and Metallurgy, 125–139.

Butcher, A.R., Helms, T.A., Gottlieb, P., Bateman, R., Ellis, S. & Johnson, N.W. 2000. Advances in the quantification of gold deportment by QEM-SCAN®. *In:* Proceedings of 7th Mill Operators Conference, October 12–14 2000, Kalgoorlie, Australia 2000. Australasian Institute of Mining and Metallurgy, 267–271.

Craw, D., Youngson, J.H., Koons, P.O. & Minter, W.E.L. 1999. Gold dispersal and placer formation in an active oblique collisional mountain belt, Southern Alps, New Zealand. *Economic Geology*, **94**, 605–614.

Dredge, L., Kerr, D. & Ward, B. 2003. *Surficial geology, Point Lake, District of Mackenzie, Northwest Territories*. Geological Survey of Canada, Map 1890A.

Dredge, L.A., Kerr, D.E. & Wolfe, S.A. 1999. Surficial materials and related ground ice conditions, Slave Province, N.W.T., Canada. *Canadian Journal of Earth Sciences*, **36**, 1227–1238.

Eppinger, R.G., Kelley, K.D., Fey, D.L., Giles, S.A. & Smith, S.M. 2011. Exploration case study using indicator minerals in till at the giant Pebble porphyry Cu-Au-Mo deposit, southwest Alaska, USA. *Vuorimiesyhdistyksen Tutkimusseloste. Sarja B*, **92-4**, 41–48.

Gaboardi, M. & Humayun, M. 2009. Elemental fractionation during LA-ICP-MS analysis of silicate glasses: implications for matrix-independent standardization. *Journal of Analytical Atomic Spectrometry*, **24**, 1188–1197.

Giessmann, U. & Greb, U. 1994. High-resolution ICP-MS - a new concept for elemental mass-spectrometry. *Journal of Analytical Chemistry*, **350**, 186–193.

Glaus, R., Kaegi, R., Krumeich, F. & Gunther, D. 2010. Phenomenological studies on structure and elemental composition of nanosecond and femtosecond laser-generated aerosols with implications on laser ablation inductively coupled plasma mass spectrometry. *Spectrochimica Acta Part B-Atomic Spectroscopy*, **65**, 812–822.

Gonzalez, J.J., Liu, C.Y., Wen, S.B., Mao, X.L. & Russo, R.E. 2007. Metal particles produced by laser ablation for ICP-MS measurements. *Talanta*, **73**, 567–576.

Gottlieb, P., Butcher, A.R., Tun, E.H. & Sutherland, D.N. 2000. Applications of automated process mineralogy. *In: Proceedings*. International Congress on Applied Mineralogy, **6**, 321–323.

Gu, Y., Schouwstra, R. & Rule, C. 2012. The value of automated mineralogy. *In:* Innovative Processing for Sustainable Growth. 26th International Mineral Processing Congress, September 24–28 2012, New Delhi, India, 1726–1732.

Guillong, M., Hametner, K., Reusser, E., Wilson, S.A. & Guenther, D. 2005. Preliminary characterisation of new glass reference materials (GSA-1G, GSC-1G, GSD-1G and GSE-1G) by laser ablation-inductively coupled plasma-mass spectrometry using 193 nm, 213 nm and 266 nm wavelengths. *Geostandards and Geoanalytical Research*, **29**, 315–331.

Gunther, D. & Heinrich, C.A. 1999. Comparison of the ablation behaviour of 266 nm Nd: YAG and 193 nm ArF excimer lasers for LA-ICP-MS analysis. J*ournal of Analytical Atomic Spectrometry*, **14**, 1369–1374.

Gunther, D., Horn, I. & Hattendorf, B. 2000. Recent trends and developments in laser ablation-ICP-mass spectrometry. *Fresenius Journal of Analytical Chemistry*, **368**, 4–14.

Hale, M., Thompson, M. & Wheatley, M.R. 1984, Laser ablation of stream-sediment pebble coatings for simultaneous multi-element analysis in geochemical exploration. *Journal of Geochemical Exploration*, **21**, 361–371.

Hartner, R., Walters, S.G. & Berry, R. 2011. Optical and SEM-based microscopy integration for optimisation of geometallurgical modelling and ore deposit characterisation. *In:* Proceedings of 1st AusIMM International Geometallurgy Conference 2011, GeoMet 2011, September 5–7 2011, Brisbane, 157–162.

Hicken, A. 2012. Glacial Dispersal Of Indicator Minerals From The Izok Lake Zn-Cu-Pb-Ag Vms Deposit, Nunavut, Canada. M.Sc. thesis, Queen's University, Kingston, Ontario.

Hicken, A.K., McClenaghan, M.B., Paulen, R.C., Layton-Matthews, D., Averill, S.A. & Crabtree, D. 2013. *Indicator mineral signatures of the Izok Lake Zn-Cu-Pb-Ag volcanogenic massive sulphide deposit, Nunavut: Part 2 till*. Geological Survey of Canada, Open File **7343**. doi:10.4095/293033

Hill, S.J. 2007. *Inductively Coupled Plasma Spectrometry and its Applications*. Wiley-Blackwell.

Hirata, T., Asada, Y., Apinya, T., Ohno, T., Iizuka, T., Hayano, Y., Tanimizu, M. & Orihashi, Y. 2004. Improvements in the precision and accuracy of elemental and isotopic analyses of geochemical samples by a laser ablation-ICP-mass spectrometer. *Bunseki Kagaku*, **53**, 491–501.

Horn, I. 2008. Comparison of femtosecond and nanosecond laser interactions with geologic matrices and their influence on accuracy and precision of LA-ICP-MS data. In: Sylvester, P. (ed.) Laser Ablation ICP–MS in the Earth Sciences: Current Practices and Outstanding Issues. Mineralogical Association of Canada, Short Course **40**, 53–65.

Jackson, S.E., Longerich, H.P., Dunning, G.R. & Fryer, B.J. 1992. The application of laser-ablation microprobe - inductively coupled plasma-mass spectrometry (LAM-ICP-MS) to in situ trace-element determinations in minerals. *Canadian Mineralogist*, **30**, 1049–1064.

Jakubowski, N., Moens, L. & Vanhaecke, F. 1998, Sector field mass spectrometers in ICP-MS. *Spectrochimica Acta Part B-Atomic Spectroscopy*, **53**, 1739–1763.

Jochum, K.P., Dingwell, D.B., Rocholl, A., Stoll, B., Hofmann, A.W., Becker, S., Besmehn, A., Bessette, D., Dietze, H. J., Dulski, P., Erzinger, J., Hellebrand, E., Hoppe, P., Horn, I., Janssens, K., Jenner, G. A., Klein, M., McDonough, W.F., Maetz, M., Mezger, K., Muenker, C., Nikogosian, I.K., Pickhardt, C., Raczek, I., Rhede, D., Seufert, H.M., Simakin, S.G., Sobolev, A.V., Spettel, B., Straub, S., Vincze, L., Wallianos, A., Weckwerth, G., Weyer, S., Wolf, D. & Zimmer, M. 2000. The preparation and preliminary characterisation of eight geological MPI-DING reference glasses for in-situ microanalysis. *Geostandards and Geoanalytical Research*, **24**, 87–133.

Jochum, K.P. & Nohl, U. 2008, Reference materials in geochemistry and environmental research and the GeoReM database. *Chemical Geology*, **253**, 50–53.

Jochum, K.P., Nohl, U., Rothbarth, N., Schwager, B., Stoll, B. & Weis, U. 2012. Geostandards and Geoanalytical Research Bibliographic Review 2011. *Geostandards and Geoanalytical Research*, **36**, 415–419.

Jochum, K.P., Stoll, B., Herwig, K. & Willbold, M. 2007. Validation of LA-ICP-MS trace element analysis of geological glasses using a new solid-state 193 nm Nd: YAG laser and matrix-matched calibration. *Journal of Analytical Atomic Spectrometry*, **22**, 112–121.

Jochum, K. P., Stoll, B., Herwig, K., Willbold, M., Hofmann, A. W., Amini, M., Aarburg, S., Abouchami, W., Hellebrand, E., Mocek, B., Raczek, I., Stracke, A., Alard, O., Bouman, C., Becker, S., Duecking, M., Braetz, H., Klemd, R., de Bruin, D., Canil, D., Cornell, D., de Hoog, C.-J., Dalpe, C., Danyushevsky, L., Eisenhauer, A., Gao, Y., Snow, J. E., Groschopf, N., Guenther, D., Latkoczy, C., Guillong, M., Hauri, E.H., Hoefer, H.E., Lahaye, Y., Horz, K., Jacob, D.E., Kasemann, S.A., Kent, A.J.R., Ludwig, T., Zack, T., Mason, P.R.D., Meixner, A., Rosner, M., Misawa, K., Nash, B.P., Pfaender, J., Premo, W.R., Sun, W.D., Tiepolo, M., Vannucci, R., Vennemann, T., Wayne, D. & Woodhead, J.D. 2006, MPI-DING reference glasses for in situ microanalysis; new reference values for element concentrations and isotope ratios. *Geochemistry, Geophysics, Geosystems G3*, **7**. doi:10.1029/2005GC001060

Jochum, K.P., Willbold, M., Raczek, I., Stoll, B. & Herwig, K. 2005. Chemical characterisation of the USGS reference glasses GSA 1G, GSC-1G, GSD-1G, GSE-1G, BCR-2G, BHVO-2G and BIR-1G using EPMA, Id-Tims, ID-ICP-MS and LA-ICP-MS. *Geostandards and Geoanalytical Research*, **29**, 285–302.

Kaiyun, C., Honglin, Y., Zhian, B., Chunlei, Z. & Mengning, D. 2013. Precise and accurate in situ determination of lead isotope Ratios in NIST, USGS, MPI-DING and CGSG glass reference materials using Femtosecond laser

ablation MC-ICP-MS. *Geostandards and Geoanalytical Research*, doi:10.1111/j.1751-908X.2013.00223.x

Kelley, K.D., Lang, J. & Eppinger, R.G., 2010. Exploration geochemistry at the giant Pebble porphyry Cu-Au-Mo deposit, Alaska. *SEG Newsletter*, **80**, 18–23.

Kerr, D.E., Dredge, L.A., Ward, B.C. & Gebert, J.S. 1995. Quaternary geology and implications for drift prospecting in the Napaktulik Lake, Point Lake, and Contwoyto Lake map areas, Northwest Slave Province, Northwest Territories. *In: Current Research*. Geological Survey of Canada, Paper **1995-E**, 201–209.

Koch, J. & Gunther, D. 2011. Review of the state-of-the-art of laser ablation inductively coupled plasma mass spectrometry. *Applied Spectroscopy*, **65**, 155A–162A.

Lehtonen, M.L., Marmo, J.S., Nissinen, A.J., Johanson, B.S. & Pakkanen, L.K. 2005. Glacial dispersal studies using indicator minerals and till geochemistry around two eastern Finland kimberlites. *Journal of Geochemical Exploration*, **87**, 19–43.

McClenaghan, M.B. 2002, Indicator mineral and till geochemical methods for kimberlite exploration in glaciated terrain. *CIM Bulletin*, **95**, 79–84.

McClenaghan, M.B. 2005. Indicator mineral methods in mineral exploration. *Geochemistry: Exploration, Environment, Analysis*, **5**, 233–245.

McClenaghan, M.B. 2013. Volcanogenic massive sulphide exploration in glaciated terrain using till geochemistry and indicator minerals. *In:* Paulen, R.C. (ed.) *New Frontiers for Exploration in Glaciated Terrain*. Geological Survey of Canada, Open-File **7374**, 53–64.

McClenaghan, M.B. & Kjarsgaard, B.A. 2001. Indicator mineral and geochemical methods for diamond exploration in glaciated terrain in Canada. *In:* McClenaghan, M.B. (ed.) *Drift Exploration in Glaciated Terrain*. Geological Society, Special Publication **185**, p. 83-123.

McClenaghan, B. & Kjarsgaard, B.A. 2007. Indicator mineral and surficial geochemical exploration methods for kimberlite in glaciated terrain: examples from Canada. *In:* Goodfellow, W.D. (ed.) *Mineral Deposits of Canada: A Synthesis of Major Deposit Types, District Metallogeny, the Evolution of Geological Provinces, and Exploration Methods*. Geological Association of Canada, Mineral Deposits Division, Special Publication **5**, 983–1006.

McClenaghan, M.B. & Peter, J. 2013. Volcanogenic massive sulphide exploration in glaciated terrain using till geochemistry and indicator minerals. *In:* Paulen, R.C. (ed.) *New Frontiers for Exploration in Glaciated Terrain*. Geological Survey of Canada, Open-File **7374**, 53–64.

McClenaghan, M.B., Thorleifson, L.H. & Dilabio, R.N.W. 2000. Till geochemical and indicator mineral methods in mineral exploration. *Ore Geology Reviews*, **16**, 145–166. doi:10.1016/S0169-1368

McClenaghan, M.B., Ward, B.C., Kjarsgaard, I.M., Kjarsgaard, B.A., Kerr, D.E. & Dredge, L.A. 2002. Indicator mineral and till geochemical dispersal patterns associated with the Ranch Lake kimberlite, Lac de Gras region, NWT, Canada. *Geochemistry - Exploration, Environment, Analysis*, **2**, 299–319.

McClenaghan, M.B., Averill, S.A., Kjarsgaard, I.M., Layton-Matthews, D. & Matile, G. 2011. Indicator mineral signatures of magmatic Ni-Cu deposits, Thompson Nickel Belt, central Canada. *Vuorimiesyhdistyksen Tutkimusseloste, Sarja B*, **92-4**, 67–72.

McClenaghan, B., Budulan, G., Averill, S., Layton-Matthews, D. & Parkhill, M.A. 2012a. *Indicator mineral abundance data for bedrock and till samples from the Halfmile Lake Zn-Pb-Cu volcanogenic massive sulphide deposit, Bathurst Mining Camp, New Brunswick*. Geological Survey of Canada, Open File **7076**.

McClenaghan, B., Hicken, A.K., Averill, S., Paulen, R. & Layton-Matthews, D. 2012b. *Indicator mineral abundance data for bedrock and till samples from the Izok Lake Zn-Cu-Pb-Ag volcanogenic massive sulphide deposit, Nunavut*. Geological Survey of Canada, Open File **7075**.

McClenaghan, B., Hicken, A.K., Paulen, R. & Layton-Matthews, D. 2012c. *Indicator mineral counts for regional till samples around the Izok Lake Zn-Cu-Pb-Ag VMS deposit, Nunavut*. Geological Survey of Canada, Open File **7029**.

McMartin, I. and McClenaghan, M.B. 2001, Till geochemistry and sampling techniques in glaciated shield terrain; a review. *In:* McClenaghan, M.B. (ed.) *Drift Exploration in Glaciated Terrain*. Geological Society. Special Publications, 185, 19–43.

Morris, T.F., Sage, R.P. Ayer, J.A. & Crabtree, D.C. 2002. A study in clinopyroxene composition: implications for kimberlite exploration. *Geochemistry - Exploration, Environment, Analysis*, **2**, 321–331.

Mortensen, J.K., Thorpe, R.I., Padgham, W.A., King, J.E. & Davis, W.J. 1988. U-Pb zircon ages for felsic volcanism in Slave Province, N.W.T. *In: Radiogenic Age and Isotopic Studies: Report 2*. Geological Survey of Canada, Paper **88-2**, 85–95.

Motelica-Hieno, M. & Donard, O.F.X. 2001. Comparison of UV and IR laser ablation ICP-MS on silicate reference materials and implementation of normalisation factors for quantitative measurements. *Geostandards Newsletter-the Journal of Geostandards and Geoanalysis*, **25**, 345–359.

Paulen, R.C., McClenaghan, B. & Hicken, A.K. 2013. Regional and local ice-flow history in the vicinity of the Izok Lake Zn-Cu-Pb-Ag deposit, Nunavut. *Canadian Journal of Earth Sciences*. doi:10.1139/cjes-2013-0064

Pirrie, D., Butcher, A.R., Power, M.R., Gottlieb, P. & Miller, G.L. 2004. Rapid quantitative mineral and phase analysis using automated scanning electron microscopy (QEMSCAN®); potential applications in forensic geoscience. *In:* Pye, K. & Croft, D.J. (eds.) *Forensic Geoscience, Principles, Techniques and Applications*. Geological Society, Special Publication **232**, 123–136.

Pirrie, D. & Rollinson, G. 2009. Use of automated mineral analysis using QEMSCAN® in the characterisation of mine tailings. *Applied Earth Science*, **118**, 32.

Poitrasson, F., Mao, X.L., Mao, S.S., Freydier, R. & Russo, R.E. 2003. Comparison of ultraviolet femtosecond and nanosecond laser ablation inductively coupled plasma mass spectrometry analysis in glass, monazite, and zircon. *Analytical Chemistry*, **75**, 6184–6190.

Rogers, R.R., Fricke, H.C., Addona, V., Canavan, R.R., Dwyer, C.N., Harwood, C.L., Koenig, A.E., Murray, R., Thole, J.T. & Williams, J. 2010. Using laser ablation-inductively coupled plasma-mass spectrometry (LA-ICP-MS) to explore geochemical taphonomy of vertebrate fossils in the upper cretaceous two medicine and Judith River formations of Montana. *Palaios*, **25**, 183–195.

Saetveit, N.J., Bajic, S.J., Baldwin, D.P. & Houk, R.S. 2008. Influence of particle size on fractionation with nanosecond and femtosecond laser ablation in brass by online differential mobility analysis and inductively coupled plasma mass spectrometry. *Journal of Analytical Atomic Spectrometry*, **23**, 54–61.

Sarala, P. & Peuraniemi, V. 2007. Exploration using till geochemistry and heavy minerals in the ribbed moraine area of southern Finnish Lapland. *Geochemistry - Exploration, Environment, Analysis*, **7**, 195–205.

Sauerbrei, J.A., Pattison, E.F. & Averill, S.A. 1987. Till sampling in the Casa-Berardi gold area, Quebec: a case history in orientation and discovery (Canada). *Journal of Geochemical Exploration*, **28**, 297–314.

Stacey, J.S. & Kramers, J.D. 1975, Approximation of terrestrial lead isotope evolution by a two-stage model. *Earth Planet. Science Letters*, **26**, 207–221.

Sylvester, P.J. 2012. Use Of the mineral liberation analyzer (MLA) for mineralogical studies of sediments and sedimentary rocks. *In:* Sylvester, P.J. (ed.) *Quantitative Mineralogy and Microanalysis of Sediments and Sedimentary Rocks*. Mineralogical Association of Canada, Short Course **42**, 285.

Thorleifson, L.H. 1993. Kimberlite indicator mineral tracing on the Canadian Prairie. *Canadian Mining and Metallurgical Bulletin*, **86**, 70.

van Staal, C.R., Wilson, R.A., Rogers, N., Fyffe, L.R., Langton, J.P., McCutcheon, S.R., McNicoll, V. & Ravenhurst, C.E. 2003. Geology and tectonic history of the Bathurst Supergroup, Bathurst mining camp, and its relationships to coeval rocks in southwestern New Brunswick and adjacent mine; a synthesis. *In:* Goodfellow, W.D., McCutcheon, S.R. & Peter, J.M. (eds.) *Massive Sulfide Deposits of the Bathurst Mining Camp, New Brunswick, and Northern Maine*. Economic Geology, Monograph **11**, 37–60.

Ward, B.C., Dredge, L.A., Kerr, D.E. & Kjarsgaard, I.M. 1996. Kimberlite indicator minerals in glacial deposits, Lac de Gras area, NWT. In: LeCheminant, A.N., Richardson, D.G., DiLabio, R.N.W. & Richardson, K.A. (eds.) *Searching for Diamonds in Canada*. Geological Survey of Canada, Open File **3228**, 191–195.

Willard, H.H. 1988. *Instrumental Methods of Analysis*. Wadsworth Publishing Company, 895 p.

Micro-analytical innovation for indicator mineral exploration

P.D. Agnew

Chief Geologist –Technical Support & Technology Development - Project Generation Group, Rio Tinto, 1 Research Avenue, Bundoora, 3083, Australia

**Corresponding author's e-mail: paul.agnew@riotinto.com*

The use of indicator minerals in mineral exploration goes back centuries, to the earliest prospectors panning for specks of gold. In many ways things have not changed much; we still look for specks of something, generally in a heavy mineral concentrate, in the hopes it will lead us to mineralization. What has changed is the range of indicator minerals now used in exploration for a wide range of commodities. In the 1970s, kimberlitic indicator mineral methods for diamond exploration ushered in an era where the major and minor elemental composition of indicator minerals added another layer of capability and complexity to the art of indicator mineral exploration. It is in diamond exploration that indicator mineral exploration came of age and truly demonstrated the power of combining appropriate sampling and mineral concentration/separation methods with mineralogical, and textural and chemical analysis. Now we find ourselves in the dawn of a new era of unprecedented micro-analytical capability where low-cost, high-volume mineral identification, and major and trace element analyses offer a whole new world of capability (and complexity) for indicator mineral exploration.

Like so many step-changes in exploration methods, the "indicator mineral revolution", which is well and truly upon us, is being driven by new and improved analytical techniques. Rio Tinto Exploration (RTX) is integrating three pre-existing analytical technologies to build a unique "in-house" micro-analytical capability that will drive development and operational implementation of innovative indicator mineral exploration methods for decades to come: 1) The Mineral Liberation Analyser (MLA) for low-cost rapid detection and accurate quantification of potential indicator minerals; 2) Improved energy-dispersive X-ray spectroscopy (EDS) major element quantification for rapid, low-cost major element chemistry of target phases; and 3) Laser Ablation ICP-MS (LAM) for trace element and isotope analyses of confirmed target phases. In combination, this analytical configuration is providing high-volume, low-cost mineralogy and mineral chemistry on a scale that has the potential to transform the art of indicator mineral exploration for Rio Tinto.

Using the MLA to rapidly scan large numbers of grains in order to identify potential indicator minerals removes the reliance on manual optical picking, which is slow and often inaccurate or inconsistent. Instead of detailed grain-by-grain selection and mounting, large populations of grains can be mounted for probing (up to 20,000 mounted on a single epoxy block), which dramatically improves the chances of finding rare mineral phases that can be difficult or impossible to identify optically, particularly those phases included inside another mineral grain.

The MLA can also collect long count EDS spectra on specified phases that are identified during the mineralogy scan. Although still widely considered to be a semi-quantitative micro-analytical technique, using proprietary EDS quantification software developed by CSIRO, RTX is now producing high-quality major element mineral chemistry at a fraction of the time and cost required to produce the same data on a wavelength-dispersive spectrometry (WDS) microprobe system. In 2012, RTX generated >700,000 major element mineral chemistry analyses in support of global diamonds exploration programs, at a cost of <50¢ per analysis.

Innovative integration of the LAM with the MLA has provided an unrivalled capability for automated trace element analysis on a scale not currently available in commercial or university analytical facilities. A Large Format CellTM was developed by the New Wave Research Division of ESI in collaboration with Rio Tinto. The cell holds up to 12 epoxy blocks and is interchangeable between the MLA and the LAM. Grain coordinates and major element internal calibration data are transferred between the MLA and LAM using proprietary software. The semi-automated system can produce up to 400 trace element analyses a day.

In recent years, RTX have utilized the innovative MLA-LAM micro-analytical configuration to develop new indicator mineral exploration techniques for copper, uranium, nickel, and bauxite. Internal and external research and development is showing mineral chemistry has enormous potential to characterize ore systems, as well as potentially vector towards them, and to assess fertility potential. In particular, the pioneering "Greenrocks" research undertaken by CODES, which uses epidote and chlorite mineral chemistry to vector towards porphyry Cu systems and assess their fertility, shows great promise. RTX is actively utilizing the MLA-LAM analytical configuration to refine the "Greenrocks" methodology and apply it operationally in support of global copper exploration programs.

Overview of titanite as an indicator mineral

R.L. Linnen[1*], X.D. Che[2] & H. Blumenthal[3]

[1]Department of Earth Sciences, University of Western Ontario, London, Ontario, Canada N6A 5B7
[2]School of Earth Sciences and Engineering, Nanjing University, Nanjing 210093, China
[3]Stantec, 101-401 Wellington Street West, Stantec, Toronto, Ontario, Canada M5V 1E7
[4]Perilya Limited, P.O. Box 5001, Broken Hill, New South Wales 2880, Australia
**Corresponding author's e-mail: rlinnen@uwo.ca*

Titanite ($CaTiSiO_5$) has many of the characteristics of indicator minerals that are used in mineral exploration, and some features that other minerals lack. It is a common mineral, present in igneous, metamorphic, sedimentary, and hydrothermally altered rocks and it is resistant to weathering. It commonly retains its original composition because solid-state diffusion rates in this mineral are slow and primary zoning typically is preserved. Substitutions involving a wide range of metals are common (Mazdab *et al.* 2007). In addition, titanite is used for U-Pb age dating (Li *et al.* 2010), analyzed for a variety of other radiogenic isotopes, and has been used as a geothermometer (Haden *et al.* 2008). In spite of these attributes, titanite has received very little attention as an indicator mineral.

The Ca in titanite can be substituted by Na, Ba, Sr, Y, and REE and Ti can be replaced by Sn, Zr, Si, Al, Fe^{2+}, Fe^{3+}, Sb, V, Nb, and Ta. OH and F can also replace O and, because of the different valences of these elements, a number of coupled substitutions have been proposed; two common ones are $Al^{3+} + Fe^{3+} = 2\ Ti^{4+}$ and $Al^{3+} + Nb^{5+} = 2\ Ti^{4+}$. A number of economically important elements are concentrated in titanite. For example, titanite is known to contain up to 3.9 wt% REE_2O_3 and 2.8 wt% ZrO_2 (Hode Vuorinen & Halenius 2005), 10.56 wt% Nb_2O_5 (Cempírek *et al.* 2008). Tin is well known to substitute for Ti in a variety of minerals and titanite at the Qitianling granite in China, is reported to contain up to 26 wt% SnO_2 (Xie *et al.* 2010). Up to 1300 ppm WO_3 has been reported in titanite from the Mt. Lindsay Sn-W skarn in Australia (Kwak 1983). Che et al (2013) studied the concentrations of lithophile and high field strength elements in titanite from W-Mo deposits in British Columbia and Yukon, Canada. Elsewhere, Linnen *et al.* (2009) studied titanite in fractures around the Dibs rare-metal pegmatite at Manitoba, Canada and Blumenthal (2010) included analyses of magmatic and hydrothermal titanite from a porphyry Cu prospect in southwestern Yukon, Canada. This paper draws on these three studies to provide an overview of the potential use of titanite as an indicator mineral for exploration.

ANALYTICAL METHODS

Different facilities were used by the three principle studies considered below: electron microprobe (University of Toronto and the University of Manitoba) and LA-ICP-MS (University of Windsor, University of Manitoba and Laurentian University). Electron microprobe typically utilized a 15 to 20 kV accelerating voltage and 20 to 65 nA beam current. Elements analyzed were Si, Ti, Ca, Al, Fe, Y, Mn, Sn, Zr, Ce, Nb, Mo, Yb, W, and F. For La-ICP-MS analyses, NIST 610 glass was used as an external standard, Femtosecond (785 nm), Nd:YAG (213 nm).

TITANITE IN W-Mo DEPOSTS

Che *et al.* (2013) studied magmatic and hydrothermal titanite from W-Mo deposits in the Canadian Cordillera: the Risby, Ray Gulch, Mactung, and Fox W skarn deposits; the Northern Dancer and Jersey Emerald W skarn-Mo stockwork systems; and the Boss Mountain and Max porphyry Mo deposits.

Igneous rocks from all of the deposits were examined, but magmatic titanite was observed only in granodiorite associated with the Ray Gulch W and Boss Mountain Mo deposits. The titanite grains were interpreted to be magmatic based on their euhedral shapes and sharp planar contacts with other magmatic minerals (plagioclase, K-feldspar, hornblende, quartz, and magnetite; Fig .1A). Titanite is typically zoned in backscattered electron images (BSE), with lighter cores and darker rims. Hydrothermal titanite is common where biotite is altered to muscovite and chlorite. Hydrothermal titanite is also present in scheelite- and molybdenite-bearing quartz veins that crosscut hornfels. Typically this style of titanite is not zoned in BSE images. Finally, metasomatic titanite is a common mineral in calc-silicate hornfels and skarn samples. Most grains are strongly zoned in BSE images, with lighter cores and darker rims with locallized oscillatory zoning (Fig. 1B).

The stoichiometries of titanite were calculated from electron microprobe analyses assuming five equivalent oxygen atoms per formula unit and all iron and Fe^{3+}. Compared to hydrothermal titanite, magmatic titanite contains higher Ti but lower Fe^{3+}, compared to hydrothermal titanite, magmatic titanite contains lower F. There is a strong negative correlation between Ca+Ti and REE+Al+Fe^{3+} contents, which is indicative of a $Ca^{2+} + Ti^{4+} = REE^{3+} + (Al,Fe)^{3+}$ exchange. Magmatic titanite has relatively high Ca+Ti but low REE+Al+Fe^{3+} contents.

Magmatic titanite in the study of Che *et al.* (2013) has relatively consistent REE patterns on chondrite normalized diagrams. Cores are LREE-enriched, up to roughly 10,000 times chondrite, and exhibit negative slopes. Grains can exhibit either positive or negative Ce and Eu anomalies. Hydrothermal, skarn, and hornfels titanite contain much lower REE concentrations producing variable patterns with negative to positive slopes, as well as inverted U-shapes.

Magmatic titanite can also be enriched in trace elements of interest: titanite from Boss Mountain contains up to 174 ppm Mo, and Ray Gulch, up to 103 ppm W (Che *et al.* 2013). These values indicate that titanite has the potential to be used to discriminate between Mo-W barren intrusions and fertile ones.

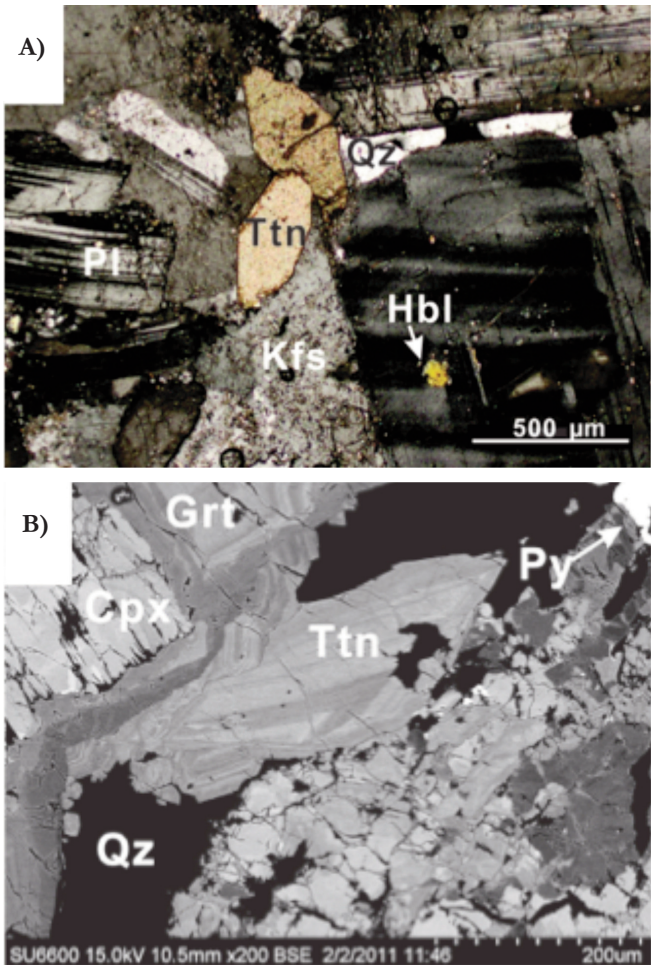

Fig. 1. Images of titanite from Che *et al.* (2013). A) cross-polarized light photomicrograph of magmatic titantite from Boss Mountain. Titanite (Ttn) intergrown with quartz (Qz), plagioclase (Pl), K-feldspar (Kfs) and hornblende (Hbl). B) Backscatter image of titanite with oscillatory zoning from W skarn at the Max deposit. Titanite (Tnt), garnet (Grt), clinopyroxene (Cpx), quartz (Qz) and pyrite (Py) are the other skarn minerals.

The cores of most titanite from skarns contain elevated contents of Y, W, Nb, Ta, Zr, and Hf, including up to 570 ppm W from a W skarn external to the Max Mo deposit (Che *et al.* 2013). Hydrothermal titanite in some mineralized systems contains up to 243 ppm W, but the Mo contents of skarn and hydrothermal titanite rarely exceeds 100 ppm. By contrast skarn and hydrothermal titanite are commonly enriched in Sn and Nb, maximum values observed in (Che *et al.* 2013) this study are 1904 and 23300 ppm, respectively.

TITANITE IN PROPYLITIC ALTERATION

The second example of titanite examined here is from propylitic alteration, interpreted to be peripheral to a porphyry Cu system (Blumenthal 2010). This study consisted of an investigation of chacopyrite-molybdenite mineralization associated with quartz-carbonate-chlorite-titanite alteration at the Hopper property, Yukon, Canada.

Although titanite is used extensively for age–dating, it is only rarely used to obtain direct ages of mineralization (e.g. Li *et al.* 2010). At the Hopper property, chalcopyrite is associated with

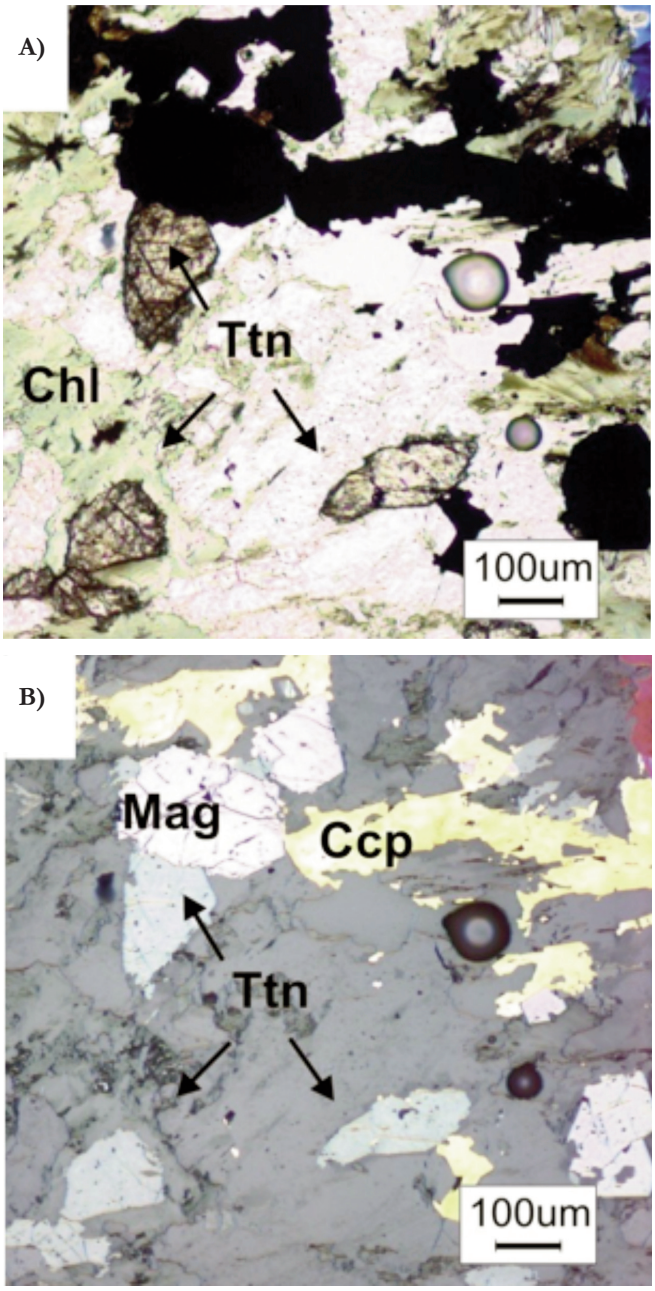

Fig. 2. Titanite mineralized propylitic alteration from the Hopper Cu prospect, from Blumenthal (2010): **(A)** plane polarized light and **(B)** reflected light. Abbreviations: Ccp = chalcopyrite, Chl = chlorite, Mag = magnetite, Ttn = titanite.

propylitic alteration (Fig. 2), thus the age of the titanite and the age of mineralization are the same. LA-ICP-MS dates of zircon and ID-TIMS U-Pb dates of zircon, as well as hydrothermal and magmatic titanite, all indicated the same age, which strongly suggests a porphyry system. Titanite is thus demonstrated to be an excellent mineral for dating mineralization.

At the Hopper property, the chemical differences between the magmatic and the hydrothermal titanite are relatively minor (Blumenthal 2010). The magmatic titanite is characterized by lower TiO_2, in contrast to the W-Mo study of Che *et al.* (2013), but has higher Al, Fe Nb, Zr, Ce, and Y (Blumenthal 2010). Copper contents of both magmatic and hydrothermal titanite are low, roughly 10 ppm, Mo contents are higher, with a maxi-

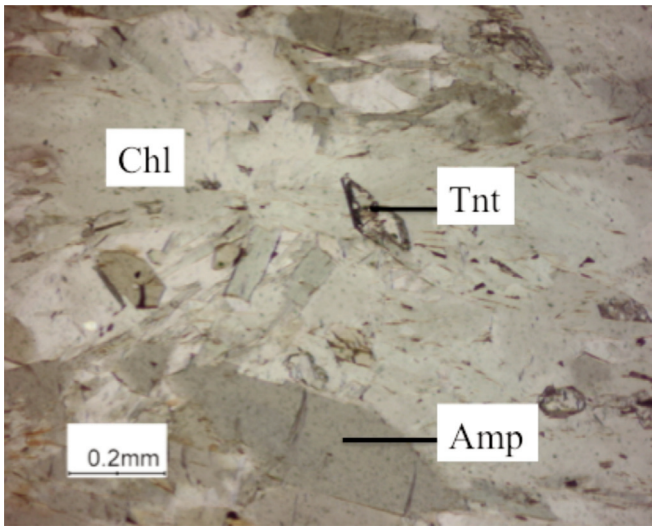

Fig. 3. Plane-polarized light photomicrograph of titanite (Tnt), chlorite (Chl), and amphibole (Amp) in a vein from the aureole around the Dibs pegmatite.

mum of 222 ppm in magmatic titanite and 61 ppm in hydrothermal titanite (Blumenthal 2010). For comparison W contents are on the order of 20 ppm and Nb and Sn contents are also low, generally less than 1000 and 100 ppm, respectively (Blumenthal 2010).

TITANITE IN RARE-METAL PEGMATITE AUREOLES

The third example comes from the Dibs rare-metal (Li-Cs-Ta) pegmatite, located near the Tanco pegmatite in southeastern Manitoba, Canada (Galeschuk & Vanstone 2005; Linnen *et al.* 2009). This buried, well zoned pegmatite is approximately 100 m below the surface, hosted entirely within metagabbro, and therefore is an ideal for establishing the dispersion of elements around the pegmatite. The study of Linnen *et al.* (2009) includes the following analyses of titanite, amphibole, biotite, and chlorite in fractures and veins in the host metagabbro (Fig. 3). Hydrothermal titanite contains up to 20 ppm Li at a distance of 70 m from the pegmatite contact, but chlorite records the involvement of Li-rich fluids much better. It could be predicted that titanite associated with rare-metal pegmatite mineralization should be enriched in Ta-Nb-Sn. Hydrothermal titanite in the metabasite contains up to 3324 ppm Sn, 2696 ppm Nb, and 335 ppm Ta. However, beyond approximately 1 metre from the pegmatite contacts, Sn contents drop to less than 10 ppm and Nb to less than 100 ppm. It thus appears that Sn, Nb, and Ta metasomatism is extremely limited, i.e., fluids were not enriched in these elements. By contrast, chlorite in the same veins and fractures proved to be an excellent indicator mineral. The Li content of chlorite in fractures at the contact with the pegmatite is in excess of 2000 ppm. This Li content decreases systematically with distance from the pegmatite, but values are 200 to 400 ppm at the tops of drillholes, roughly 80 m above the Dibs pegmatite contact. This compares to a value of 30 ppm Li for whole-rock. Thus, for rare metal pegmatite, chlorite shows much greater promise than titanite as an indicator mineral.

ACKNOWLEDGEMENTS

We gratefully acknowledge financial support from NSERC, the Yukon Geological Survey, Strategic Metals Ltd., Tantalum Mining Corporation (Tanco), and numerous other people involved with these studies: A. Brand, D. Davis, C. Galeschuk, L. Groat, N. Halden, B. Kamber, L. Lau, T. Ulrich, and R.-C. Wang.

REFERENCES

Blumenthal, H. 2010. *A Geochemical Study of the Mineralization at the Hopper deposit, Yukon: A Case Study of an Atypical Copper Occurrence*. M.Sc. thesis, University of Waterloo, London, Ontario, 107 p.

Cempírek, J., Houzar, S. & Novák, M. 2008. Complexly zoned niobian titanite from hedenbergite skarn at Písek, Czech Republic, constrained by substitutions $Al(Nb,Ta)Ti_{-2}$, $Al(F,OH)(TiO)_{-1}$ and $SnTi_{-1}$. *Mineralogical Magazine*, **72**, 1293–1305.

Che, X.D., Linnen, R.L., Wang, R.C., Groat, L.A. & Brand, A.A. 2013. Distribution of trace and rare earth elements in the titanite from tungsten and molybdenum deposits in Yukon and British Columbia, Canada. *Canadian Mineralogist*, **51**, 415–438.

Galeschuk, C.R. & Vanstone, P.J. 2005, Exploration for buried rare-element pegmatites in the Bernic Lake area of southeastern Manitoba. *In:* Linnen, R.L. & Samson, I.M. (eds.) R*are-Element Geochemistry and Mineral Deposits*. Geological Association of Canada, Short Course Notes 17, 153–167.

Hayden, L.A., Watson, E.B. & Wark, D.A. 2008. A thermobarometer for sphene (titanite). *Contributions to Mineralogy and Petrology*, **155**, 529–540.

Hode Vuorinen, J. & Hålenius, U. 2005. Nb-, Zr- and LREE-rich titanite from the Alno alkaline complex: Crystal chemistry and its importance as a petrogenetic indicator. *Lithos*, **83**, 128–142.

Kwak, T.A.P. 1983. The geology and geochemistry of the zoned, Sn-W-Be skarns at Mt. Lindsay, Tasmania, Australia. *Economic Geology*, **78**, 1440–1465.

Li, J.W., Deng, X.D., Zhou, M.F., Liu, Y.S., Zhao, X.F. & Guo, J.L. 2010. Laser ablation ICP-MS titanite U-Th-Pb dating of hydrothermal ore deposits: A case study of the Tonglushan Cu-Fe-Au skarn deposit, SE Hubei Province, China. *Chemical Geology*, **270**, 56–67.

Linnen, R.L., Galeschuk, C., Halden, N. & Lau, L. 2009. Dispersion haloes around rare-metal pegmatites: A case study of the Dibs LCT pegmatite, Manitoba, Canada. *In: Proceedings of the 4th International Symposium on Granitic Pegmatites - PEG 2009*. Recife, Brazil, 30 August–2 September, 2009, 23–25.

Mazdab, F.K., Wooden, J.L. & Barth, A.P. 2007, Trace-element variability in titanite from diverse geologic environments *In: Abstracts with Programs*. Geological Society of America, **39**, 406.

Trace element compositions of silicates and oxides as exploration guides to metamorphosed massive sulphide deposits: examples from Broken Hill, Australia, and Stollberg, Sweden

P.G. Spry[1*], J.J. O'Brien[1] K.S. Frank[1], G.S. Teale[2], A. Koenig[3], N. Jansson[4], R. Allen[5] & H. Raat[5]

[1]Department of Geological and Atmospheric Sciences, 253 Science I, Iowa State University, Ames, Iowa 50011-3212, U.S.A.
[2]Teale & Associates, P.O. Box 740, North Adelaide, South Australia 5006, Australia
[3]U.S. Geological Survey, Denver Federal Center, Denver, Colorado 80225, U.S.A.
[4]Department of Civil, Environmental and Natural Resources Engineering, Luleå University, SE-971 87 Luleå, Sweden
[5]Exploration Department, Boliden Mineral, SE-776 98, Garpenberg, Sweden
**Corresponding author's e-mail: pgspry@iastate.edu*

Although the presence of indicator minerals has long been used as a guide in the exploration for various ore deposits on a regional scale (e.g. Spry 2000; McClenaghan 2005), the composition of these minerals has also helped to target sulphide mineralisation on a more local scale. Using major element compositions, an increase in the Mg/(Mg+Fe) ratio of ferromagnesian silicates, including garnet, biotite, tourmaline, chlorite, staurolite, cordierite, and amphibole, has been used to indicate proximity to metamorphosed ore deposits in low- to high-grade metamorphic terranes (e.g. Nesbitt 1986; Bryndzia & Scott 1987). More recently, trace element studies using various techniques (e.g. electron microprobe, laser ablation-inductively coupled plasma-mass spectrometry (LA-ICP-MS), proton-induced X-ray emission (PIXE)) have allowed the provenance of minerals and their composition in various ore deposits to be determined. Such techniques facilitate the measurement of many elements at concentrations as low as parts per billion (e.g. Jackson, 1992). Trace element studies of minerals spatially related to metallic mineral deposits include titanite in porphyry Cu deposits (Xu *et al.* 2014), magnetite in porphyry Cu-Mo, orogenic Au, skarn, iron oxide-copper-gold (IOCG), volcanogenic massive sulphide (VMS), and Ni-Cu-platinum-group element deposits (e.g. Dupuis & Beaudoin 2011; Nadoll *et al.* 2012, 2014), maghemite and hematite in IOCG deposits (e.g. Schmidt Mumm *et al.* 2012), garnet in skarn (e.g. Gaspar *et al.* 2008) and Broken Hill-type (BHT) deposits (Spry *et al.* 2007), and chromite (e.g. Pagé & Barnes 2009), and ilmenite (e.g. Dare *et al.* 2012) in magmatic sulphide deposits. Nine minerals (feldspar, calcite, garnet, pyroxene, amphibole, allanite, epidote-group minerals, titanite, and apatite) were analyzed by Ismail *et al.* (2014) in a study of the Hillside IOCG deposit, South Australia.

The use of trace element studies of minerals to vector to metamorphosed massive sulphide has received minimal attention but has largely focused on gahnite (e.g. Clark & Williams-Jones 2004; Layton-Matthews *et al.* 2013; O'Brien *et al.* 2013a, 2015a, b), garnet (Spry *et al.* 2007; Heimann *et al.* 2009, 2011), and tourmaline (Griffin *et al.* 1996), with the most detailed work being done on BHT deposits. The present contribution focuses on the trace element composition of gahnite from BHT deposits and metamorphosed VMS, sedimentary exhalative (SEDEX), and non-sulphide zinc (NSZ) deposits, garnet from BHT deposits in the southern Curnamona Province, Australia (including the supergiant Broken Hill Pb-Zn-Ag deposit), and preliminary data for magnetite, garnet, and biotite from the Stollberg Zn-Pb-Ag and magnetite field, Sweden. The analytical methods used in this study are described in O'Brien *et al.* (2015a) and are not repeated here. The aim of study is to evaluate the use of trace elements of these minerals in guiding exploration, with a discussion of the physicochemical parameters that affect their trace element composition in metamorphosed metallic base metal deposits.

TRACE ELEMENT COMPOSITIONS OF SILICATES AND OXIDES

Gahnite

The major element chemistry of gahnite (AB_2O_4) is comprised of varying proportions of Zn^{2+}, Fe^{2+}, Mg^{2+} and lesser amounts of Mn^{2+} in the tetrahedral site (A), where Zn > (Fe + Mg), and dominantly Al^{3+} in the octahedral site (B), with minor amounts of Fe^{3+} also in the octahedral site. The most extensive gahnite horizons known occur in the Proterozoic Broken Hill domain of the southern Curnamona Province, New South Wales, Australia. Gahnite occurs in blue quartz-gahnite lode rocks in and along strike from the Broken Hill Pb-Zn-Ag deposit as well as minor BHT deposits. These rocks form part of the so-called "lode horizon", which occurs intermittently for >300 km throughout the Broken Hill domain, and also contains quartz garnetite and lesser amounts of garnetite and lode pegmatite. In addition to blue quartz-gahnite lode, gahnite occurs in minor to trace amounts in sillimanite gneiss, lode pegmatite, tourmalinite, iron formation, quartz-feldspar-garnet gneiss, and amphibolite. O'Brien *et al.* (2015a) evaluated the composition of gahnite from various rock types, including 11 minor BHT deposits and the main Broken Hill deposit. The aim of their study was to find a compositional fingerprint that could be used to distinguish gahnite associated with sulphides from those in rocks devoid of sulphides. Based on >500 major and trace element compositions of gahnite from various rocks types, O'Brien *et al.* found that gahnite from the Broken Hill deposit can be distinguished from that associated with unmineralized lode pegmatite and sillimanite gneiss using a principal component analysis and a plot of Zn/Fe versus Ni+Cr+V. Bivariate plots of Zn/Fe versus Ga,

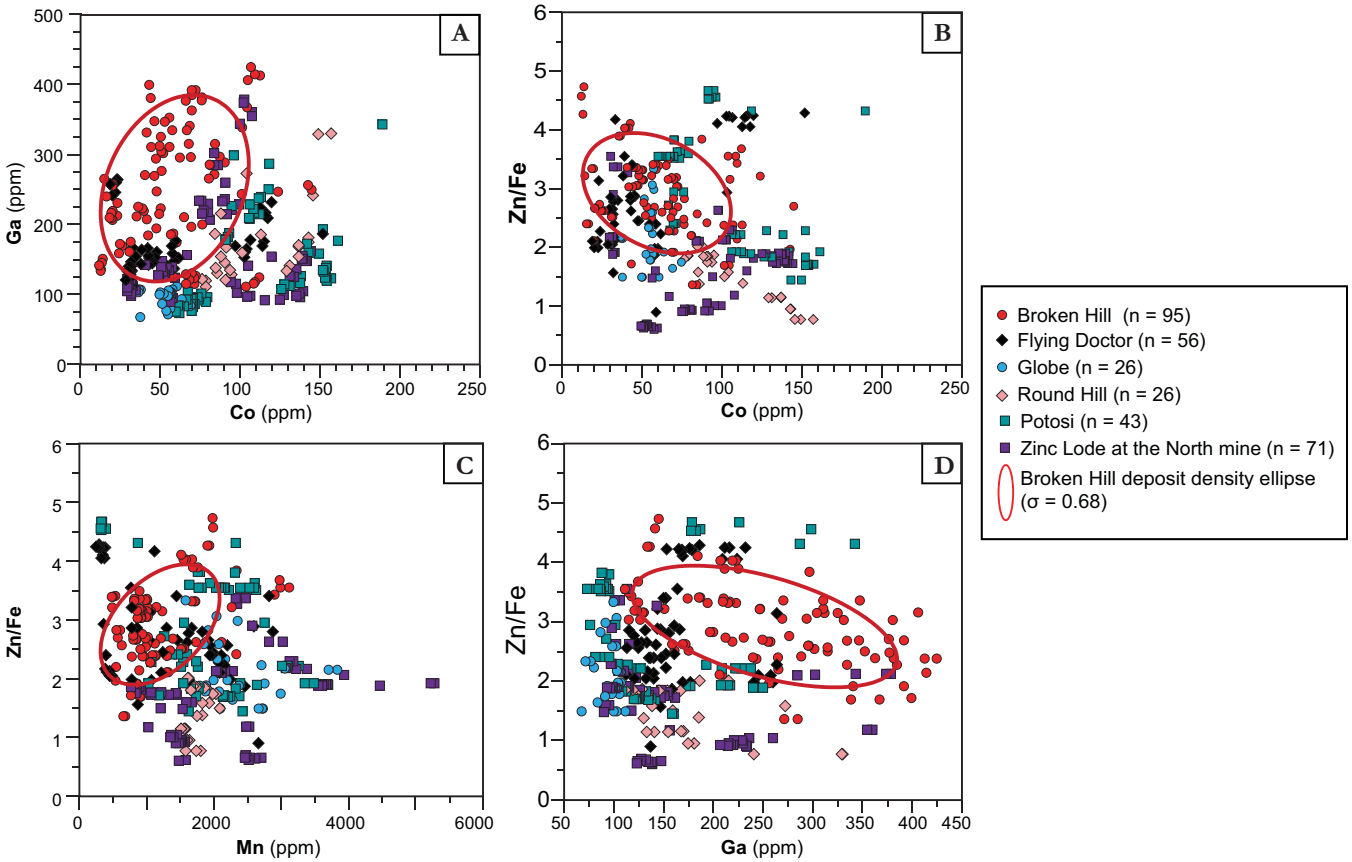

Fig. 1. Bivariate plots of gahnite compositions from Flying Doctor, Globe, Round Hill, Potosi, and Zinc lode at the North mine, and Broken Hill deposits (Broken Hill domain): **A)** Ga (ppm) vs. Co (ppm), **B)** Zn/Fe vs. Co (ppm), **C)** Zn/Fe vs. Mn (ppm), and **D)** Zn/Fe vs. Ga (ppm). A compositional field for the Broken Hill deposit is shown as a density ellipse (σ = 0.68) (after O'Brien et al. 2015b).

Co, and Mn, or Ga versus Co showed that gahnite from the Broken Hill deposit has a relatively restricted compositional range and that it overlaps with the composition of gahnite from some minor BHT occurrences (Fig. 1). O'Brien *et al.* (2015b) further evaluated the same data set using a linear discriminant analysis and a relatively new statistical technique known as Random Forests to discriminate the composition of gahnite in the Broken Hill deposit from those in minor BHT deposits (Fig. 2). The use of Random Forests was particularly valuable, more so than the linear discriminant analysis, in identifying compositional factors (i.e. the so-called "spinel elements": Mg, Al, V, Cr, Mn, Fe, Co, Ni, Zn, Ga, and Cd) that can be used for discrimination purposes.

Garnet in the Stollberg ore field (~12 Mt), Bergslagen district, Sweden, occurs in a variety of strongly altered (i.e. gedrite-albite, garnet-biotite, and garnet-pyroxene-carbonate alteration) rocks associated with massive Zn-Pb-Ag sulphides and magnetite deposits, and in unaltered to weakly altered 1.9 Ga bimodal felsic (dominated by rhyolitic ash-siltstone) and mafic rocks metamorphosed to the amphibolite facies. Sulphides are hosted by volcanic rocks and skarn, and occur as massive to semi-massive base metal lenses. Jansson *et al.* (2013) considered the deposits to be part of a synvolcanic, seafloor hydrothermal system, which was partly exhalative (iron oxide) and partly carbonate-replacive (sulphides + more iron oxides). Garnet in garnet-biotite alteration and high-grade sulphides is almandine-rich, whereas that in skarn and garnet-pyroxene alteration contains significantly higher proportions of the grossular and spessartine components (e.g. Jansson *et al.* 2013). In general, garnet contains elevated concentrations of Sc, Ti, V, Cr, Co, Zn, Ga, Ge, Y, and REEs, with Sc, Ga, and Ti being derived exclusively from a volcaniclastic (rather than a hydrothermal) component (Jansson *et al.* 2013). Overall, chondrite-normalized REE patterns of garnet in quartz garnetite at Broken Hill (Fig. 3) are similar to those for garnet in the Stollberg ore field (Fig. 4). Garnet in unaltered (or slightly altered) rhyolitic ash-siltstone at Stollberg typically shows no Eu anomaly and low concentrations of Zn, Ga, Cr, and V. In contrast, garnet in garnet-biotite and garnet-pyroxene alteration, which are strongly altered equivalents of rhyolitic ash-siltstone, shows a strong positive Eu anomaly and contains elevated concentrations of Zn and Ga, and low Ti contents. Garnet in gedrite-albite alteration, which likely represents part of a footwall feeder pipe to deposits on the eastern side of the Stollberg ore field, exhibits a relatively flat chondrite-normalized REE profile and contains elevated Sc content and low concentrations of V, Cr, and Zn. Garnet in mafic dykes and marble contains the highest amounts of Cr, Co, V, and Ti.

Magnetite

Magnetite occurs in a variety of metamorphic, sedimentary, and igneous rocks, as accumulations in iron formations and as an accessory phase in a large variety of ore deposits (e.g. Dupuis & Beaudoin, 2011; Nadoll *et al.* 2012, 2014). Of all the accessory minerals associated with ore deposits, magnetite is the most studied because it occurs in so many different types

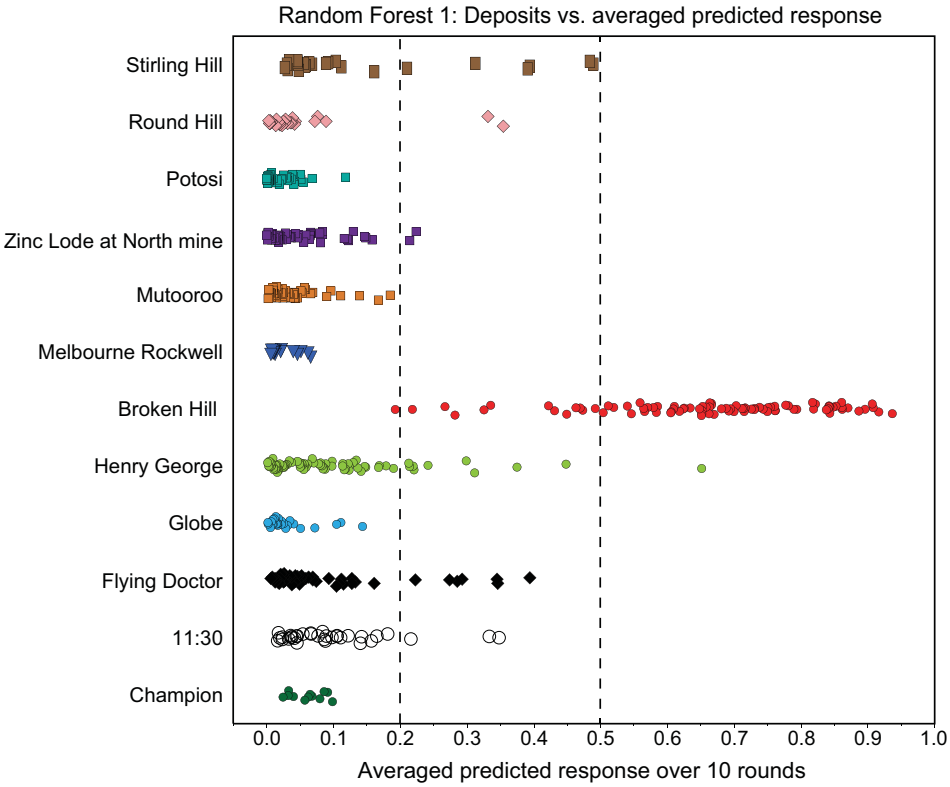

Fig. 2. Percentage of votes by Random Forests for compositions of gahnite from the Broken Hill deposit versus minor Broken Hill-type occurrences (Broken Hill domain). Predictions represent an average over ten 10-fold cross-validations (after O'Brien *et al.* 2015b).

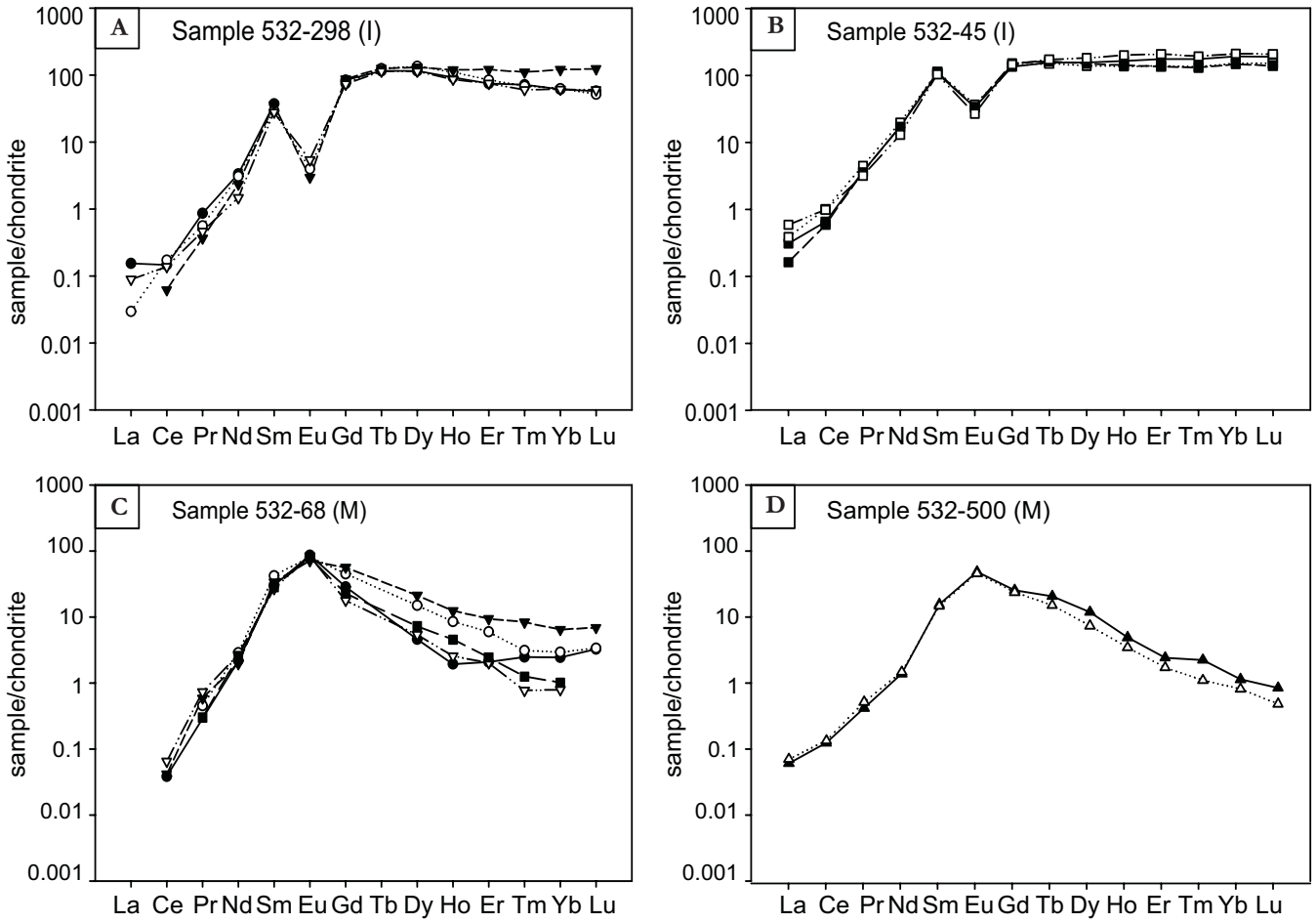

Fig. 3. Chondrite-normalized rare earth element patterns of garnet in **(A & B)** quartz garnetite, and **(C & D)** metasomatic garnet in post-peak metamorphic quartz-garnet rock (Broken Hill, Australia) (modified from Spry *et al.* 2007).

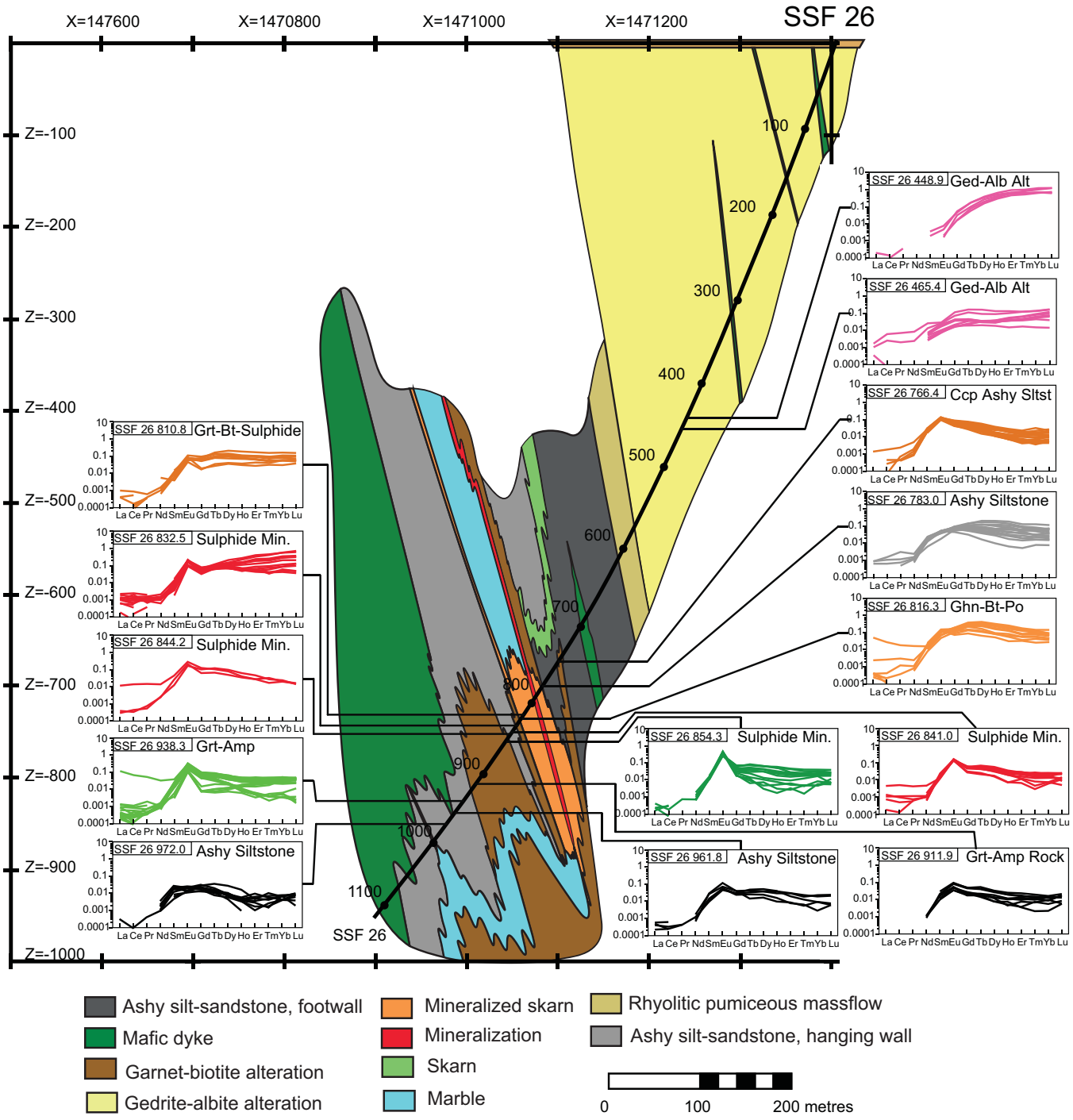

Fig. 4. Cross-section through the Dammberget deposit, Stollberg ore field, Sweden, showing the rare earth element patterns of garnet in various samples from drillhole SSF 26. Note the positive Eu anomalies in garnet in and adjacent to the ore zone, particularly in garnet-biotite alteration, and the negative Eu anomalies in garnet-bearing samples distal to ore. Abbreviations: Alb = albite, Amp = amphibole, Bt = biotite, Ccp = chalcopyrite, Ged = gedrite, Ghn = gahnite, Grt = garnet, Sltst = siltstone.

of ores. Despite numerous studies being conducted on the trace element composition of magnetite associated with metallic mineral deposits, those involving magnetite in VMS deposits are limited in number (e.g. Singoyi *et al.* 2006; Dupuis & Beaudoin, 2011).

The lithological variability in the Stollberg ore field makes this location ideal to evaluate the physico-chemical parameters that affect the chemistry of magnetite in a district that contains exhalative and replacement base metal sulphide mineralisation metamorphosed to the amphibolite facies. The district has many of the same characteristics as a VMS district but it is atypical in that mineralisation has a high iron-oxide/sulphide ratio, it commonly occurs in limestone, and it lacks massive pyritic rocks. Trace element compositions of magnetite in high-grade ore, skarn, massive magnetite, and garnet-biotite, gedrite-albite, garnet-pyroxene alteration throughout the district show a wide range (Figs. 5 & 6). Such a broad compositional range is inconsistent with previous studies in other ore

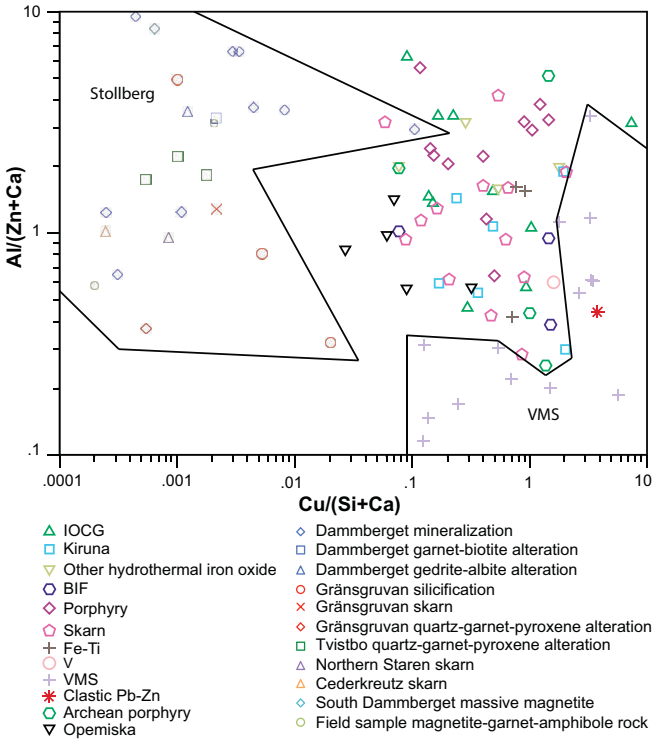

Fig. 5. Plot of Al/(Zn+Ca) versus Cu/(Si+Ca) for magnetite in various rocks types in the Stollberg ore superimposed on the composition of magnetite from various ore types identified by Dupuis & Beaudoin (2011).

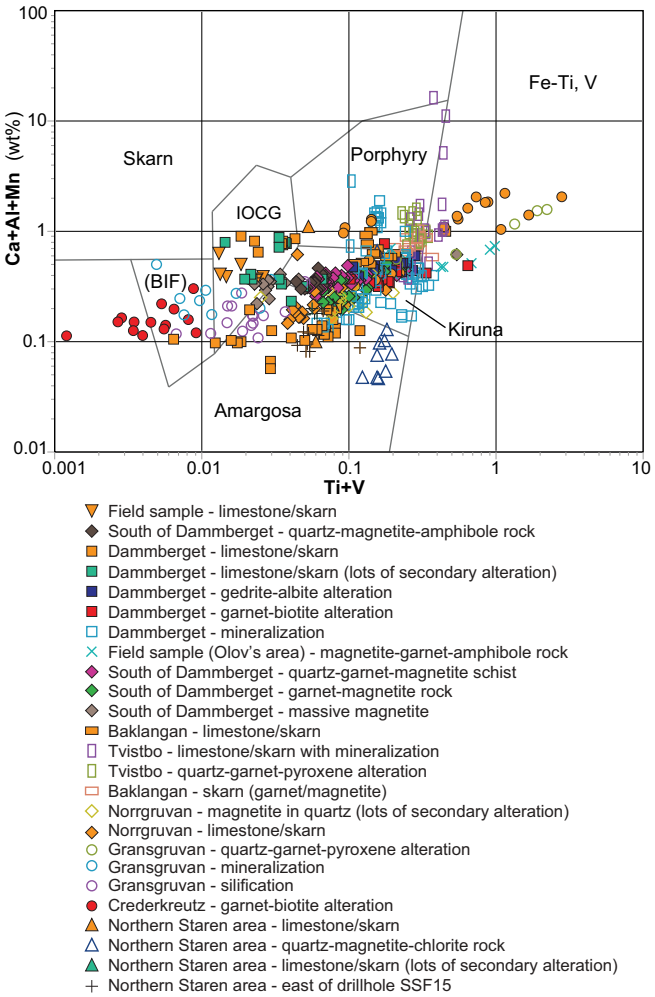

Fig. 6. Plot of Ca+Al+Mn versus TI+V for magnetite in various rocks types in the Stollberg ore field superimposed on the composition of magnetite from various ore types identified by Dupuis & Beaudoin (2011).

fields, which have suggested that magnetite chemistry can be used to define compositional fields for different ore deposit types (e.g. Al/(Zn+Ca) vs Cu/(Si+Ca) (Fig. 5); Ca+Al+Mn vs Ti+V (Fig. 6)) or can be used to approximate the temperature of the ore-forming fluid (e.g. Dupuis & Beaudoin 2011; Nadoll *et al.* 2014). Magnetite in garnet-biotite and gedrite-albite alteration spatially associated with the Dammberget deposit typically contains >200 ppm Ga, >10 ppm Sn, and has Ti/V ratios of >10, whereas magnetite in garnet-biotite alteration associated with the smaller Cedarkreutz deposit contains less Ga, Sn, and lower Ti/V ratios. Magnetite in garnet-biotite alteration associated with the Gränsgruvan deposit contains >10 ppm Sn, 20 to 180 ppm Ga, and has Ti/V ratios of 0.1 to 2. These and other trace element compositions of magnetite in altered host rocks show potential as exploration guides to ore in the Stollberg district.

Biotite

Biotite is a common mineral in metamorphic rocks and is locally intergrown with gahnite and garnet in both the Broken Hill and Stollberg deposits. Although trace elements of biotite have been obtained on rocks in metamorphic terranes (e.g. Yang & Rivers, 2000), their application as a vector to metamorphosed sulphide deposits has not previously been conducted. None-the-less the trace element composition of biotite intergrown with garnet and gahnite in the Broken Hill deposit was evaluated by O'Brien *et al.* (2013b). The focus of the O'Brien *et al.* study was to gauge how trace elements partition among gahnite, biotite, and garnet, with the view of determining how the concentration of "spinel elements" in gahnite was affected by the composition of coexisting minerals. The compositions of biotite in gahnite-bearing rocks from the Broken Hill deposit show solid solution between annite and phlogopite end-members, with X_{Mg} = Mg/(Mg+Fe) ranging from 0.29 to 0.60 and VI_{Al} ranging from 0.41 to 1.30. Beryllium, Cr, Co, Ni, Ga, Cd, and to a lesser extent V strongly partition into gahnite, whereas Li, Mg, Ti, Ge, Rb, Sr, Sn, Ba, Pb, Bi, Th, and REEs partition into biotite (Fig. 7).

Trace element compositions of biotite in various altered rocks in the Stollberg ore field were also evaluated. Preliminary studies show elevated concentrations of Cs and Tl in drillholes that cross-cut the Dammberget deposit over a distance of 100 m in its stratigraphic hanging wall, and appear to be the best indicators of proximity to ore (Fig. 8). It should be noted here that high bulk rock concentrations of Tl in the hanging walls of VMS deposits were reported by Large *et al.* (2001) and was considered by them to be a good guide to ore.

DISCUSSION AND CONCLUSIONS

Previous and ongoing studies suggest that various chemical plots and discrimination diagrams using the concentration of certain elements, or combinations of elements, are valuable for exploration purposes and for determining mineral provenance. For example, based on the major and trace element chemistry of gahnite, the best guides to high-grade ore in the Broken Hill

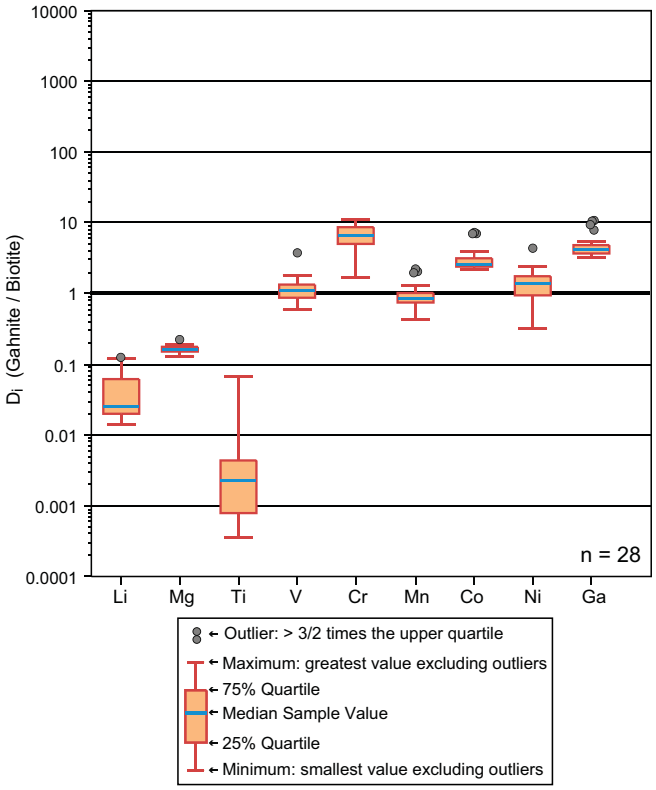

Fig. 7. Distribution coefficients for coexisting gahnite and biotite in blue quartz-gahnite rock from the Broken Hill deposit. Note that gahnite preferentially incorporates Cr, Co, and Ga relative to biotite, whereas biotite preferentially incorporates Li, Mg, and Ti (after O'Brien *et al.* 2013a).

domain involve the following chemical parameters: Zn/Fe = 2 to 4 versus Co = 10–110 ppm, Ga = 110–400 ppm, and Mn = 500–2,250 ppm; and Co = 25–100 ppm versus Ga 125–375 ppm (O'Brien *et al.* 2015a). In addition, garnet from the Broken Hill deposit is enriched in Zn (>400 ppm), Cr (>140 ppm), and Eu (up to 6 ppm and positive Eu anomalies), and depleted in Co, Ti, and Y compared to garnet in other garnet-rich rocks from other localities in the southern Curnamona Province. These values, as well as MnO contents of >15 wt% and Eu/Eu* >1, were only found in garnet from the Broken Hill deposit and appear to be good pathfinders to BHT mineralisation (Heimann *et al.* 2011). Garnet in massive sulphides and sulphide-bearing alteration assemblages in the Stollberg ore field can be distinguished from sulphide-poor or sulphide-free rocks of the same alteration type on the basis of a positive Eu anomaly, and the concentrations of Zn, Ga, and Ti. The compositions of magnetite and biotite in the Stollberg ore field also appear to show great promise as pathfinder minerals because the composition of magnetite in altered versus unaltered rocks, and larger versus smaller hydrothermal systems can be distinguished. The Tl and Cs content of biotite also appear to be more elevated in the hanging wall of sulphide mineralisation with proximity to ore (Fig. 8).

Although discrimination diagrams were developed by Dupuis & Beaudoin (2011) and O'Brien *et al.* (2013a) to assist in determining the provenance of magnetite and gahnite, respectively, they must be considered to be preliminary at best due to the limited number of compositional data that were used in both studies. In the discrimination diagrams used by O'Brien *et al.* (2013a), individual analyses were plotted; however for diagrams presented by Dupuis & Beaudoin (2011), fields that apparently characterize different types of ore

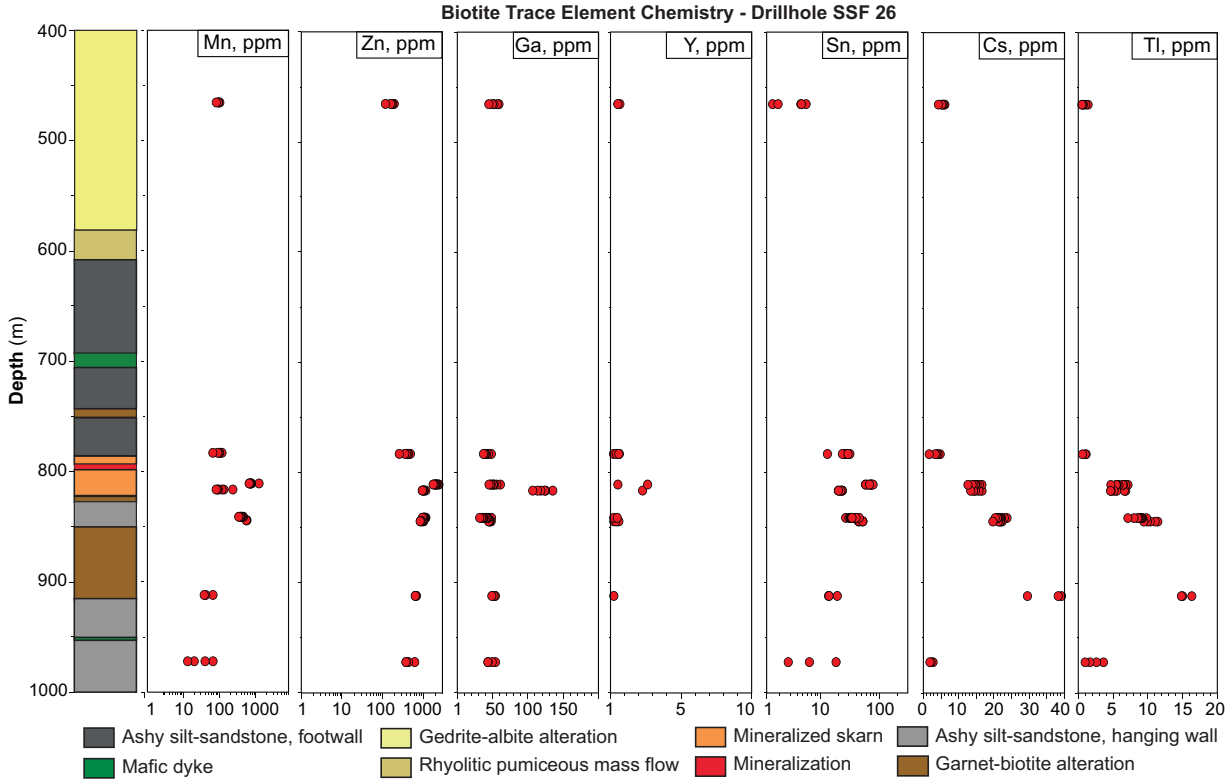

Fig. 8. Trace element composition (Mn, Zn, Ga, Y, Sn, Cs, and Tl) of biotite with depth along drillhole SSF 26, which intersects the Dammberget deposit, Stollberg ore field, Sweden. The stratigraphic bottom (i.e. gedrite-albite alteration) is at the top of the vertical section on the left.

deposits are based upon the average composition of magnetite from individual deposits, regardless of the number of data that were collected from that deposit. Such an approach, in the absence of error bars, is questionable, given that data from individual deposits from a specific ore type (e.g. sulphide mineralisation in the Stollberg ore field) can cover much of the diagram and plot in the fields of several different deposit types. Variability in trace element composition of a given mineral in metamorphosed massive base metal deposits is dependent upon several variables, including different physicochemical conditions during mineral growth, crystal-chemical controls (i.e. the major element chemistry of the mineral), pre-metamorphic alteration, the chemistry of precursor minerals, the partitioning of elements between coexisting minerals, fO_2, fS_2, temperature, pressure, and host-rock geochemistry. The effect of most of these parameters on the trace element composition of oxides and silicates is unknown and, consequently, trying to assess the relative importance of these parameters is difficult at best, notwithstanding the possibility that some minerals may be subject to post-peak modification during retrograde metamorphism. For example, gahnite can break down to biotite, chlorite, and staurolite, all of which are known to contain elevated concentrations of Zn (e.g. Spry 2000), and both biotite and garnet can convert to chlorite.

Although considerably more work needs to be done on the minerals evaluated here (i.e. gahnite, magnetite, garnet, and biotite), the study of other silicates (e.g. tourmaline, staurolite, chlorite, titanite, amphibole, aluminosilicates, quartz, and pyroxene), and oxides (ilmenite, rutile, högbomite, and ecandrewsite) is also warranted.

Given the complexity of the physicochemical parameters that affect mineral trace element chemistry, and the large amount of data that can be collected in a short amount of time using EMPA and LA-ICP-MS techniques, application of various types of statistical analyses of data are also important in refining or identifying new empirical parameters that can be used for targeting purposes (e.g. Dupuis & Beaudoin 2011; O'Brien *et al.* 2015a, b).

REFERENCES

Bryndzia, L.T. & Scott, S.D. 1987. Application of chlorite sulfide oxide equilibria to metamorphosed sulfide ores, Snow Lake area, Manitoba. *Economic Geology*, **82**, 963- 970.

Clark, J.R. & Williams-Jones, A.E. 2004. *Rutile as a potential indicator mineral for metamorphosed metallic ore deposits*. Montreal, Diversification de L'Exploration Minérale au Québec, Sous-projet SC2 Final Report, 17 p.

Dare, S.A.S., Barnes, S.J. & Beaudoin, G. 2012. Variation in trace element content of magnetite crystallized from a fractionating sulfide liquid, Sudbury, Canada: Implications for provenance discrimination. *Geochimica et Cosmochimica Acta*, **88**, 27–50.

Dupuis, C. & Beaudoin, G., 2011. Discriminant diagrams for iron oxide trace element fingerprinting of mineral deposit types. Mineralium Deposita, 46, 319–335.

Gaspar, M., Knaack, C., Meinert, L.D. & Moretti, R. 2008. REE in skarn systems: a LA-ICP-MS study of garnets from the Crown Jewel gold deposit. *Geochimica et Cosmochimica Acta*, **72**, 185–205.

Griffin, W.L., Slack, J.F., Ramsden, A.R., Win, T.T. & Ryan, C.G. 1996. Trace elements in tourmalines from massive sulfides deposits and tourmalinites; geochemical controls and exploration applications. *Economic Geology*, **91**, 657–675.

Heimann, A., Spry, P.G., Teale, G.S., Conor, C.H.H. & Leyh, W.R. 2009. Geochemistry of garnet-rich rocks in the southern Curnamona province, Australia, and their genetic relationship to Broken Hill-type Pb-Zn-Ag mineralization. *Economic Geology*, **104**, 687–712.

Heimann, A., Spry, P.G. & Teale, G.S. 2011. Chemical and crystallographic constraints on the geochemistry of garnet in garnet-rich rocks, southern Proterozoic Curnamona Province, Australia. *Mineralogy and Petrology*, **101**, 49–74.

Ismail, R., Ciobanu, C.L., Cook, N.J., Teale, G.S., Giles, D., Schmidt Mumm, A. & Wade, B. 2014. Rare earths and other trace elements in minerals from skarn assemblages, Hillside iron oxide-copper-gold deposit, Yorke Peninsula, South Australia. *Lithos*, **184-187**, 456–477.

Jackson, S.E., Longerich, H.P., Dunning, G.R. & Freyer, B.J. 1992. The application of laser-ablation microprobe; inductively coupled plasma-mass spectrometry (LAM-ICP-MS) to in situ trace-element determinations in minerals. *Canadian Mineralogist*, **30**, 1049–1064.

Jansson, N.F., Erismann, F., Lundstam, E. & Allen, R.L. 2013. Evolution of the Paleoproterozoic volcanic-limestone-hydrothermal sediment succession and Zn-Pb-Ag and Fe-oxide deposits at Stollberg, Bergslagen, Sweden. *Economic Geology*, **108**, 309–335.

Large, R.R., McPhie, J., Gemmell, J.B., Herrmann, W. & Davidson, G.J. 2001. The spectrum of ore deposit types, volcanic environments, alteration halos, and related exploration vectors in submarine volcanic successions - Some examples from Australia. *Economic Geology*, **96**, 913–938.

Layton-Matthews, D., Hamilton, D.C. & McClenaghan, M.B. 2013. Mineral chemistry: modern techniques and applications to exploration, *In: Application of Indicator Methods to Mineral Exploration*. 26th International Applied Geochemistry, Rotorua, New Zealand, Short Course Notes, 9-18.

McClenaghan, M.B. 2005. Indicator mineral methods in exploration. *Geochemistry: Exploration, Environmental, Analysis*, **5**, 233–345.

Nadoll, P., Mauk, J.L., Hayes, T.S., Koenig, A.E. & Box, S.E. 2012. Geochemistry of magnetite from hydrothermal ore deposits and host rocks of the Mesoproterozoic Belt Supergroup, United States. *Economic Geology*, **107**, 1275–1292.

Nadoll, P., Angerer, T., Mauk, J. L., French, D. & Walshe, J. 2014. The chemistry of hydrothermal magnetite: A review. *Ore Geology Reviews*, **61**, 1–32.

Nesbitt, B.E. 1986. Oxide sulfide silicate equilibria associated with metamorphosed ore deposits. Part I: Theoretical considerations. *Economic Geology*, **81**, 831-840.

O'Brien, J.J., Spry, P.G., Teale, G.S., Jackson, S.E. & Rogers, D. 2013a. Major-trace element chemistry of gahnite in metamorphosed massive sulfide deposits: The use of discrimination diagrams to determine provenance, *In: Application of Indicator Methods to Mineral Exploration*. 26th International Applied Geochemistry, Rotorua, New Zealand, Short Course Notes, 29–33.

O'Brien, J.J., Spry, P.G., Teale, G.S., Jackson, S.E. & Rogers, D. 2013b. Trace element partitioning between gahnite, garnet, and biotite in gahnite-bearing rocks: Implications for metamorphic processes and exploration for Pb-Zn-Ag mineralization. *In: Abstract Volume*. Society of Economic Geologists Meeting, Whistler, British Columbia, 45–46.

O'Brien, J.J., Spry, P.G., Teale, G.S., Jackson, S.E. & Rogers, D. 2015a. Major and trace element chemistry of gahnite as an exploration guide to Broken Hill-type Pb-Zn-Ag mineralization in the Broken Hill domain, New South Wales, Australia. *Economic Geology* **110**, in press.

O'Brien, J.J., Spry, P.G., Nettleton, D., Ruo, X., Teale, G.S., Jackson, S.E. & Rogers, D. 2015b. Random forests as a statistical method for distinguishing gahnite compositions as an exploration guide to Broken Hill-type Pb-Zn-Ag deposits in the Broken Hill domain, Australia. *Journal of Geochemical Exploration*, **149**, 74–86.

Pagé, P. & Barnes, S.J. 2009. Using trace elements in chromites to constrain the origin of podiform chromitites in the Thetford mines ophiolite, Québec, Canada. *Economic Geology*, **104**, 997–1018.

Schmidt Mumm, A., Dart, R.C. & Say, P. 2012. Hematite/maghemite trace element geochemistry in base metal exploration. *Journal of Geochemical Exploration*, **118**, 1–13.

Singoyi, B., Danyushevsky, L., Davidson, G.J., Large, R. & Zaw, K. 2006. Determination of trace elements in magnetites from hydrothermal deposits using the LA ICP-MS technique, I*n: SEG Keystone Conference Notes*. Society of Economic Geologist, CD-ROM.

Spry, P.G. 2000. Sulfidation and oxidation haloes as guides in the exploration for metamorphosed massive sulfide deposits. *Reviews in Economic Geology*, **11**, 149-161.

Spry, P.G., Heimann, A., Messerly, J.D., Houk, R.S. & Teale, G.S. 2007. Discrimination of metamorphic and metasomatic processes at the Broken Hill lead-zinc-silver deposit, Australia: Rare earth element signatures of garnet in garnet-rich rocks. *Economic Geology*, **102**, 471–494.

Yang, P. & Rivers, T. 2000. Trace element partitioning between coexisting biotite and muscovite from metamorphic rocks, western Labrador: structural, compositional and thermal controls. *Geochimica et Cosmochimica Acta*, **64**, 1451-1472.

Xu, L., Bi, X., Hu, R., Tang, Y., Wang, X. & Xu, Y. 2014. LA-ICP-MS mineral chemistry of titanite and the geological implications for exploration of porphyry Cu deposits in the Jinshajiang – Red River alkaline igneous belt, SW China. *Mineralogy and Petrology*, doi10.1007/s00710-014-0359-x

Tourmaline: the universal indicator?

John Chapman[1*], Alain Plouffe[2] & Travis Ferbey[3]

[1]Natural Resources Canada – Geological Survey of Canada, 1500-605 Robson Street, Vancouver, British Columbia, Canada V6B 5J3

[2]Natural Resources Canada – Geological Survey of Canada, 601 Booth Street, Ottawa, Ontario, Canada K1A 0E8

[3]British Columbia Geological Survey, PO Box 9333 Stn. Prov. Govt., Victoria, British Columbia, Canada V8W 9N3

**Corresponding author's e-mail: john.chapman@nrcan-rncan.gc.ca*

The tourmaline supergroup comprises 30 different minerals recognized by the International Mineralogical Association (IMA, Table 1), which share the borate-bearing cyclosilicate 'tourmaline' structure. In addition to these IMA-recognized end-member mineral species, there are numerous unofficial and intermediate solid-solution species that occur naturally. Tourmaline minerals as a group are some of the most common boron-bearing minerals in the natural environment; they occur within rocks of widely variable origins including igneous, metamorphic, and hydrothermal settings, as well as within sediments derived from these precursors. Even within sedimentary settings, tourmaline may grow as a result of common diagenetic processes, either as an authigenic overgrowth to existing detrital tourmaline grains or as newly formed minerals within cements and void spaces (Deer *et al.* 1986). Tourmaline species share many other beneficial characteristics that make them ideally suited for use as indicator minerals for sediment provenance studies, as well as for targeting a wide variety of economically significant mineral deposits.

In the past decade, the tourmaline group has seen a surge in interest amongst researchers from across a broad spectrum of the geosciences. In large part, this increase in activity has been driven by advances in a number of geochemical microanalysis techniques, which have had improved accuracy and precision, while driving down sample spot sizes, the time taken to perform an analysis, and the costs of equipment. Hence, geological records locked within tourmaline minerals at scales previously too fine for us to access are now amenable to interrogation. The breadth and depth of those records may be unequalled amongst commonly occurring silicate minerals. George Calas's recent editorial in *Elements* magazine likened a single tourmaline grain to "Ali Baba's cave", stacked high with treasures (Calas 2011). Members of the tourmaline family are stable across a huge range of pressure and temperature conditions, from sedimentary diagenetic settings to ultra-high pressure metamorphic settings, and to temperatures of over 750°C. As a consequence, tourmaline minerals are common constituents of many diverse rock types. The complex crystal structure of tourmaline, incorporating triangular, tetrahedral, and octahedral coordination environments, permits incorporation of a wide array of major, minor, and trace element components.

Such elemental flexibility gives tourmaline almost unparalleled ability to reflect and record the chemical composition of the environment within which it formed. Already, many workers have documented systematic and interpretable chemical signatures associated with distinct geological environments, including within and between different ore-forming settings. Tourmaline's piezo- and pyroelectric properties also give rise to systematic intra-mineral chemical variability, which may allow the mineral to be used as a single crystal geothermometer and -barometer. In addition to simple abundances, tourmaline also incorporates a wide range of isotopically interesting elements that record both stable and radiogenic (including geochronological) signatures. Such information is preserved through many subsequent episodes of weathering and hydrothermal or metamorphic alteration, owing to tourmaline's stability and very limited chemical diffusivity, even at elevated temperatures.

Fortunately, for those of us working in mineral exploration research, in addition to its superlative ability to record and preserve complex geological information, tourmaline also possess hardness equal to or greater than quartz, lacks cleavage, and has a density of up to 3.3 g/cm^3. Hence, tourmaline is a common resistate phase in clastic sedimentary and surficial settings, and is often recovered as a component of a heavy mineral concentrate. In addition to simple grain abundances and broad mineralogical classification, more detailed analysis of tourmaline recovered from such samples can reveal much more detail of the sediment provenance, including the presence and type of any possible mineral deposit.

This presentation will provide an overview of the complex sphere of tourmaline structure and chemistry. It will cover some aspects of appropriate analytical methods and limitations to be considered when seeking to employ tourmaline within a study. The presentation will conclude with a case study examining the bedrock and surficial occurrence of tourmaline minerals within and around the Woodjam alkalic porphyry Cu-Au deposits of central British Columbia, and demonstrate that, in tandem, tourmaline grain abundance and chemical analyses provide powerful tools to identify and locate porphyry-related mineral deposits.

TOURMALINE CRYSTAL STRUCTURE

Minerals of the tourmaline supergroup share the general chemical formula:

$$XY_3Z_6(T_6O_{18})(BO_3)_3V_3W$$

By inspection of this formula, it immediately becomes apparent that the only stoichiometrically required elements within a tourmaline are oxygen and boron. The other lettered sites within the generalized formula commonly take only a limited range of major elemental components:

X = □, Na, K, Ca, Pb^{2+}
Y = Li, Mg, Fe^{2+}, Mn^{2+}, Cu^{2+}, Al, V^{3+}, Cr^{3+}, Fe3+, Mn^{3+}, Ti^{4+}
Z = Mg, Fe^{2+}, Al, V^{3+}, Cr^{3+}, Fe^{3+}
T = Si, Al, B
V = OH, O
W = OH, F, O

Table 1. Tourmaline species approved by the International Mineralogical Association (September 2014).

Name	Formula	IMA Year-#	Country	Reference[1]
Adachiite	$CaFe^{2+}_3Al_6(Si_5AlO_{18})(BO_3)_3(OH)_3(OH)$	2012-101	Japan	Mineralogical Magazine, **77** (2013), 2695
Chromium-dravite	$NaMg_3Cr_6(Si_6O_{18})(BO_3)_3(OH)_3(OH)$	1982-055	Russia	European Journal of Mineralogy, **16** (2004), 345
Chromo-alumino-povondraite	$NaCr_3(Al_4Mg_2)(Si_6O_{18})(BO_3)_3(OH)_3O$	2013-089	Russia	American Mineralogist, **99** (2014), 1767
Darrellhenryite	$Na(Al_2Li)Al_6(Si_6O_{18})(BO_3)_3(OH)_3O$	2012-026	Czech Republic	American Mineralogist, **98** (2013), 1886
Dravite	$NaMg_3Al_6(Si_6O_{18})(BO_3)_3(OH)_3(OH)$	1884	Slovenia	Canadian Mineralogist, **49** (2011), 29
Elbaite	$Na(Al_{1.5}Li_{1.5})Al_6(Si_6O_{18})(BO_3)_3(OH)_3(OH)$	1913	Italy	Canadian Mineralogist, **32** (1994), 31
Feruvite	$CaFe^{2+}_3(Al_5Mg)(Si_6O_{18})(BO_3)_3(OH)_3(OH)$	1987-057	New Zealand	Canadian Mineralogist, **52** (2014), 285
Fluor-buergerite (Buergerite[2])	$NaFe^{3+}_3Al_6(Si_6O_{18})(BO_3)_3O_3F$	1965-005	Mexico	American Mineralogist, **51** (1966), 198
Fluor-dravite	$NaMg_3Al_6(Si_6O_{18})(BO_3)_3(OH)_3F$	2009-089	USA	Canadian Mineralogist, **49** (2011), 57
Fluor-elbaite	$Na(Li_{1.5}Al_{1.5})Al_6(Si_6O_{18})(BO_3)_3(OH)_3F$	2011-071	Brazil	American Mineralogist, **98** (2013), 297
Fluor-liddicoatite (Liddicoatite[3])	$Ca(Li_2Al)Al_6(Si_6O_{18})(BO_3)_3(OH)_3F$	1976-041	Madagascar	American Mineralogist, **96** (2011), 895
Fluor-schorl	$NaFe^{2+}_3Al_6(Si_6VO_{18})(BO_3)_3(OH)_3F$	2010-067	Germany/Italy	Mineralogical Magazine, **75** (2011), 289
Fluor-tsilaisite	$NaMn^{2+}_3Al_6(Si_6O_{18})(BO_3)_3(OH)_3F$	2012-044	Italy	Mineralogical Magazine, **76** (2012), 1281
Fluor-uvite	$CaMg_3(Al_5Mg)(Si_6O_{18})(BO_3)_3(OH)_3F$	2011 s.p.	Sri Lanka	Mineralogical Record, **8** (1977), 100
Foitite	$\square(Fe^{2+}_2Al)Al_6(Si_6O_{18})(BO_3)_3(OH)_3(OH)$	1992-034	USA	American Mineralogist, **96** (2011), 895
Luinaite-(OH)	$(Na,\square)(Fe^{2+},Mg)_3Al_6(BO_3)_3Si_6O_{18}(OH)4$	2009-046	Australia	Norsk Bergverksmuseet Skrift, **50** (2013), 23
Magnesio-foitite	$\square(Mg_2Al)Al_6(Si_6O_{18})(BO_3)_3OH)_3(OH)$	1998-037	Japan	Canadian Mineralogist, **44** (2006), 959
Maruyamaite	$K(MgAl_2)(Al_5Mg)(BO_3)_3(Si6O_{18})(OH)_3O$	2013-123	Kazakhstan	Mineralogical Magazine, **78** (2014), 549
Olenite	$NaAl_3Al_6(Si_6O_{18})(BO_3)_3O_3(OH)$	1985-006	Russia	European Journal of Mineralogy, **14** (2002), 935
Oxy-chromium-dravite	$NaCr_3(Cr_4Mg_2)(Si_6O18)(BO_3)_3(OH)_3O$	2011-097	Russia	American Mineralogist, **97** (2012), 2024
Oxy-dravite	$Na(Al_2Mg)(Al_5Mg)(Si_6O_{18})(BO_3)_3(OH)_3O$	2012-004a	Kenya	Mineralogical Magazine, **78** (2014), 681
Oxy-schorl	$Na(Fe^{2+}_2Al)Al_6(Si_6O_{18})(BO_3)_3(OH)_3O$	2011-011	Czech Rep./Slovakia	American Mineralogist, **98** (2013), 485
Oxy-vanadium-dravite[4]	$NaV_3(V_4Mg_2)(Si_6O_{18})(BO_3)_3(OH)_3O$	2012 s.p.	Russia	American Mineralogist, **98** (2013), 501
Povondraite[5]	$NaFe^{3+}3(Fe^{3+}_4Mg_2)(Si_6O_{18})(BO_3)_3(OH)_3O$	1990 s.p.	Bolivia	American Mineralogist, **78** (1993), 433
Rossmanite	$\square(Al_2Li)Al_6(Si_6O_{18})(BO_3)_3(OH)_3(OH)$	1996-018	Czech Republic	American Mineralogist, **83** (1998), 896
Schorl	$NaFe^{2+}3Al_6(Si_6O_{18})(BO_3)_3(OH)_3OH)$	2007 s.p.	Germany	American Mineralogist, **90** (2005), 1784
Tsilaisite	$NaMn^{2+}_3Al_6(Si_6O_{18})(BO_3)_3(OH)_3(OH)$	2011-047	Italy	American Mineralogist, **97** (2012), 989
Uvite	$CaMg_3(Al_5Mg)(Si_6O_{18})(BO_3)_3(OH)_3(OH)$	2000-030a	Brazil	Mineralogical Magazine, **74** (2010), 375
Vanadio-oxy-chromium-dravite	$NaV_3(Cr_4Mg_2)(Si_6O_{18})(BO_3)_3(OH)_3O$	2012-034	Russia	American Mineralogist, **99** (2014), 1155
Vanadio-oxy-dravite	$NaV_3(Al_4Mg_2)(Si_6O_{18})(BO_3)_3(OH)_3O$	2012-074	Russia	American Mineralogist, **99** (2014), 218

[1]Reference provided refers to the most recent or most complete study for each mineral, not the original study.
[2]Originally named 'buergerite', the mineral was renamed in 2011 as the type mineral is F-bearing.
[3]Originally named 'liddicoatite', the mineral was renamed in 2011 as the type mineral is F-bearing.
[4]Originally named 'vanadium-dravite', the mineral was renamed in 2011 to conform to existing oxysubgroup nomenclature.
[5]Originally named 'ferridravite', the mineral was renamed in 1990 as the original site assignments were incorrect.

where □ represents a structural vacancy at the *X*-site (Hawthorn & Dirlam 2011). The 30 IMA-approved mineral species detailed in Table 1 give a good indication of the most common and more idiosyncratic combinations of site occupancies seen in nature. In addition to these major element components, each site can also play host to minor and trace element substitutions that give tourmaline minerals possibly the greatest and most complex range of elemental possibilities within any abundant mineral group.

Compositional compliance is imparted by the variety of structural settings that the complex tourmaline crystal provides. The *T*-site is tetrahedrally coordinated by four oxygen atoms, and although dominantly occupied by silicon it may also contain either aluminum (e.g. adachiite, Table 1) or boron. Six oxygen atoms are shared at the corners of six conjoined *T*-site tetrahedra, forming the basic, six-membered-ring T_6O_{18} unit of the cyclosilicate tourmaline structure. Although possessing six-fold rotational symmetry in plan view, these cyclosilicate rings are asymmetrical in profile. The apices of all TO_4 tetrahedrons point in the same direction within each ring, and within a tourmaline crystal all apices point toward the −c pole. It is this strong structural asymmetry that imparts the tourmaline's pyroelectric and piezoelectric properties.

Between the cyclosilicate rings, linking them, are the *Y* and *Z* octahedrally coordinated sites. The *Y*-site locations are relatively large and regular, located as a trimer toward the centre of the silicate rings, and can be occupied by a very wide variety of cations with a multitude of valence states (e.g. Li^+ vs. Ti^{4+}). In contrast, the *Z*-site octahedra are smaller and distorted, and are located at the periphery of the *Y*-site trimer. These are dominantly occupied by trivalent cations, but may contain significant proportions of divalent cations (e.g. Mg^{2+}) if sufficient charge balancing substitutions occur elsewhere.

At the centre of the cyclosilicate axis of symmetry, although out of plane, the *X*-site is in ninefold-coordination, and although dominantly occupied by sodium or potassium in some species (e.g. foitite) the site may be largely vacant. Also positioned along the central axis, the *W*-site is dominantly occupied by the OH^- anion or O^{2-}. The *W*-site is also significant as it is the only position into which the F^- anion can be

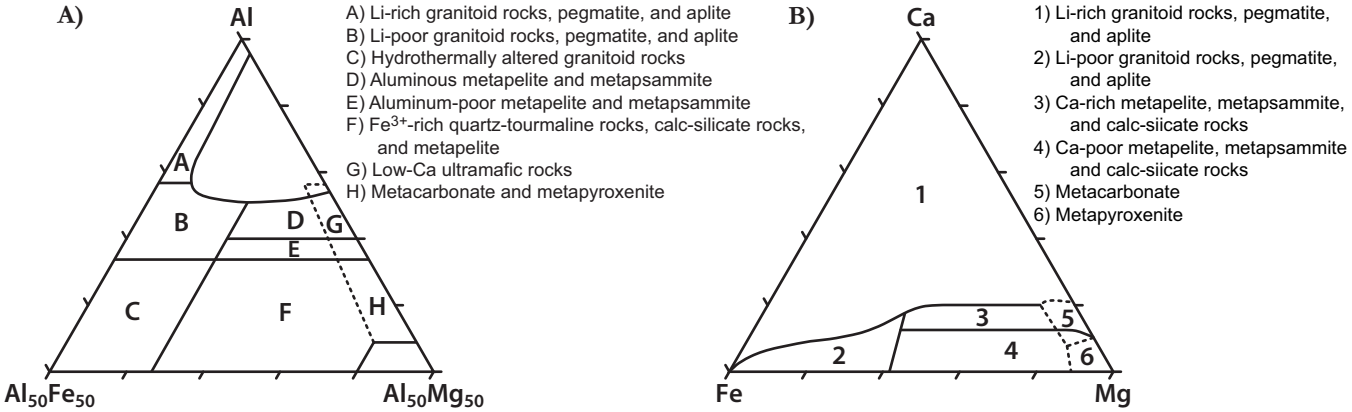

Fig. 1. The tourmaline provenance discrimination Al-Fe^T-Mg and Ca-Fe^T-Mg ternary diagrams of Henry & Guidotti (1985), modified from Mange & Morton (2007). Cation proportions are atoms per formula unit.

partitioned. Under these circumstances, vacancy at the *X*-site is precluded.

TOURMALINE MINERALOGY

Many illustrious careers have been built largely on the study of tourmaline mineralogy. The variety of chemical compositions and site substitutions, coupled to the diversity of environments within which tourmaline can be formed, mean that naturally occurring tourmaline crystals can adopt an almost unlimited range of colours and a very wide range of morphological habits. Such complexity, recognized since antiquity, has acted to obscure the true identity of many of the currently recognized end-member species, as many previous tourmaline mineralogical classification schemes were based on colour, texture, or paragenetic associations.

As recently as the turn of the 21st century, approximately a dozen tourmaline minerals were officially recognized by the IMA. Table 1 shows that the rapid expansion of research into tourmaline that has occurred in the last decade has increased the stock of known tourmaline minerals to 30, the most recent of which, chromo-alumino-povondraite, was only added to the official list in 2013. In addition, a number of species that have been recognized for many decades have had their crystal chemistry refined and redefined, either through recognition of inadequacies in original analyses of the type specimens (e.g. buergerite and liddicoatite, renamed fluor-buergerite and fluor-liddicoatite in 2011, respectively) or through the splitting of previously mixed compositions into unique minerals (e.g. F-bearing fluor-uvite distinguished from OH-bearing uvite in 2008). Even schorl, for which the first recognized published reference dates from 1505 (Ertl 2006), has had its mineralogy and chemistry refined in the first decade of the new millennium.

Detailed discussions on the mineralogy of tourmaline were presented as papers within two broad reviews of tourmaline research, both published in 2011: Dutrow & Henry (2011) and van Hinsberg *et al.* (2011). These special issues of the journals *Elements* and *The Canadian Mineralogist* are recommended texts for any researcher wanting a more detailed introduction to tourmaline and its geological significance and applications. That year also saw a comprehensive re-examination and restatement of the system for tourmaline nomenclature by the Subcommittee on Tourmaline Nomenclature of the IMA's Commission on New Minerals, Nomenclature and Classification, including protocols for the naming of unrecognized and intermediate species (Henry *et al.* 2011). As well as refining the system of mineral names and specific tourmaline compositions, the Henry *et al.* (2011) study also proposed a number of compositional diagrams to aid classification of tourmaline minerals.

Following this scheme, tourmaline species may be classified into three broad primary groups, based on the cation occupancy of the *X*-site, and three general species subgroups based on the anion occupancy of the *W*-site. Those species whose *X*-site is dominated by sodium or potassium are classified as 'alkali' group; those that have calcium as the dominant *X* cation are classified as the 'calcic' group; and those that have a vacancy dominant in the *X* position form the '*X*-vacant' group. The subgroup assignments are made in a similar fashion, with those species whose *W*-site occupancy is dominated by F^-, OH^-, or O^{2-} classified to 'fluor-', 'hydroxy-' or 'oxy-' subgroups, respectively (Henry *et al.* 2011).

Dominant end-member species commonly form solid-solution intermediate series with one or more other species, with near-complete compositional spectra. The most common of these is the alkali group schorl–dravite–elbaite series, members of which can be distinguished and classified using a ternary diagram based on the relative Fe^{2+}, Mg^{2+}, or Li^{1+} occupancy of the *Y*-site. Similar ternary diagrams can be constructed to aid in the classification of the *X*-vacant rossmanite–foitite–magnesiofoitite and the calcic liddicoatite–feruvite–uvite series.

Such diagrams not only allow individual crystal analyses to be assigned to specific groupings, but as they graphically represent subtle compositional variation they can also be employed to describe the compositional distribution within and between different sample populations. Additional compositional ternary, bivariate, and ratio plots can be devised and constructed as required for any particular application, and from these the expected compositional variation associated with tourmaline from a particular geological setting can be plotted and discriminated for use in sediment-provenance and mineral-vectoring studies. Many studies of this kind have been performed for a variety of igneous and metamorphic tourmaline species, and their results are summarized in Figure 1. Studies of tourmaline mineralogy and chemistry are less developed for hydrothermal mineral deposit settings, although coverage of these is improving annually and are summarized in the following section. An example of this latter application will be discussed below, applied to a series of till samples taken from within and surrounding the Woodjam porphyry-related Cu-Au deposits of central British Columbia.

TOURMALINE IN HYDROTHERMAL SYSTEMS

Tourmaline minerals form common components in the gangue assemblage of many hydrothermal metallic mineral deposits, and this association with ore-forming systems has been recognized for centuries. Indeed, the first known reference to the mineral schorl is taken from a description of placer tin deposits in Germany published in 1505 (Ertl 2006), where the target cassiterite was noted as traveling in stream sediments with a black tourmaline species. One of the most comprehensive and detailed reviews of a very broad spectrum of mineral deposit-related tourmaline occurrences and chemistry was published by John Slack in the 1996 *Reviews in Mineralogy and Geochemistry*, volume 33 (Slack 1996). This work, which includes numerous ternary diagrams presenting data compiled from many literature sources, should be on all researchers' shelves if they intend to employ tourmaline as a part of an ongoing study. In the last decade this work has been augmented by many detailed studies that have documented tourmaline occurrences at a variety of specific ore deposits.

Trace amounts of tourmaline may be found in a very wide range of ore-forming settings, but it is most common in those systems associated with (a) plutonic granitoid magmatism, including porphyry deposits, magmatic-hydrothermal breccia, skarn, granite-associated veins and greisen; b) stratabound and stratiform systems and their associated tourmalinite rocks, such as volcanogenic massive sulphide (VMS) and sedimentary exhalative (SEDEX) deposits; c) metamorphic and intrusion-related gold systems; and d) volcanic veins. However, in some systems tourmaline, although clearly spatially related and locally elevated in abundance, cannot clearly be related directly to the formation of metal-bearing minerals. Rather, in many cases tourmaline appears either pre- or post-ore within the deposit paragenesis.

However, despite in many cases an unclear direct association, tourmaline minerals from many deposit types appear to have characteristic mineralogical and chemical compositions that can be used both to investigate and interpret the ore-forming system itself, as well as allowing ore-associated tourmaline to be distinguished from regional background in sediment provenance studies. Tourmaline species associated with granitoid deposits are commonly schorl to near-dravite. Tourmaline associated with porphyry Cu-Au systems has significantly elevated Fe^{3+} content in comparison to similar schorl-rich assemblages that occur within granitoid Sn-W systems. In addition, many studied Cu-Au systems contain tourmaline that plots significantly below the schorl−dravite join on the discrimination plot of Henry & Giudotti (1985; Fig. 1). A review of tourmaline composition within a range of porphyry Cu-Au, Au, and Sn-W deposits suggested that for many of the more oxidized systems, tourmaline mineral evolution followed the magnesio-foitite−povondraite join, rather than a simple schorl−dravite trend (Baksheev *et al.* 2012). Very few samples from these settings show significant lithium concentrations (Slack 1996).

Within vein and stratabound ore-system gangue assemblages, many studies have documented a transition in dominant species from schorl-rich assemblages in the deeper, fluid source-proximal portions of the deposit, to a dravitic assemblage in the shallower and fluid source-distal portions of the deposit. In many cases, this is thought to represent a combination of reducing temperatures, changes in the relative fluid-rock ratio, depletion of iron within the metal source rocks, and/or variations in the relative proportions of iron-rich hydrothermal fluids and magnesium-rich seawater within the tourmaline-forming fluids (Slack 1996). Evolutionary trends within these deposits commonly follow a simple $MgFe_{-1}$ vector, although stratabound deposits may display a very wide range of major element variability, including significant proportions of alkali defect and uvite compositions.

EXPLORATION CASE STUDY: THE WOODJAM PORPHYRY Cu-Au DEPOSITS, BRITISH COLUMBIA

The Woodjam property in central British Columbia, Canada, encompasses a number of discrete porphyry-related Cu-Au and Cu-Mo deposits, which are thought to be related to the Takomkane batholith underlying and immediately to the south of the property (Fig. 2A). The individual deposits span a very narrow range in age (ca. 197 Ma) and are interpreted to represent portions of the same genetic system. Despite this relationship, mineralization styles within the deposits range from calc-alkalic Cu-Mo types in the Southeast Zone bodies, to alkalic Cu-Au mineralization in the Takom Zone. Mineralization in the Deerhorn Zone falls between these two, displaying many characteristics of both alkalic Cu-Au deposits as well as some features of more typical Cu-Mo calc-alkalic systems (del Real *et al.* 2014). The deposits have only very limited surface outcrop. Glacial sediments reaching a thickness of over 200 m in places mantle and obscure many of the mineralized zones. The stratigraphy of the glacial sediment succession is not well known. The last glacial event in the Woodjam district included two vectors of ice flow: first to the southwest, followed by a second event to the northwest (Fig. 2B).

Tourmaline at the Woodjam properties occurs principally in the Deerhorn and Takom zones. Within each of these, tourmaline forms a complex series of spatial and paragenetic associations with a number of other silicate and sulphide minerals. In many cases these occur in barren to very weakly mineralized portions of the deposits, but some tourmaline does appear to be intimately linked to significant copper sulphide (principally chalcopyrite) mineralization, although this is possibly a later addition rather than being coeval with the copper-bearing stage. To characterize and investigate its spatial and genetic relationship to the ore-forming process, samples of tourmaline and associated Cu-Au mineralization and hydrothermally altered host rocks were taken from exploration diamond-drill core from the Takom and Deerhorn zones, as well as surface samples from albite-epidote-tourmaline alteration of regional volcanic rocks, and tourmaline-cemented breccias, that occur at surface over the Takom Zone. From these samples, polished thin sections were prepared (Fig. 3) and analyzed by optical and scanning electron microscopy, prior to elemental analysis by electron probe microanalysis (EPMA).

In addition to the bedrock samples, to investigate the utility and resolution of tourmaline as a porphyry exploration vector in glaciated terrain, till samples were recovered from numerous sites in and around the Woodjam property. From these till samples, mid-density and heavy mineral concentrates were prepared. Tourmaline content of the till samples was determined for the mid-density (2.8–3.2 g/cm^3) 0.25–0.5 mm fraction and normalized to a 10 kg sample weight (Fig. 2B). Broadly, the tourmaline abundance anomaly describes a halo that is approximately 10 km from east to west and runs from the southern margin of the deposits to a point approximately 10 km north

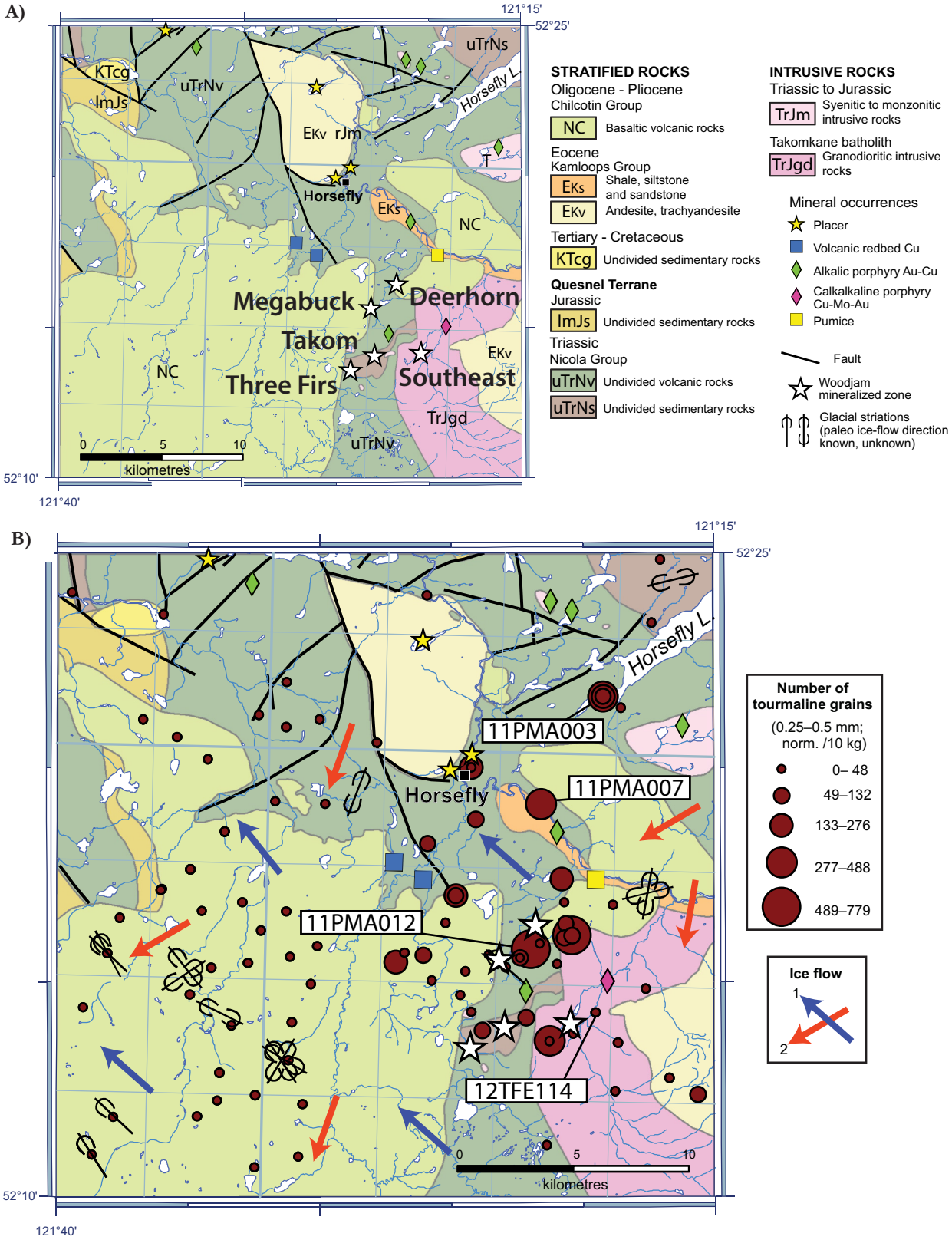

Fig. 2. Bedrock geology, mineral deposits and sample locations in the vicinity of the Woodjam property, central British Columbia: **A)** bedrock geology and major mineralized zones, Woodjam zones are named; **B)** glacial striations, dominant ice-flow directions, and abundance of tourmaline in the mid-density (3.0–3.2 g/cm^3) 0.25–0.5 mm fraction of till, normalized to 10 kg bulk sediment (<2 mm). Till samples for which tourmaline major element compositions have been determined are labelled. Bedrock geology modified from Massey *et al.* (2005).

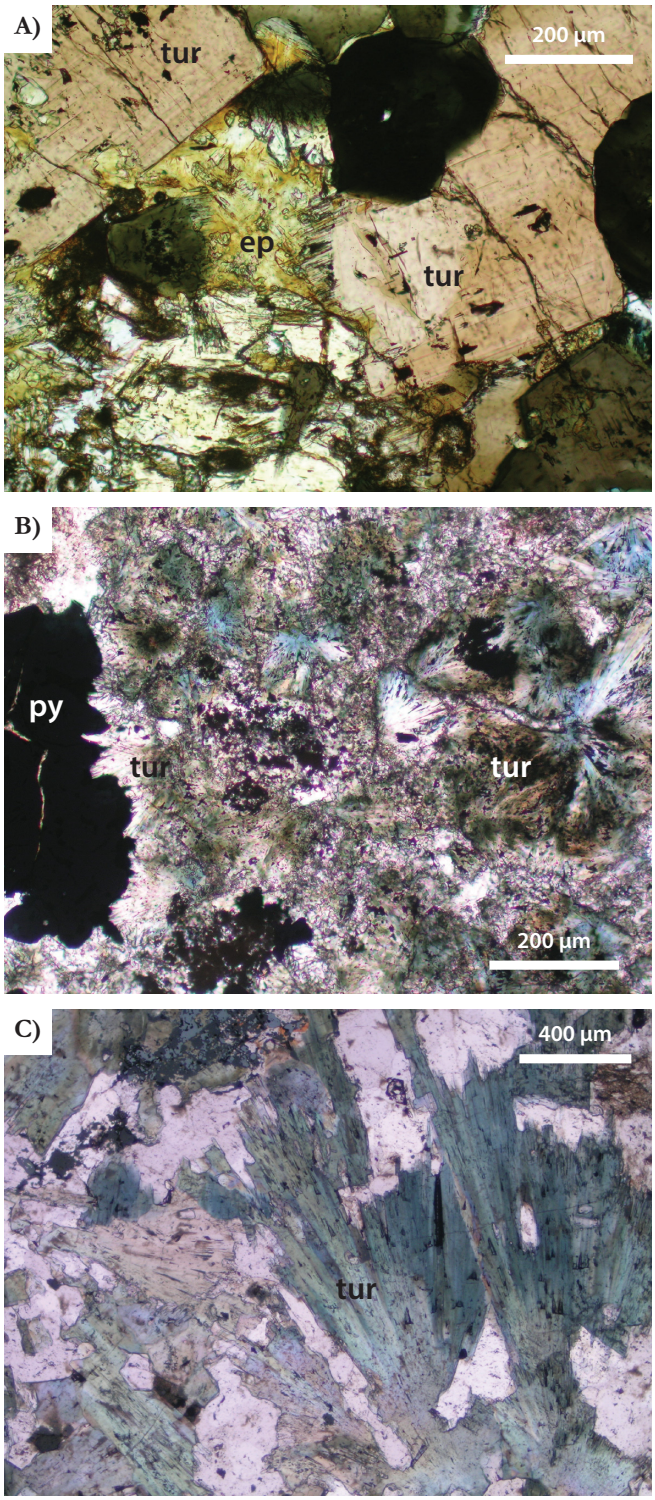

Fig. 3. Plane polarized light optical photomicrographs of typical tourmaline species and habits from within the Takom and Deerhorn zones: **a)** mid- to dark brown, equant schorl-dravite from albite-epidote-tourmaline-altered mafic country rocks at surface in the Takom zone; **b)** fine, fibrous, felted, dark to pale green dravite overgrowing and almost entirely replacing earlier potassic-altered monzonite from a subsurface sample at the Deerhorn Zone, the tourmaline directly adjacent to the late pyrite is colourless; **c)** large, radiating, acicular, blue-grey dravite forming rosettes intimately associated with contemporaneous chalcopyrite-bearing potassic alteration of host monzonite, from subsurface sampling of the Takom Zone.

of the Deerhorn Zone. Four of these samples were selected for further study: sample 11PMA003, taken from a site at the southwest end of Horsefly Lake with tourmaline unlikely to be derived from Woodjam; sample 11PMA007, taken from a site located 6.5 km north of Deerhorn containing tourmaline that is unlikely to be derived from the Woodjam mineralization; sample 11PMA012, taken from a site located in between Megabuck and Deerhorn and likely derived from known mineralization; and sample 12TFE114, taken ~1 km northeast of the Southeast Zone and therefore its tourmaline is unlikely derived from the known mineralization. As with samples taken from the bedrock, till tourmaline grains were mounted in epoxy, polished, and their major element chemistry was determined using EPMA.

Based on major element chemistry discriminant plots, the majority of bedrock tourmaline samples analyzed are dravitic, although with a significant subset of albite-associated tourmaline from the surficial outcrop at Takom Zone falling along the chemical-evolution trend to moderately schorl-rich compositions. Samples from both deposits have many of the characteristics identified by Baksheev *et al.* (2012) as typical for tourmaline in porphyry copper systems: magnesium content is approximately 2 atoms-per-formula unit, and they lie on the $FeAl_{-1}$ isomorphic substitution trend (Fig. 4A). The dominance of this substitution is reinforced by most samples plotting on the Mg-foitite–povondraite join and above the schorl–dravite join in an Fe-Al-Mg ternary (Fig. 4B). Both of these substitution trends are thought to represent the evolution of an ore-forming fluid from an initial iron-dominant magmatic-hydrothermal precursor to a magnesium-dominant effluent fluid. While the magnesium content (i.e. atomic percentage) varies comparatively little, as iron is stripped from the fluid and the fluid pH is lowered, both through the iron-bearing sulphide precipitation and the substitution of aluminum for iron in the *Y*-site is promoted (Baksheev *et al.* 2012). Hence, the evidence for these evolution trends may be considered a fingerprint for the tourmaline-forming fluid having also formed iron sulphide upstream of the tourmaline deposition site.

These element evolution trends are important for the interpretation and application of unknown populations, as can be seen in the major element chemical plots for till tourmaline taken from the vicinity of the Woodjam deposits (Fig. 4C, D). Although samples 11PMA003, 11PMA007 and 12TFE114 are dominated by tourmaline that has chemical compositions that, in part, resemble those of Baksheev *et al.*'s (2012) porphyry tourmaline fingerprint, the scatter and evolutionary trends described by these samples do not follow either the $FeAl_{-1}$ trend within the $Fe_{(t)}$-Mg plot (Fig. 4C), nor the magnesio-foitite–povondraite join in an Fe-Al-Mg ternary plot (Fig. 4D). In both cases these tourmaline populations more closely resemble a simple cooling or fluid-rock ratio variation trend, and do not appear to have originated in fluids that have participated in a porphyry-forming sulphide-deposition process. In contrast, the tourmaline population within sample 11PMA012 plots directly over tourmaline taken from Deerhorn and particularly Takom Zone bedrock samples in both an $Fe_{(t)}$-Mg plot and Fe-Al-Mg ternary plot (Fig. 4C, D).

Of the four till samples analysed, only sample 11PMA012 contains a tourmaline population that unequivocally fits both the Baksheev *et al.* (2012) porphyry Cu-Au tourmaline model and the range of compositions recorded in local Woodjam mineralized bedrock. This sample site sits directly over the cen-

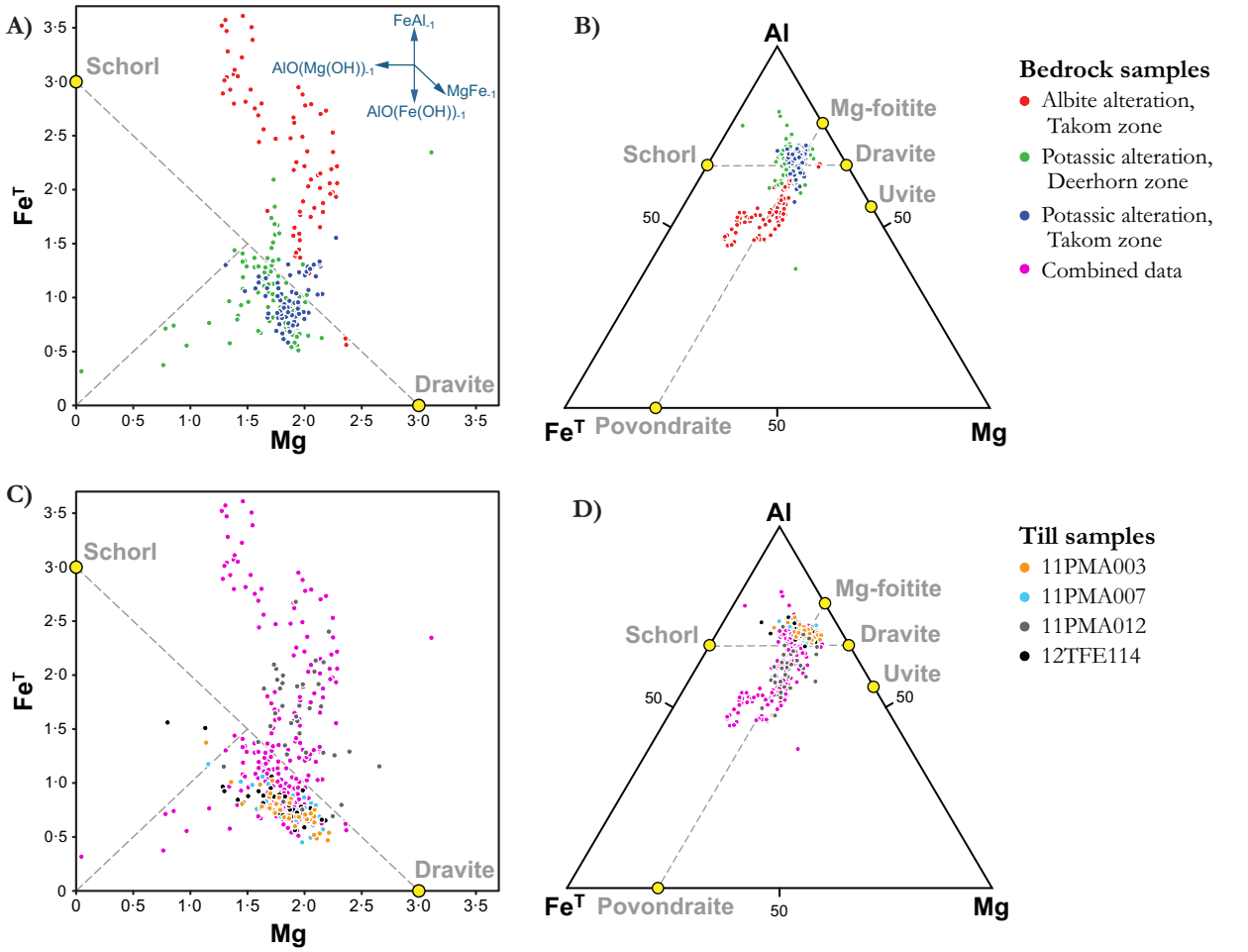

Fig. 4. Tourmaline major element cation ratio discrimination plots for bedrock samples (A & B) and till (C & D) tourmaline samples described in this study: **A)** Fe^T vs. Mg plot for bedrock samples, all three populations lie dominantly along the $FeAl_{-1}$ substitution vector; **B)** an Al-Fe^T-Mg ternary plot of bedrock tourmaline data, although most samples plot at or above the schorl–dravite join, they dominantly scatter along the magnesio-foitite–povondraite join; **C)** till tourmaline sample data overlain on to bedrock data in the same Fe^T versus Mg plot as used in (A), demonstrating that although the Mg-cation count is approximately 2 apfu, all three distal populations describe a substitution trend parallel to the $MgFe_{-1}$ trend, though only the sample taken directly over the deposits (sample 11PMA012) scatters along the $FeAl_{-1}$ substitution vector; **D)** till tourmaline sample data overlain on bedrock data in the same Al-Fe^T-Mg ternary plot used in (B), only sample 11PMA012 data scatters along the magnesio-foitite–povondraite join.

tre of the mineralized district and less than one kilometre down-ice from the Deerhorn Zone. Were the locations of the deposit centres unknown, the spatially restricted anomaly described by the tourmaline chemical fingerprint would give a more precise exploration target than the approximately 10 by 20 km target defined by simple tourmaline grain abundances. At present we cannot explain the looser spatial association of abundant tourmaline with some porphyry characteristics.

REFERENCES

Baksheev, I.A., Prokof'ev, V.Y., Zaraisky, G.P., Chitalin, A.F., Yapaskurt, V.O., Nikolaev, Y.N., Tikhomirov, P.L., Nagornaya, E.V., Rogacheva, L.Ä.I., Gorelikova, N.V. & Kononov, O.V. 2012. Tourmaline as a prospecting guide for the porphyry-style deposits. *European Journal of Mineralogy*, **24**, 957–979

Calas, G. 2011. Tourmaline Research: Unlocking Ali Baba's Cave. *Elements*, **7**, 291

Deer, W.A., Howie, R.A. & Zussman, J. 1986. *Rock-Forming Minerals, Volume 1B: Disilicates and Ring Silicates* (2nd ed.). John Wiley & Sons, Inc., New York.

del Real, I., Hart, C.J.R., Bouzari, F., Blackwell, J.L., Rainbow, A. & Sherlock, R. 2014. Relationships between calcalkalic and alkalic mineralization styles at the copper-molybdenum Southeast Zone and copper-gold Deerhorn porphyry deposits, Woodjam Property, Central British Columbia (NTS 093A), *In: Summary of Activities 2013*. Geoscience BC, Report 2014-1, 63–82.

Dutrow, B.L. & Henry, D.J. (eds.) 2011. Tourmaline. *Elements*, **7/5**, 360 p.

Ertl, A. 2006. Über die Etymologie und die Typlokalitäten des Minerals Schörl (About the etymology and the type-localities of schorl). *Mitteilungen der Österreichischen Mineralogischen Gesellschaft*, **152**, 7–16 (German with English abstract.)

Hawthorne, F.C. & Dirlam, D.M. 2011. Tourmaline the indicator mineral: from atomic arrangement to Viking navigation. *Elements*, **7/5**, 307–312

Henry, D.J. & Guidotti, C.V. 1985. Tourmaline as a petrogenetic indicator mineral: an example from the staurolite-grade metapelites of NW Maine. *American Mineralogist*, **70**, 1–15

Henry, D.J., Novák, M., Hawthorne, F.C., Ertl, A., Dutrow, B.L., Uher, P. & Pezzotta, F. 2011. Nomenclature of the tourmaline-supergroup minerals. *American Mineralogist*, **96**, 895–913

Mange, M.A. & Morton, A.C. 2007. Geochemistry of Heavy Minerals, Chapter 13 *In:* Mange, M.A. & Wright, D.T. (eds.) *Heavy Minerals in Use*. Developments in Sedimentology, 58, 345–391

Massey, N.W.D., MacIntyre, D.G., Desjardins, P.J. & Cooney, R.T. 2005. *Digital Map of British Columbia: Tile NN10 Central B.C.* British Columbia Ministry of Energy and Mines, GeoFile 2005-6

Slack, J.F. 1996. Tourmaline associations with hydrothermal ore deposits. *Reviews in Mineralogy and Geochemistry*, **33**, 559–643

van Hinsberg, V.J., Henry, D.J. & Marschall, H.R. (eds.) 2011. Tourmaline: An ideal indicator of its host environment. *The Canadian Mineralogist*, **49/1**, 405 p.

Direct and indirect indicator minerals in exploration for carbonatite and related ore deposits — an orientation survey, British Columbia, Canada

G.J. Simandl[1,2*], D.A.R. Mackay[1], X. Ma[3], P. Luck[2] , J. Gravel[3], B. Grcic[4] & M. Redfearn[4]

[1]School of Earth and Ocean Sciences, University of Victoria, Victoria, British Columbia, Canada V8P 5C2
[2]British Columbia Geological Survey, Ministry of Energy and Mines, Victoria, British Columbia, Canada V8W 9N3
[3]Bureau Veritas Commodities Canada Ltd., Geo-analytical Division, 9050 Shaughnessy Street, Vancouver, British Columbia, Canada V6P 6E5
[4]Bureau Veritas Commodities Canada Ltd, Metallurgical Division, 11620 Horseshoe Way, Richmond, British Columbia, Canada V7A 4V5
**Corresponding author's e-mail: George.Simandl@gov.bc.ca*

CARBONATITE AS AN EXPLORATION TARGET

Specialty metals, and more specifically Nb, Ta, and rare earth elements (REE), are concentrated in a variety of deposit types, including carbonatite, peralkaline intrusions, pegmatite, and peraluminous granite (Mackay & Simandl 2014a; Simandl 2014). Carbonatite-related deposits, such as Mountain Pass (California) and Bayan Obo (Inner Mongolia), are the main sources of light rare earth elements (LREE), and Araxá and Catalão (Brazil) and St. Honoré (Quebec) type deposits are the main sources of Nb and ferroniobium. Palabora is an exceptional example of a carbonatite complex with important resources of Cu, natural zirconia (badelleite), vermiculite, phosphate (apatite), and U (Clarke 1981). A discussion of the overall economic importance of carbonatite can be found in Mariano (1989a, b), Richardson & Birkett (1996a, b), and Birkett & Simandl (1999).

Airborne geophysical methods of particular importance for carbonatite exploration are aeromagnetic, radiometric, and gravity. These have been used successfully to discover new, or delimit known carbonatite complexes (Satterly 1970; Thomas *et al.* 2011; Drenth 2014). In addition to traditional prospecting, geochemical exploration methods, including boulder tracing and indicator minerals, are ideally suited for ground follow-up.

INDICATOR MINERALS — BACKGROUND

Background information regarding the use of indicator minerals and traditional processing methodologies for regional- or country-wide scale surveys is provided in McClenaghan (2005, 2011) and McCurdy *et al.* (2006, 2009). Since the development of the indicator mineral method for diamond exploration by Gurney (1984) and popularization by Gurney & Zweistra (1995), Muggeridge (1995), Fipke *et al.* (1995), and McClenaghan & Kjarsgaard (2001), its use has expanded to include exploration for other commodities, such as base metals (e.g. Averill 2001; Paulen *et al.* 2009, 2011). Traditional indicator mineral surveys are processing intensive and involve mineral-picking. As such, they are relatively expensive and time consuming in comparison to regional geochemical surveys. Indicator mineral concentration flow-charts (e.g. Fig. 8 *in* Crabtree 2003) illustrate the number of consecutive processing steps used in traditional regional, multi-target surveys. In summary, samples are sieved to a range of size fractions and selected fractions undergo a variety of density and magnetic separations, panning, grain counting, acid washing, and hand-picking to produce a suite of kimberlite and metamorphic/magmatic massive sulphide indicator minerals (Crabtree 2003; McClenaghan 2011).

One of the objectives of the specialty metals component of the Targeted Geoscience Initiative 4 (TGI-4), a Canadian federal government collaborative geoscience program, was to find efficient and cost-effective methods for vectoring towards carbonatite intrusions and related specialty metal deposits, and by default, towards a wide variety of other carbonatite-related deposit types. During 2013 and 2014 in the framework of this program, limited field and laboratory orientation surveys were undertaken to test the concept of customized indicator mineral methods for carbonatite exploration, to complement traditional regional stream sediment surveys, to follow-up on geophysical anomalies possibly attributable to carbonatite, and to follow-up on REE, Nb, and Ta anomalies detected during regional geochemical and indicator mineral surveys. By extrapolation, the research and ensuing successful methods may be applied in the exploration of other deposit types in regions challenged by extensive and/or transported cover.

SIMPLIFICATION OF INDICATOR MINERAL METHODOLOGY IN EXPLORATION FOR CARBONATITE

Orientation-centric research concentrated on five aspects of indicator mineral surveys that target carbonatite and related deposits in the North American Cordillera:

(a) identification of potential carbonatite indicator minerals;
(b) identification of an optimal grain-size fraction;
(c) simplification of the processing methodology;
(d) use of Quantitative Evaluation of Minerals by Scanning electron microscopy (QEMSCAN®);
(e) improvement of existing and development of new discrimination diagrams that could be used for target identification.

Potential carbonatite indicator minerals

The pyrochlore supergroup (as defined by Atencio *et al.* 2010), the columbite-tantalite series (as defined by Černý & Ercit 1985; Černý *et al.* 1992), the REE-bearing fluorocarbonate minerals (such as bastnaesite and synchysite), and monazite are direct carbonatite indicator minerals (Table 1). They contain high concentrations of key carbonatite pathfinder elements

Table 1. Principal (shown in red) and potential carbonatite indicator minerals. Density data is from Anthony *et al.* (2004). Table is simplified from Mackay *et al.* (2015b).

Mineral Name	Chemical Formula	Density (g/cm^3)
Pyrochlore supergroup	$(Ca,Na)_2(Nb,Ti,Ta)_2O_6(O,OH,F)$	4.2–6.4
Columbite-tantalite series	$(Fe,Mn)(Ta,Nb)_2O_6$	5.3–8.2
Fersmite	$(Ca,Ce,Na)(Nb,Ta,Ti)_2(O,OH,F)_6$	4.69–4.79
Bastnaesite	$Ce(CO_3)F$	4.95–5.00
Synchysite	$Ca(Ce,La)(CO_3)_2F$	3.90–4.15
Monazite	$(Ce,La,Nd,Th)PO_4$	4.8–5.5
Allanite	$(Ce,Ca,Y)_2(Al,Fe)_3(SiO_4)_4(OH)$	3.3–4.2
Fluorite	CaF_2	3.2–3.6
Zircon	$ZrSiO_4$	4.6–4.7
Apatite	$Ca_5(PO_4)_3(OH,F,Cl)$	3.16–3.22
Magnetite	Fe_3O_4	5.1–5.2
Arfvedsonite	$Na_3[(Fe,Mg)_4Fe]Si_8O_{22}(OH)_2$	3.44–3.45
Richterite	$Na(Ca,Na)(Mg,Fe)_5(Si_8O_{22}(OH)_2$	2.97–3.45
Aegerine	$NaFeSi_2O_6$	5.50–5.54
Barite	$BaSO_4$	4.48
Celestine	$SrSO_4$	3.9–4.0
Perovskite	$CaTiO_3$	4.0–4.3
Rutile	TiO_2	4.23

Fig 1. Location of the Aley, Wicheeda, and Lonnie carbonatite complexs, British Columbia alkaline province.

(Nb, La, Ce, Pr, and Nd) in their crystal structure. Their presence can be established using traditional chemical analyses (Li borate fusion followed by ICP-MS) and portable X-ray fluorescence spectroscopy (Luck & Simandl 2014; Mackay & Simandl 2014b, c). Barium and Sr sulphate minerals (barite-celestine solution series), Na-pyroxene minerals (commonly aegirine), Na and K amphibole (e.g. arfvedsonite and richterite), baddeleyite, fluorite (Makin *et al.* 2014, Nb-rutile, Ti-Zr garnet, magnetite, apatite (Belusova *et al.* 2002a), zircon (Belusova *et al.* 2002b), and others are also potential carbonatite indicator minerals.

Identification of the ideal sediment grain-size fraction

Three representative carbonatite complexes located in the British Columbia alkaline province (Fig. 1) were selected for orientation surveys. They differ greatly in size, shape, ore mineralogy, and grade. The Aley carbonatite complex, which has been defined by drilling, is exposed over an irregularly shaped, 2 by 3 km area. It has a measured resource of 113 million tonnes grading at 0.41% Nb_2O_5, an indicated resource of 173 million tonnes at 0.35% Nb_2O_5 with a cut-off grade of 0.20% Nb_2O_5 (Jones *et al.* 2014), and relatively low REE content (Simandl *et al.* 2014b). The Wicheeda Lake carbonatite forms an elongated cluster of poorly exposed carbonatite and syenite occurrences. It represents the most developed LREE resource in British Columbia (Lane 2009). A discussion of the geology of the Wicheeda Lake carbonatite can be found in Trofanenko *et al.* (2014). The Lonnie carbonatite complex has been traced by trenching over 650 metres along strike and has been found to reach widths of up to 50 metres. It is oriented at 120ºE/60ºSW (Hankinson 1958; Rowe 1958). An approximately 530 metre long, 17 metre wide zone within this complex grades 0.21% Nb_2O_5 (Rowe 1958; Chisholm 1960). However, limited sampling in 2013 was unable to confirm this grade (Simandl *et al.* 2013).

The Lonnie, Aley, and Wicheeda Lake stream sediment studies (Luck & Simandl 2014; Mackay & Simandl 2014b, c) identified the 0.125–0.250 mm fraction as optimal for carbonatite indicator mineral studies. This fraction consistently contained high pathfinder element concentrations (e.g. Wicheeda Lake carbonatite area; Fig. 2) and routinely yielded an acceptable mass for testing by QEMSCAN®. The 0.125–0.250 mm fraction is well within the QEMSCAN®'s optimal operational range, and leaves the 0.250–0.500 mm and coarser fractions for traditional mineral picking. Sample sites, sizes, and location as well as distance from deposits and sampling methodology are described by Luck & Simandl (2014) and Mackay & Simandl (2014b, c).

Minimum required processing

The key REE-bearing fluorocarbonate and Nb- and Ta-bearing carbonatite indicator minerals (3.9–8.2 g/cm^3, Table 1) have a good density contrast with common rock-forming minerals and lithic fragments (2.5–3.4 g/cm^3) that make-up the bulk of stream sediments. Splits of the 0.125–0.250 mm size fraction of samples downstream from the Aley carbonatite were successfully processed using Mozley C800 and Wilfley #13 concentrator tables (Mackay *et al.* 2015a, b). Both tables are simple, efficient, and widely available. Concentrates prepared using Mozley C800 tables were found to have increased Nb content by a factor of 2.8 to 3.7 (average of 3.3), Ta by a factor of 2.1 to 2.9 (average of 2.4), and LREE by a factor of 1.7 to 3.1 (average of 2.5) relative to the corresponding raw samples. The Nb content of Wilfley #13 concentrates increased by a factor of 3.9 to 5.6 (average of 4.8) relative to raw samples. Similarly, Ta increased by a factor of 2.3 to 4.9 (average of 3.6) and LREE content increased by a factor of 1.8 to 5.1 (average of 3.9). High coefficients of determination (R^2>0.9) for Nb, LREE (Σ La, Ce, Pr, and Nd), U, Th, and Ba in Mozley C800 and Wilfley #13 table concentrates relative to their unprocessed 0.125-0.250 mm fractions indicate the concentrators produced a predicable degree of enrichment under constant operating conditions.

The Mozley C800 table was preferred to the Wilfley #13 table because it was more user-friendly and permitted efficient processing of relatively small samples (approximately 75 grams

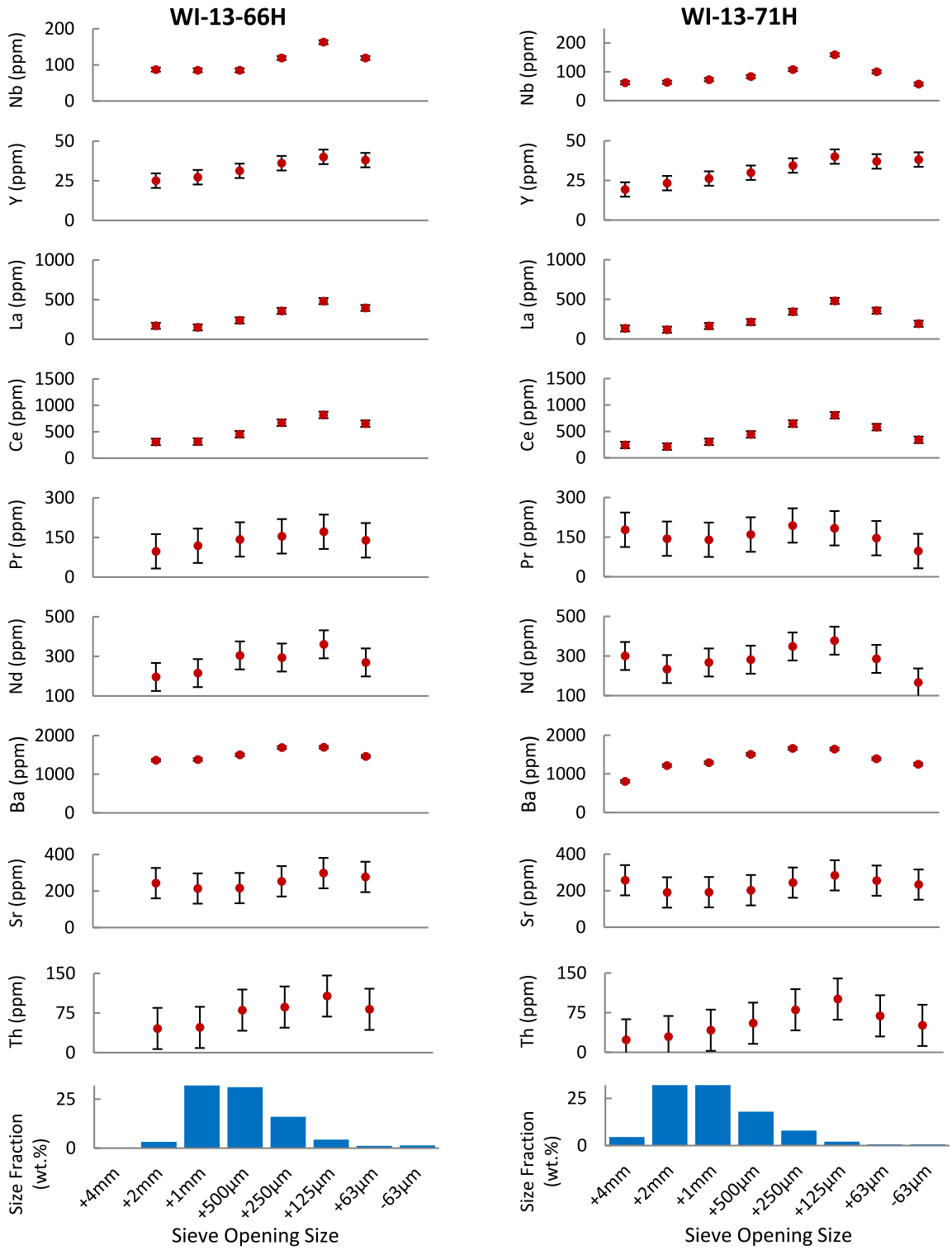

Fig 2. Particle size distribution and content of key carbonatite pathfinder elements in stream sediment samples, Wicheeda Lake carbonatite, British Columbia (Mackay & Simandl, 2014c).

of the 0.125–0.250 mm size fractions in case of Aley and Lonnie samples). Difficulty in obtaining a sufficient mass of the 0.125–0.250 mm size fractions for samples from the Wicheeda Lake area prevented systematic comparison of Mozley C800 and Wilfley #13 table at that location. At the Wicheeda carbonatite, the concentrations of carbonatite indicator minerals in raw stream sediments were too low to obtain sufficient quantities of concentrate for both QEMSCAN® studies and chemical analyses using pXRF , according to the method described in Simandl *et al.* (2014a) and Luck & Simandl (2014).

QEMSCAN® as a substitute for hand-picking of indicator minerals

Automated scanning electron microscope analysis (QEMSCAN®) is a powerful tool used mainly by metallurgists to

Table 2. Concentrations of minerals in the 0.125–0.250 mm size fraction of stream sediment samples determined by QEMSCAN® (wt%) prior to and after processing with a Mozley C800 concentrator table.

Sample number	AL-13-01		AL-13-04		AL-13-16	
Northing*	6252228		6256338		6251818	
Easting*	443432		454355		445779	
Sample type	RAW	CON	RAW	CON	RAW	CON
Fersmite	0.01	0.04	0.26	0.06	0.35	0.04
Pyrochlore	0.64	1.42	0.11	2.17	0.06	1.02
Columbite-Fe	0.32	1.36	1.88	3.02	0.87	1.12
Monazite	0.63	1.45	0.49	1.92	0.47	1.61
REE-fluorocarbonates	0.07	0.32	0.31	0.25	0.17	0.38
Zircon	0.14	0.36	0.08	0.35	0.17	0.41
Pyrite	0.06	0.19	0.43	0.92	0.18	0.20
Magnetite	2.03	3.76	0.67	7.07	1.29	6.16
Hematite	5.18		13.54	19.21	8.51	6.68
Goethite	0.22	0.29	0.64	0.32	0.36	0.24
Ilmenite	0.14	0.21	0.08	0.18	0.11	0.19
Quartz	19.10	9.65	3.23	1.36	18.43	11.83
Clinochlore/Chamosite	1.20	1.03	1.44	1.05	1.05	0.99
Muscovite	2.97	1.33	0.39	0.16	2.99	1.12
Biotite/Phlogopite	0.78	0.20	0.15	0.08	0.64	0.23
K-Feldspars	4.62	0.93	0.28	0.15	4.98	1.75
Feldspar Albite	1.34	0.63	0.46	0.25	1.17	0.71
Dolomite	40.07	41.03	47.68	28.89	38.24	44.87
Apatite	6.22	13.10	19.26	27.40	6.42	10.66
Calcite	10.33	6.49	0.84	0.26	9.52	5.57
Ankerite	1.71	1.14	4.29	2.27	1.73	1.87
Fluorite	0.00	0.03	0.00	0.00	0.00	0.03
Amphibole/Pyroxene	1.49	1.42	2.73	2.25	1.12	1.69
Epidote	0.05	0.18	0.01	0.01	0.06	0.09
Rutile/Anatase	0.14	0.24	0.15	0.20	0.13	0.18
Garnet	0.09	0.05	0.02	0.04	0.06	0.04
Kaolinite	0.05	0.07	0.01	0.01	0.07	0.04
Talc/Serpentine	0.06	0.04	0.43	0.08	0.13	0.09
Barite	0.16	0.26	0.01	0.01	0.14	0.06
Others	0.18	0.04	0.12	0.06	0.59	0.13
TOTAL	100.00	100.00	100.00	100.00	100.00	100.00

*Locations for UTM zone 10, NAD 83

RAW - result of QEMSCAN® analysis on the 0.125–0.250 mm size fraction prior to processing on a Mozley 800C concentrator table

CON - result of QEMSCAN® analysis on the 0.125–0.250 mm size fraction after processing on a Mozley 800C concentrator table

Red text - proven direct Nb indicator minerals

Blue text - proven direct REE indicator minerals

Green text - potential indirect indicator minerals

assess degree of mineral liberation following comminution. In our orientation survey, it provided mainly grain counts of indicator and rock-forming minerals and their weight % equivalents, detailed grain-size analysis on a mineral-by-mineral basis, quantitative assessment of abundances of free and composite (multi-mineral) grains, and mineral associations within composite grains. Another important advantage of QEMSCAN® analysis over traditional mineral picking is that it can operate on grain-size fractions considered too small for hand picking.

The QEMSCAN® orientation (carried out at the Bureau Veritas Commodities Canada Ltd., Inspectorate Metallurgical Division in Richmond, British Columbia) examined representative Aley carbonatite stream sediment samples testing the 0.125 to 0.250 mm fraction of raw (unprocessed) sediment and corresponding Mozley C800 concentrates. Results of these tests demonstrate that a 2 g sample split yields 12,000 to 35,000; (average = 20,000) exposed grains in a polished smear thin section. To ensure that pyrochlore supergroup, columbite-tantalite series minerals, monazite, and REE-bearing fluorocarbonate in low-grade samples are adequately concentrated (Table 2) before preparation of polished smear thin sections for QEMSCAN® and microprobe analysis, sample splits were

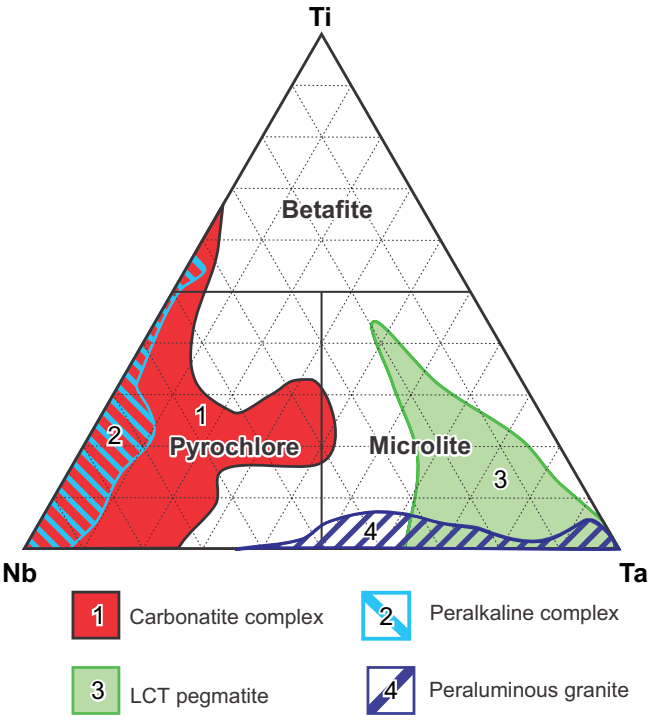

Fig. 3. Nb-Ta-Ti discrimination diagram for minerals of pyrochlore supergroup showing carbonatite field (Mackay & Simandl, 2015).

processed on the Mozley C800 table under constant, controlled conditions. However, even without Mozley C800 table concentration, QEMSCAN® detected pyrochlore supergroup and columbite-tantalite series grains in samples collected more than 11 km downstream of the Aley carbonatite (Nb deposit).

Results of QEMSCAN® analysis were compared to the concentration of pathfinder elements determined by XRF and Li-borate fusion with ICP-MS in the 125–250 μm fraction of three unprocessed samples and five Mozley C800 concentrates from the Aley carbonatite study area. There is a high coefficient of determination ($R^2 = 0.90$) between the concentration of key Nb-bearing minerals in wt% obtained by QEMSCAN® and Nb content determined by XRF. An R^2 of 0.92 was obtained when plotting the QEMSCAN® monazite concentration in wt% against (Σ La, Ce, Pr, Nd) content by ICP-MS. Excellent fit (R^2) between the abundance of pathfinder elements and concentrations of direct indicator minerals (wt%) in the 125–250 μm fraction of stream sediments provides the option to analyze all the samples chemically but use QEMSCAN® only on selected samples. The combination of these two methods would provide the low-cost advantage of geochemical surveys with the high interpretative power of both indicator mineral and geochemical surveys.

Discrimination diagrams

Discrimination diagrams are the key to successful targeting and vectoring towards mineralization. This is illustrated by highly-evolved garnet, chromite, clinopyroxene, olivine, and ilmenite discrimination diagrams used by the diamond exploration industry (Gurney & Zweistra 2005).

The pyrochlore supergroup and columbite-tantalite series discrimination diagrams (Figs. 3 & 4), developed for general specialty-metal exploration, are most appropriate for carbonatite exploration (Mackay & Simandl 2015). They permit iden-

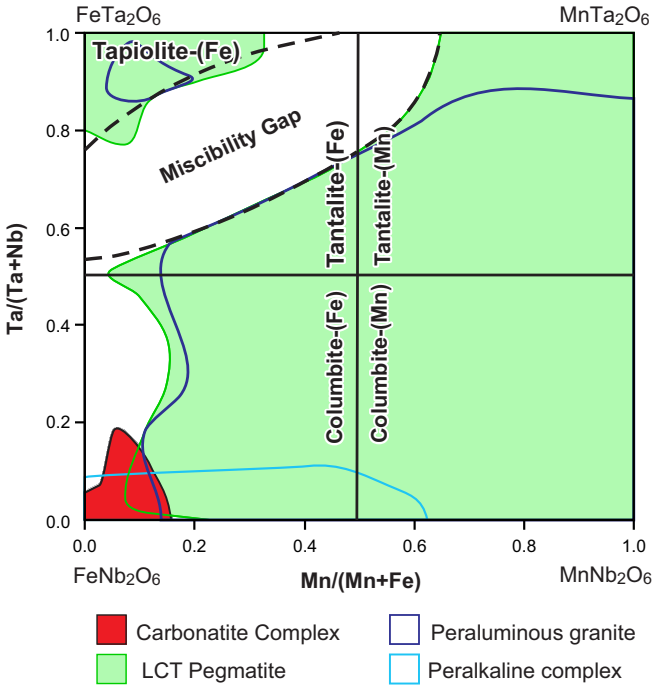

Fig. 4. Columbite-tantalite series discrimination diagram showing compositional field for carbonatite derived grains (Mackay & Simandl, 2015).

tification of the deposit type(s) from which the indicator mineral grains were derived (eg. carbonatite-, peralkaline intrusion, peraluminous granite- or pegmatite-related deposits as defined in Mackay & Simandl (2014a) and Simandl (2014)) based on microprobe analyses (no LA-ICP-MS required). There are other diagrams that can be employed for carbonatite exploration; however, many of these are based on small data sets. For example, the apatite discrimination diagram (Fig. 5A) from Belusova *et al.* (2002a) is based on 61 analyses of apatite from 4 carbonatite rocks. By plotting an additional 250 apatite (*sensu lato*) analyses from 12 fresh and weathered carbonatite, the Mn range of the carbonatite field expands from 40–450 ppm to 4-2320 ppm (Fig. 5B), and the Sr range expands from approximately 2000–9500 ppm to 1310–93330 ppm.

Other potential indicator minerals could be used in exploration for carbonatite if appropriate carbonatite-sensitive discrimination diagrams were successfully developed. Some of them are Ba and Sr sulphate, Na-pyroxene, Na- and K-amphibole, baddeleyite, monazite, fluorite (Makin *et al.* 2014), Nb-rutile, Ti-Zr garnet, perovskite, magnetite, and zircon (Belousova *et al.* 2002b). While discrimination diagrams for some of these minerals exist, the carbonatite field on these diagrams is either poorly constrained or not known. Most of these minerals occur as gangue and/or constituents of fenitized zones associated with carbonatite.

CONCLUSION

Pyrochlore supergroup and columbite-tantalite series minerals and REE-fluorocarbonate are useful direct indicator minerals in exploration for carbonatite and associated mineral deposits. They have very high densities relative to all common rock-forming minerals and to most other potential carbonatite-indicator minerals. Their presence is detectable in the favourable (in our case 0.125–0.250 mm) size fractions of unprocessed sediment downstream of known carbonatite by traditional chemical analyses (ICP-MS and XRF) and pXRF for Nb, Ta, and REEs, and also directly with QEMSCAN®.

If the concentrations of these elements are too low in raw samples, no more than single-step gravity concentration (eg. Mozley C800 or Wilfley #13 tables) is required to enrich the 0.125–0.250 mm size fraction of the samples for QEMSCAN® and microprobe analyses.

High R^2 between the abundance of pathfinder elements and concentrations of direct indicator minerals (wt%) provides explorationists the option to analyze all the samples chemically and only use QEMSCAN® on selected samples. By combining analytical techniques in this way, the explorationist benefits

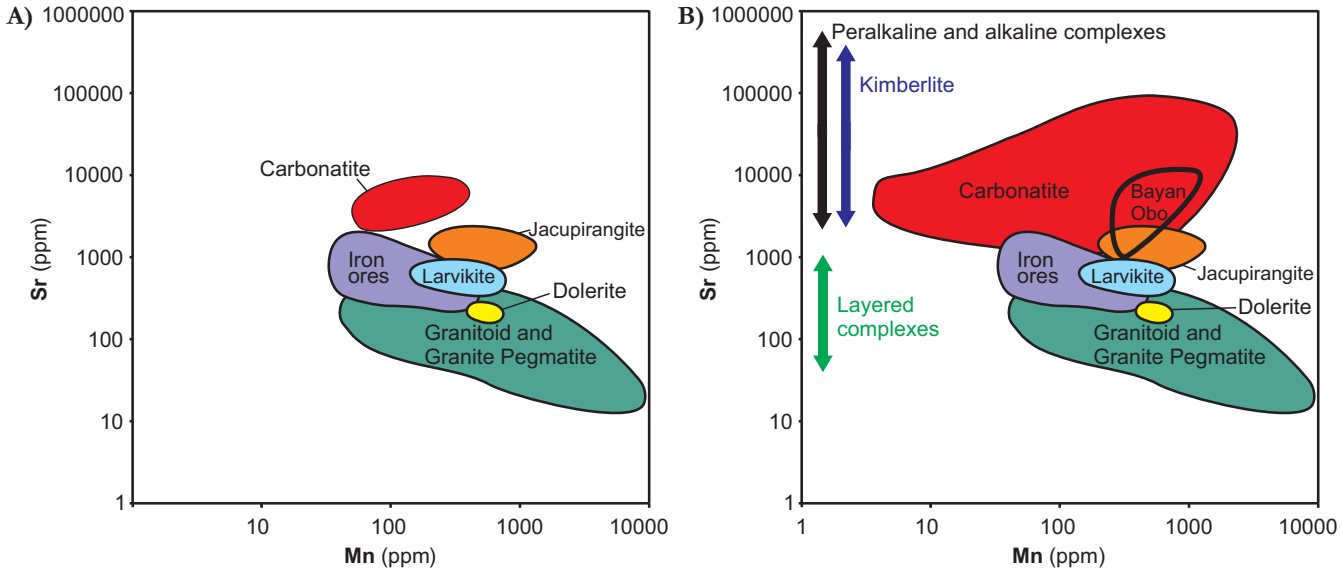

Fig. 5. A) Apatite discrimination diagram from Belousova *et al.* (2002a); and **B)** Modified apatite discrimination diagram. Carbonatite field enlarged due to incorporation of an extra 250 analyses. Carbonatite field is likely to overlap with fields of kimberlite and peralkaline intrusions at least in terms of Sr concentrations.

from the interpretational power of a combined survey at a fraction of the cost.

Discrimination diagrams (Figs. 4 & 5), designed for microprobe-quality (LA-ICP-MS analysis is not required) data, were developed for pyrochlore supergroup and columbite-tantalite series minerals. These diagrams permit screening of regional geophysical and geochemical anomalies for deposit-type without trenching or drilling.

This project focussed on exploration for carbonatite-related deposits, however, the same concepts and principles, and the experience acquired during optimization of the laboratory procedures (including QEMSCAN®), can be applied to more traditional targets such as base metals, platinum group elements, gold, gold chromite, etc.

ACKNOWLEDGMENTS

This project was supported by the Targeted Geoscience Initiative 4 (2010–2015), a Natural Resources Canada geoscience program. The Specialty Metal component of this program was carried out collaboratively by the Geological Survey of Canada and the British Columbia Geological Survey. Helicopter and logistical support during sampling by Taseko Mines Limited is greatly appreciated. Bureau Veritas Commodities Canada Ltd., Metallurgical and Geo-analytical divisions, are thanked for access to their laboratory equipment and the expert advice of their staff. Edits by Beth. M. McClenaghan (Geological Survey of Canada) are greatly appreciated.

REFERENCES

Anthony, J.W., Biduaex, R.A., Bladh, K.W. & Nichols, M.C. 2004. *Handbook of Mineralogy*. Mineralogical Society of America, Chantilly.

Atencio, D., Andrade, M.B., Christy, A.G., Gieré, R. & Kartashov, P.M. 2010. The pyrochlore supergroup of minerals: nomenclature. *The Canadian Mineralogist*, 48, 673–698.

Averill, S.A. 2001. The application of heavy indicator mineralogy in mineral exploration, *In:* McClenaghan, M.B., Cook, S., and Bobrowsky, P.T. (eds) *Drift Exploration in Glaciated Terrain*. Geological Society of London, Special Volume 185, p. 69–81.

Belousova, E.A., Griffin, W.L., O'Reilly, S.Y. & Fisher, N.I. 2002a. Apatite as an indicator mineral for mineral exploration: trace-element compositions and their relationship to host rock type. *Journal of Geochemical Exploration*, **76**, 45–69.

Belousova, E.A., Griffin, W.L., O'Reilly, S.Y. & Fisher, N.I. 2002b. Igneous zircon: trace element composition as an indicator of source rock type. *Contributions to Mineralogy and Petrology*, **143**, 602–622.

Birkett, T.C. & Simandl G.J. 1999. Carbonatite-associated deposits, *In:* Simandl ,G.J., Hora, Z.D. & Lefebure, D.V. (eds) *Selected British Columbia Mineral Deposit Profiles, Vol. 3: Industrial Minerals and Gemstones*. British Columbia Ministry of Energy, Mines and Petroleum Resources, British Columbia Geological Survey, Open File 1999-10.

Černý, P. & Ercit, T.S. 1985. Some recent advances in the mineralogy and geochemistry of Nb and Ta in rare-element granitic pegmatites. *Bulletin de Minéralogie*, **108**, 499–532.

Černý P., Ercit, T.S. & Wise, M.A. 1992. The tantalite-tapiolite gap: natural assemblages versus experimental data. *The Canadian Mineralogist*, **30**, 587–596.

Chisholm, E.O. 1960. Lonnie Columbian deposit. British Columbia Ministry of Energy and Mines property file <http://propertyfile.gov.bc.ca/showDocument.aspx?&docid=138373> accessed October 2012.

Clarke, G. 1981, The Palabora complex- triumph over low grade ores. *Industrial Minerals*, **October**, 45–62.

Crabtree, D.C. 2003. *Preliminary results from the James Bay Lowland indicator mineral sampling program*. Ontario Geological Survey, Open File Report 6108, 115 p.

Drenth, B.J. 2014. Geophysical expression of a buried niobium and rare element deposit: the Elk Creek carbonatite, Nebraska, USA. *Interpretation*, **2**, p. SJ169–SJ179. doi:10.1190/INT-2014-0002.1

Fipke, C.E., Gurney, J.J. & Moore, R.O. 1995. *Diamond exploration techniques emphasising indicator mineral geochemistry and Canadian examples*. Geological Survey of Canada, Bulletin 423, 86 p.

Gurney, J.J. 1984. A correlation between garnets and diamonds, *In:* Glover, J.E. & Harris, P.G. (eds) *Kimberlite Occurrence and Origin: A basis for conceptual models in exploration*. University of Western Australia, Department of Geology and University Extension, Publication 8, 143–166.

Gurney, J.J. & Zweistra, P. 1995. The interpretation of the major element compositions of mantle minerals in diamond exploration. *Journal of Geochemical Exploration*, **53**, 293–309.

Hankinson, J.D. 1958. *The Lonnie group columbium deposit*. B.Sc. thesis, University of British Columbia, Vancouver, British Columbia, 32 p.

Jones, S., Merriam, K., Yelland, G., Rotzinger, R. & Simpson, R.G. 2014. *Technical report on mineral reserves at the Aley project British Columbia, Canada*. Taseko Mines Limited, National Instrument 43-101, 291 p.

Lane, B. 2009. *Diamond Drilling Report on the Wicheeda Property, Cariboo Mining Division*. British Columbia Ministry of Energy, Mines, and Petroleum Resources, Assessment Report 30873, 196 p.

Luck, P. & Simandl, G.J. 2014. Portable X-ray fluorescence in stream sediment chemistry and indicator mineral surveys, Lonnie Carbonatite Complex, British Columbia, *In: Geological Fieldwork 2013*. British Columbia Ministry of Energy and Mines, British Columbia Geological Survey, Paper 2014-1, 169–182.

Mackay, D.A.R. & Simandl, G.J. 2014a. Geology, market and supply chain of niobium and tantalum–a review. *Mineralium Deposita*, **49**, 1025–1047.

Mackay, D.A.R. & Simandl, G.J. 2014b. Portable X-ray fluorescence to optimize stream sediment chemistry and indicator mineral surveys, case 1: Carbonatite-hosted Nb deposits, Aley carbonatite, British Columbia, Canada,. I*n: Geological Fieldwork 2013*. British Columbia Ministry of Energy and Mines, British Columbia Geological Survey, Paper 2014-1, 183–194.

Mackay, D.A.R. & Simandl, G.J. 2014c. Portable X-ray fluorescence to optimize stream sediment chemistry and indicator mineral surveys, case 2: Carbonatite-hosted REE deposits, Wicheeda Lake, British Columbia, Canada. *In: Geological Fieldwork 2013*. British Columbia Ministry of Energy and Mines, British Columbia Geological Survey, Paper, 2014-1, 195–206.

Mackay, D.A.R. & Simandl, G.J. 2015. Pyrochlore and columbite-tantalite as indicator minerals for specialty metal deposits. *Geochemistry: Exploration, Environment, Analysis*, In Press.

Mackay, D.A.R., Simandl, G.J., Grcic, B., Li, C., Luck, P., Redfearn, M. & Gravel, J. 2015a. Evaluation of Mozley C800 laboratory mineral separator for heavy mineral concentration of stream sediments in exploration for carbonatite-related specialty metal deposits: case study at the Aley carbonatite, British Columbia (NTS 094B), Canada. *In: Summary of Activities 2014*. Geoscience BC, Report 2015-1, 111–122.

Mackay, D.A.R., Simandl, G.J., Luck, P., Grcic, B., Li, C., Redfearn, M. & Gravel, J. 2015b. Concentration of carbonatite indicator minerals using Wilfley gravity shaking table: A case history from the Aley carbonatite, British Columbia, Canada. *In: Geological Fieldwork 2014*. British Columbia Ministry of Energy and Mines, British Columbia Geological Survey Paper 2015-1, 189-195.

Makin, S.A., Simandl, G.J. & Marshall, D. 2014. Fluorite and its potential as an indicator mineral for carbonatite related rare earth element deposits. *In: Geological Fieldwork 2013*. British Columbia Ministry of Energy and Mines, British Columbia Geological Survey, Paper 2014-1, 207–212.

Mariano, A.N. 1989a. Economic geology of rare earth minerals, *In:* Lipman, B.R. & McKay, G.A. (eds) *Geochemistry and Mineralogy of Rare Earth Elements: Reviews in Mineralogy, Volume 21*. Mineralogical Society of America, Chantilly, 303–337.

Mariano, A.N. 1989b. Nature of economic mineralization in carbonatites and related rocks, *In:* Bell, K (ed.) *Carbonatites: Genesis and Evolution*. Unwin Hyman, London, 149–176.

McClenaghan, M.B. 2005. Indicator mineral methods in mineral exploration. *Geochemistry: Exploration, Environment, Analysis*, **5**, 233–245.

McClenaghan, M.B. 2011. Overview of common processing methods for recovery of indicator minerals from sediments and bedrock in mineral exploration. *Geochemistry: Exploration, Environment, Analysis*, 11, 265–278.

McClenaghan, M.B. & Kjarsgaard, B.A. 2001. Indicator mineral and geochemical methods for diamond exploration in glaciated terrain in Canada, *In:* McClenaghan, M.B.,Bobrowsky, P.T., Hall, G.E.M.&, Cook, S.J. (eds) *Drift Exploration in Glaciated Terrain*. Geological Society, London, Special Publication 185, 83–123.

McCurdy, M.W., Prior, G.J., Friske, P.W.B., McNeil, R.J., Day, S.J.A. & Nicholl, T.J. 2006. *Geochemical, mineralogical and kimberlites indicator mineral electron microprobe data from silts, heavy mineral concentrates and water from a National Geochemical Reconnaissance stream sediment and water survey in northern and southwestern Buffalo Head Hills, northern Alberta (parts of 84B, 84C, 84F, and 84G)*. Alberta Energy and Utilities Board, Alberta Geological Survey, Special Report 76 and Geological Survey of Canada, Open File 5057, 15 p.

McCurdy, M.W., Kjarsgaard, I.M., Day, S.J.A., McNeil, R.J., Friske, P.W.B. & Plouffe, A. 2009. *Indicator mineral content and geochemistry of stream sediments and waters from northeast British Columbia (NTS 94A, 94B, 94G, 94H, 94I, 94K, 94N, 94O, 94P).* Geological Survey of Canada, Open File 6311 and Geoscience BC, Report 2009-2, 19 p.

Muggeridge, M.T. 1995. Pathfinder sampling techniques for locating primary sources of diamond: Recovery of indicator minerals, diamonds and geochemical signatures. *Journal of Geochemical Exploration,* **53**, 183–204.

Paulen, R.C., Paradis, S., Plouffe, A. & Smith, I.R. 2009. Base metal exploration using indicator minerals in glacial sediments, northwestern Alberta, Canada. *In:* Lentz, D, R., Thorne, K.G. & Beal, K.-L. (eds)*Proceedings of the 24th International Applied Geochemistry Symposium, Volume II*. Fredericton, New Brunswick, 1–9 June 2009, 557–560.

Paulen, R.C., Paradis, S., Plouffe, A. & Smith, I.R. 2011. Pb and S isotopic composition of indicator minerals in glacial sediments from northwest Alberta, Canada: implications for Zn-Pb base metal exploration. *Geochemistry: Exploration, Environment, Analysis*, **11**, 309–320.

Richardson, D.G. & Birkett, T.C. 1996a. Carbonatite associated deposits. *In:* Eckstrand, O.R., Sinclair, W.D. & Thorpe, R.I. (eds) *Geology of Canada Number 8: Geology of Canadian Mineral Deposit Types*. Geological Survey of Canada, 541–558.

Richardson, D.G. & Birkett, T.C. 1996b. Residual carbonatite-associated deposits, *In:* Eckstrand, O.R., Sinclair, W.D. & Thorpe, R.I. (eds) *Geology of Canada Number 8: Geology of Canadian Mineral Deposit Types*. Geological Survey of Canada, 108–119.

Rowe, R.B. 1958. *Niobium (Columbium) Deposits of Canada*. Geological Survey of Canada, Economic Geology Series 18, 103 p.

Satterly, J. 1970. *Aeromagnetic maps of carbonatite-alkalic complexes in Ontario*. Ontario Department of Mines and Northern Affairs, Preliminary Map No. P.452.

Simandl, G.J. 2014. Geology and market-dependent significance of rare earth element resources. *Mineralium Deposita*, **49**, 889–904.

Simandl, G.J., Reid, H.M. & Ferri, F. 2013. Geological setting of the Lonnie niobium deposit, British Columbia, Canada. *In: Geological Fieldwork 2012.* British Columbia Ministry of Energy, Mines and Natural Gas, British Columbia Geological Survey, Paper 2013-1, 127–138.

Simandl, H.J., Fajber, R. & Paradis, S. 2014a. Portable X-ray fluorescence in the assessment of rare earth element-enriched sedimentary phosphate deposits. *Geochemistry: Exploration, Environment, Analysis*, **14**, 161–169.

Simandl, G.J., Paradis, S., Stone, R.S., Fajber, R., Kressall, R., Grattan, K., Crozier, J., and Simandl, L.J. 2014b. Applicability of handheld X-ray fluorescence spectrometry in the exploration and development of carbonatite-related niobium deposits: a case study of the Aley carbonatite, British Columbia, Canada. *Geochemistry: Exploration, Environment, Analysis*, **14** (3), 211–221.

Thomas, M.D., Ford, K.L. & Keating, P. 2011. *Exploration geophysics for intrusion-hosted rare earth metals*. Geological Survey of Canada, Open File 6828. doi:10.4095/288092

Trofanenko, J., Williams-Jones, A.E. & Simandl, G.J. 2014. The nature and origin of the carbonatite-hosted Wicheeda Lake rare earth element deposit. *In: Geological Fieldwork 2013*. British Columbia Ministry of Energy and Mines, British Columbia Geological, Survey Paper 2014-1, 213–225.

Overview of porphyry Cu indicator minerals

Karen D. Kelley

U.S. Geological Survey, Box 25046, Mail Stop 973, Denver, Colorado 80225 U.S.A.

**Corresponding author's e-mail: kdkelley@usgs.gov*

The porphyry Cu indicator mineral (PCIM) method was developed by Averill (2007) with a focus on porphyry deposits in arid regions such as the Atacama Desert. Recent case studies have tested the usefulness of the method in identifying concealed deposits in glaciated environments, including those in Alaska, USA (Kelley *et al.* 2011, 2013a) and British Columbia, Canada (Bouzari *et al.* 2011; Celis *et al.* 2013; Plouffe *et al.* 2013; Hashmi *et al.* 2014; Ferbey *et al.* 2014). Results suggest that the PCIM method is a powerful tool in the exploration for porphyry deposits in arctic regions.

This overview focuses on deposits in glaciated terranes, with emphasis on southwest Alaska. The Pebble Cu-Au-Mo porphyry deposit (Fig. 1) contains one of the largest resources of copper and gold in the world (Kelley *et al.* 2013b). Except for two small surface exposures, the deposit is buried by glacial deposits, and locally by post-mineralization volcanic and sedimentary rocks that underlie the glacial deposits. Numerous additional porphyry deposits, geologically and geochemically similar to Pebble, are located within the Pebble district. In addition, the Audn-Iliamna porphyry prospect, which is southwest of Pebble, is entirely concealed by up to ~210 m of glacial materials. The PCIM method was applied to both areas, and comparison of the Alaskan examples with those from deposits in British Columbia suggest many similarities with regards to the dominant indicator mineral species present in bedrock and till, and their physical or chemical characteristics.

PORPHYRY Cu INDICATOR MINERALS IN BEDROCK AND TILL

Indicator minerals are defined as those that are heavy (>2.8 S.G.) and thus concentratable, coarse-grained, readily identifiable, and sometimes chemically stable in weathered surficial sediments (i.e. resistate). Identification of gold-grain dispersal trains in tills is perhaps the most effective, because the combination of gold-grain abundance, size, shape, flatness, and fineness may provide information about the source and transport distance. Although the gangue mineralogy of porphyry deposits and their associated alteration zones is variable, there is some commonality among resistate minerals. Apatite, garnet, rutile, titanite, and zircon are commonly associated with many calc-alkaline and alkaline porphyry deposits in Alaska and British Columbia (Table 1). Most of these minerals are stable in oxidizing conditions and thus, in studied examples, are also observed in till. Tourmaline, corundum, and epidote are occasionally components of bedrock or till near some deposits.

Many of the resistate porphyry minerals also occur in barren igneous or other rock types, and therefore their presence in rock or till samples may or may not be significant. However, unique physical or chemical properties of the minerals can indicate their association with mineralized porphyry systems. For example, garnet in porphyry deposits is typically Fe-Ca-Mn-rich (primarily andradite but also grossular or spessartine) and epidote is characteristically rich in Mn (Averill 2011). Recent studies have shown that Mn concentrations in epidote decrease systematically with distance from a deposit, suggesting it may be used to vector to mineralized porphyry systems (Cooke *et al.* 2014). Cathodoluminescence studies show that apatite associated with K-silicate altered rocks from porphyry deposits in British Columbia luminesce green compared to yellow luminescing apatite in fresh rock, reflecting differences in chemistry (Bouzari *et al.* 2011). Kelley *et al.* (2011) report very high V concentrations (avg. 6.3 wt%) in black rutile from rocks affected by potassic alteration at Pebble compared to rutile associated with barren igneous rocks, or to other porphyry deposits (0.2–1.3 wt%) for which data are available (Scott 2005).

Sulphide minerals are generally considered unstable under oxidizing conditions and therefore do not survive weathering processes. Molybdenite and chalcocite may be present in bedrock samples (e.g. Pebble) but physical characteristics (low

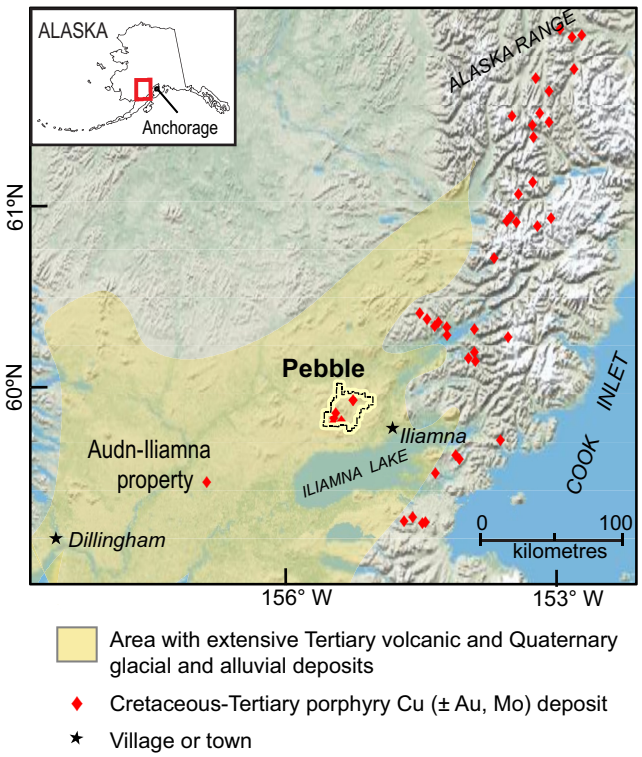

Fig. 1. Map of southwestern Alaska showing extensive cover by Tertiary and Quaternary deposits and locations of known porphyry deposits. The deposits in the Pebble district and Audn-Iliamna region were tested with the porphyry Cu indicator mineral (PCIM) method.

Table 1. Summary of major indicator minerals in bedrock and till from porphyry Cu deposits in glaciated terranes (compiled from Bouzari *et al.* 2011; Celis *et al.* 2013; Kelley *et al.* 2011, 2013; Plouffe *et al.* 2013; Hashmi *et al.* 2014).

Mineral	Present in Bedrock^	Present in Till*
Apatite	CM, GC, G, HV, L, MM, MP, P	P, MP
Chalcopyrite	present in most deposits	HV, MP
Chalcocite	P	
Epidote		AI, P, MP, WJ
Garnet	GC, L, MP	AI, P
Gold	present in most deposits	AI, MP, P
Jarosite	MM	AI, P
Magnetite	HV, MM, MP	
Molybdenite	P	
Monazite	E	
Pyrite	present in most deposits	AI, P
Rutile	BL, HV, MM P	
Titanite	CM, MM, MP, P	AI, P
Tourmaline	HV	AI
Zircon	A, CM, MM, MP	AI, P

*absence of mineral in till from British Columbia deposits is largely a result of lack of study of these deposits, not absence of mineral; lack of minerals in till from the Audn-Iliamna prospect and Pebble deposit is because mineral was not observed

^absence of mineral in bedrock from the Audn-Iliamna deposit is largely a result of lack of study of these deposits, not absence of mineral

British Columbia deposits: A - Ajax; BL - Babine Lake; CM - Copper Mountain; E - Endako; G - Granisle; GC - Galore Creek; HV - Highland Valley; L - Lorraine; MM - Mt. Milligan; MP - Mt. Polley; WJ - Woodjam

Alaskan Deposits: AI - Audn-Iliamna; P - Pebble

hardness) make them vulnerable to glacial crushing and therefore they are not observed in tills. However, some sulphides survive; for example, tills from the Highland Valley and Mt. Polley deposits contain chalcopyrite (Table 1). Chalcopyrite is known to be reasonably stable in till (Averill 2007), and thus the absence in till (e.g. Alaskan deposits; Table 1) suggests either that pre-glacial supergene alteration of the original hypogene mineralization was extreme, or there was in situ post-glacial weathering and oxidation of glacially transported chalcopyrite grains (Averill 2011; Kelley *et al.* 2011).

The presence of resistate indicator minerals in mineralized bedrock but not in till down-ice from mineralization (e.g. rutile at Pebble, Table 1) may be attributed to low overall abundance or inhomogeneous distribution in the rocks, or it may be attributable to grain size. Indicator mineral counts are reported for the >0.25 mm (>250 μm) grains. If a given mineral occurs in bedrock as fine, silt-sized grains intergrown with other minerals, these resulting particles may be >0.25 mm, explaining their detection in bedrock samples. During glaciation, rock is broken down along grain boundaries into individual mineral constituents. Therefore, a mineral such as rutile, which undoubtedly is present in the till, probably occurs in the silt-sized fraction (Kelley *et al.* 2011).

It may be even more common for indicator minerals to be detected in tills but not bedrock samples (e.g. andradite garnet, Mn-epidote, and jarosite at Pebble, Table 1). Such cases suggest either that the bedrock samples are not representative of all of the mineralogically diverse zones, or that glacial erosion took place at a higher level of the porphyry system than currently exposed in outcrop or subsurface. Of particular interest is the occurrence of jarosite in till samples down-ice of Pebble, but not in bedrock. Its presence in till suggests that a preglacial supergene cap existed over the deposit (Kelley *et al.* 2011).

CASE STUDY: SOUTHWEST ALASKA

Based on the distribution of known deposits, southwest Alaska has enormous potential for Cretaceous-Tertiary porphyry-style mineralization yet the area is largely underexplored, due in part to limited exposure and extensive cover by volcanic-sedimentary rocks and glacial deposits (Fig. 1). It is thus critical to develop new and innovative exploration methods that will assist in the search for concealed deposits. The PCIM method was applied at two known porphyry deposits/occurrences: the giant Pebble deposit and surrounding occurrences within the Pebble district and the Audn-Iliamna prospect about 90 km southwest of Pebble. The mineralogical data and details of sampling and processing methods are in Anderson *et al.* (2011).

Results show that the best indicator minerals from the Pebble (+/- Audn-Iliamna) regions are gold, andradite garnet, Mn-epidote, and jarosite. Other indicator minerals such as apatite, titanite, and zircon are present in till samples (Table 1) but based on their distribution, a direct tie to mineralization is not evident (Kelley *et al.* 2011).

Gold abundance and morphology

Gold-grain abudance includes visible gold identified during panning and that observed during processing in the laboratory; sizes of grains range from 15 to 700 μm. Most tills, including some up-ice from both the Pebble and Audn-Iliamna deposits contain gold (Fig. 2). However, tills from glacial moraines immediately adjacent to Pebble (Fig. 3a) contain 3–30 times the number of gold grains compared to samples up- or down-ice, and the number of grains decreases in the down-ice direction. Abundant gold is also present in tills near porphyry mineral occurrences/prospects in the southwest part of the Pebble district (Fig. 2a). The greatest abundance of modified and pristine grains (as opposed to reshaped grains) is in proximity to mineralization, indicating either short transport distances, or in situ weathering of transported chalcopyrite grains (host to most gold at Pebble) (Kelley *et al.* 2011).

Surprisingly similar results are shown for the Audn-Iliamna prospect (Fig. 2b) despite the fact that the entire area is covered by up to 210 m of glacial deposits from at least two major stages of glaciation, and sand dunes cover much of the central part of the claim area (Fig. 3b). Tills with the most gold grains, especially those with modified and pristine shapes occur about 5 to 10 km west of the claim blocks (Fig. 2b), consistent with the westward and southwestward directions of ice transport during the older and younger glaciation stages, respectively.

Similar anomalous abundances of gold grains in till are dispersed at least 4.9 km down-ice of the Mt. Polley deposit in British Columbia (Plouffe *et al.* 2013; Hashmi *et al.* 2014). The similarities and consistency in results from Canadian deposits with those from southwest Alaska suggest that gold-grain abundance is a potentially reliable tool for identifying porphyry Cu deposits in glaciated terranes, even those that have experienced multiple glaciation events.

Epidote, garnet, and jarosite

Yellow andradite garnet ($Ca_3Fe_2Si_3O_{12}$) is widespread and

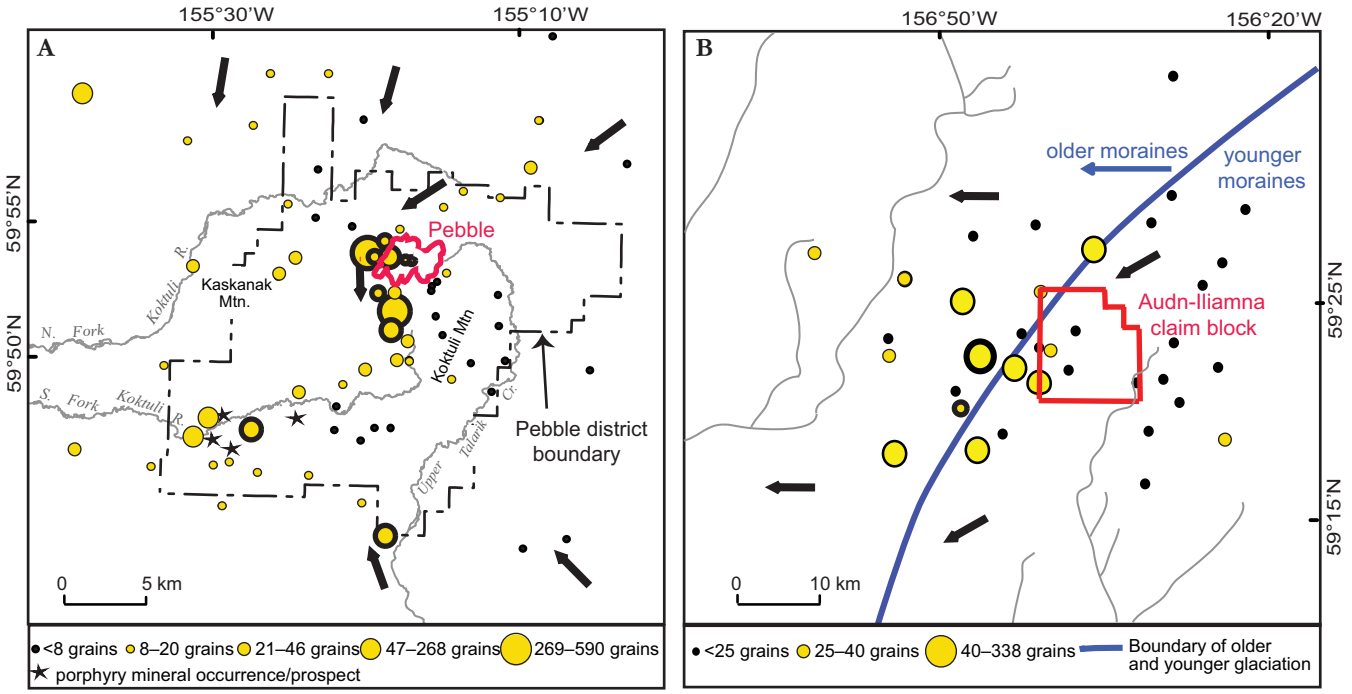

Fig. 2. Gold abundance normalized to 10 kg in till samples (15–700 µm size range). **a)** Pebble deposit and district (n = 70) and **(b)** Audn-Iliamna region (n=37). Heavy black line around symbol indicates >65% of grains are pristine or modified. Stars are porphyry mineral occurrences/prospects within the Pebble district. Heavy black arrows are ice-flow directions. Modified from Kelley et al. (2011) and Kelley et al. (2013a).

abundant in till samples (0.25–5.0 mm fraction) from Pebble (Fig. 4a). With one exception, all samples up-ice of Pebble contain <10 grains of garnet (normalized to 10 kg of till), samples adjacent to Pebble contain 10–20 grains, and samples with the most grains (>40) occur southwest and further down-ice of Pebble, in close proximity to the smaller mineral occurrences (Fig. 4a).

The lack of garnet in bedrock samples from Pebble does not preclude its presence in mineralized/altered rocks. It is common in the periphery of some deposits, for example, the Mt. Polley, Galore Creek, and Lorraine deposits in British Columbia (Bouzari *et al.* 2011). The abundance of garnet in tills from Pebble may also reflect peripheral zones or garnet-epidote-quartz skarns associated with some of the porphyry prospects (Kelley *et al.* 2011). Garnet is abundant in tills from the Audn-Iliamna area, but its distribution is not clearly linked with the location of the deposit. Three samples with the most abundant garnet grains occur west of the claim block, but many other samples northeast and east of the block also contain abundant garnet.

The distribution of Mn-epidote closely mimics the distribution of garnet in the Pebble till samples (Fig. 4a). All samples up-ice and in close proximity to Pebble are mostly free of epidote, whereas samples down-ice of Pebble that contain relatively abundant garnet also contain abundant (up to 40 grains/10 kg) epidote. Anomalous concentrations of epidote are also reported by Hashmi *et al.* (2014) in till down-ice of the Mt. Polley deposit. The results suggest that the combination of garnet and epidote in till samples is a powerful means for identifying buried porphyry Cu-Au deposits.

Jarosite occurs in about 28 till samples from Pebble (70 total) with a wide range in abundance (1–2,500 grains/10 kg; Fig. 4b). The distribution is more restricted than that of gold grains. All samples up-ice and distal from known mineralized

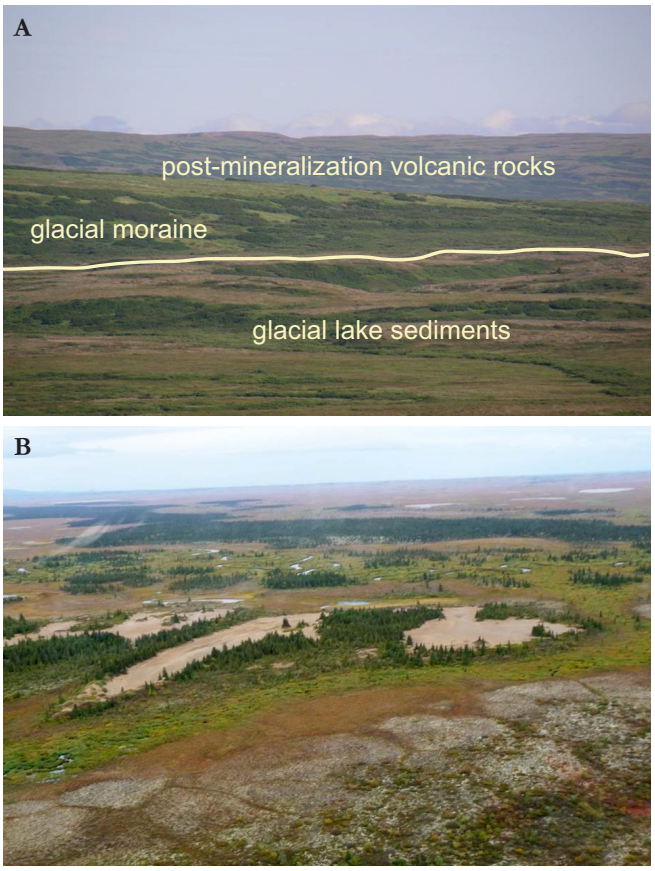

Fig. 3. Photographs taken from **(a)** the Pebble deposit looking southeast showing the extent of the glacial deposits and the Tertiary volcanic rocks that overlie the deposit, and **(b)** the Audn-Iliamna area showing the glacial deposits and sand dunes that cover much of the central part of the claim area.

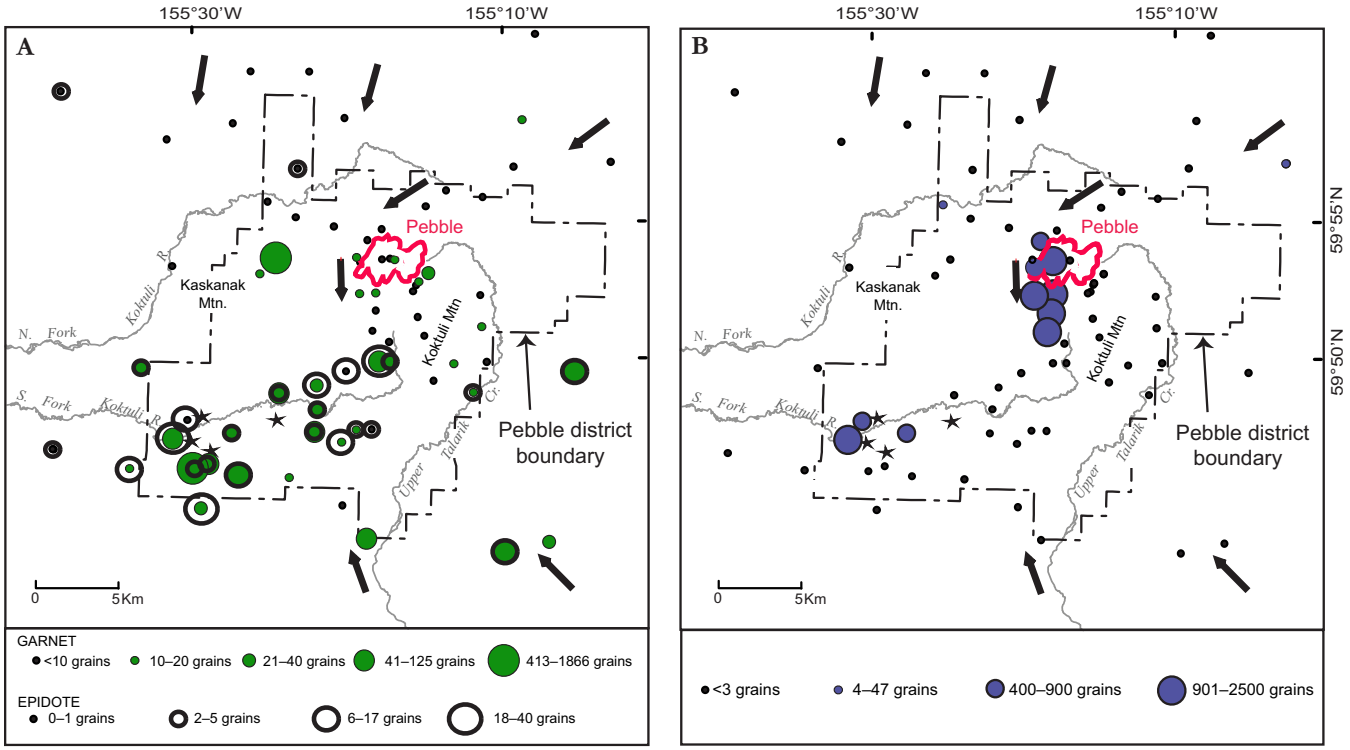

Fig. 4. Distribution of **(a)** andradite garnet and Mn-rich epidote and **(b)** jarosite in the 0.25–0.5 mm (250–500 μm) fraction of till samples from the Pebble region. Stars are porphyry mineral occurrences/prospects within the Pebble district. Heavy black arrows are ice-flow directions.

areas either lack jarosite or contain only trace amounts. The most abundant jarosite occurs in samples adjacent to and within 7 to 8 km down-ice of the Pebble deposit (Fig. 4b). Ages derived from $^{40}Ar/^{39}Ar$ dating techniques (ca. 8 Ma) suggest that the jarosite formed prior to glaciation, perhaps as a result of oxidation and supergene enrichment. Assuming this is true, it suggests that the level of erosion by glacial processes was shallow (Kelley *et al.* 2011). The jarosite grains from Pebble are among the first encountered in till samples near porphyry deposits, including other samples from Alaska and Yukon (Stu Averill, oral comm., 2008).

CONCLUSIONS

Indicator minerals in till samples are an effective tool for identifying porphyry deposits in glaciated terranes. Detailed case studies of the Pebble and Audn-Iliamna area suggest the best indicator mineral is gold, which was detected in dispersal trains that extend at least 5 to 10 km down-ice from the deposits. The distribution of andradite garnet and Mn-epidote effectively outlines the Pebble deposit and other occurrences in the district, but is less distinct at Audn-Iliamna. Jarosite distribution at Pebble is particularly informative as (1) it is the first example of a porphyry deposit with abundant jarosite in till samples, (2) it is effective in delineating the deposit, (3) it suggests formation of supergene mineralization, and (4) it indicates the level of glacial erosion was probably shallow. Comparison of Alaskan studies to those underway in Canada suggests many similarities in the characteristics of indicator minerals.

REFERENCES

Anderson, E.D., Smith, S.M., Giles, S.A., Granitto, M., Eppinger, R.G., Bedrosian, P.A., Shah, A.K., Kelley, K.D., Fey, D.L., Minsley, B.J. & Brown, P.J. 2011. *Geophysical, geochemical, and mineralogical data from the Pebble Cu-Au-Mo porphyry deposit area, southwestern Alaska: Contributions to assessment techniques for concealed mineral resources*. U.S. Geological Survey, Data Series 608, 46 p.

Averill, S.A. 2007. Recent advances in base metal indicator mineralogy: an update from Overburden Drilling Management Limited. *EXPLORE, Newsletter for the Association of Applied Geochemists*, **134**, 2–6.

Averill, S.A.2011. Viable indicator minerals in surficial sediments for two major base metal deposit types: Ni-Cu-PGE and porphyry Cu. *Geochemistry: Exploration, Environment, Analysis*, **11**, 279–297.

Bouzari, F., Hart, C.J.R., Barker, S. & Bissig, T. 2011. *Porphyry Indicator Minerals (PIMs): A new exploration tool for concealed deposits in south-central British Columbia*. Geoscience BC, Report 2011-17, 31 p. http://www.geosciencebc.com/i/project_data/GBC_Report2011-7. GBC_Report2011-07_BCMEM%20OF2011-1.pdf [November 23, 2012].

Celis, M.A., Hart, C.J.R., Bouzari, F., Bissig, T. & Ferbey, T. 2013. Porphyry Indicator Minerals (PIMs) from alkalic porphyry copper-gold deposits in south-central British Columbia (NTS 092, 093). *In: Geoscience BC Summary of Activities 2012*. Geoscience BC, Report 2013-1, 37–46. http://www.geosciencebc.com/s/DataReleases.asp.

Cooke, D.R., Baker, M., Hollings, P., Sweet, G., Chang, Z., Danyuskevsky, L., Gilbert, S., Zhou, T., White, N., Gemmell, J.B. & Inglis, S. 2014. New advances in detecting the distal geochemical footprints of porphyry systems – epidote mineral chemistry as a tool for vectoring and fertility assessments. *In:* Kelley, K.D. & Golden, H.C. (eds.) *Building Exploration Capability for the 21st Century*. Society of Economic Geologists, Special Publication 18, 127–152.

Ferbey, T., Plouffe, A. & Anderson, R.G. 2014. *An integrated approach to search for buried porphyry-style mineralization in central British Columbia using geochemistry and mineralogy: a TGI-4 project*. Geological Survey of Canada, Current Research 2014-2, 12 p. doi:10.4095/293130

Hashmi, S., Ward, B., Plouffe, A., Ferbey, T. & Leybourne, M. 2014. *Geochemical and mineralogical dispersal in till from the Mount Polley Cu-Au porphyry deposit, central British Columbia, Canada*. Geological Survey of Canada, Open File 7589, poster. doi:10.4095/293682

Kelley, K.D., Eppinger, R.G., Smith, S.M. & Fey, D.L. 2011. Porphyry copper indicator minerals in till as an exploration tool: Example from the giant Pebble porphyry Cu-Au-Mo deposit. *Geochemistry: Exploration, Environment, Analysis*, **11**, 321−334.

Kelley, K.D., Eppinger, R.G., Anderson, E.D. & Cosca, M.A. 2013a. Exploration for porphyry deposits in glaciated environments: A case study from the Iliamna/Audn region, southwest Alaska, with comparisons

to the Pebble district. *In: Abstracts*. 26th International Applied Geochemistry Symposium, Rotorua, New Zealand.

KELLEY, K.D., LANG, J. & EPPINGER, R.G. 2013b. The giant Cu-Au-Mo deposit and surrounding region, southwest Alaska: Introduction. *Economic Geology*, **108**, 397–404.

PLOUFFE, A., FERBEY, T., ANDERSON, R. G., HASHMI, S., WARD, B.C. & SACCO, D.A. 2013. *The use of till geochemistry and mineralogy to explore for buried porphyry deposits in the Cordillera – preliminary results from a TGI-4 Intrusion-related Ore Systems Project*. Geological Survey of Canada, Open File 7367, poster. doi:10.4095/292555

SCOTT, K.M. 2005. Rutile geochemistry as a guide to porphyry Cu-Au mineralization, Northparkes, New South Wales, Australia. *Geochemistry: Exploration, Environment, Analysis*, **5**, 247–253.

The Blackwater gold-spessartine-pyrolusite dispersal train, British Columbia, Canada: Influence of sampling depth on indicator mineralogy and geochemistry

Stuart A. Averill

Overburden Drilling Management Limited, 107-15 Capella Court, Nepean, Ontario, Canada K2E 7X1
**Corresponding author's e-mail: odm@storm.ca*

New Gold Inc. (New Gold), a Canadian mining company with operations in four countries, holds a highly prospective property known as Blackwater in south-central British Columbia, Canada (Fig. 1). This large property contains two significant Au-Ag deposits, Blackwater in the east and Capoose to the west (Fig. 2).

In 2011, New Gold collected 12 samples of alluvial gravel from first- and second-order drainages downslope from the Blackwater deposit and submitted these samples to the Ottawa laboratory of Overburden Drilling Management Limited (ODM) for heavy indicator mineral testing. As expected, the samples yielded only low levels of gold grains because ~90 percent of gold particles are, by nature, only of silt size (Averill 2001) and this hinders their settling to such a degree (Stokes' Law) that they are expelled rather than concentrated by high-energy, gravel transporting streams. However, some samples were found to be distinctly anomalous in another, coarser grained indicator mineral – spessartine – a manganiferous garnet ($Mn_3Al_2(Si0_4)_3$) which occurs in the altered host rocks of both the Blackwater (Simpson *et al.* 2012; Christie *et al.* 2014) and Capoose (Andrew 1988; Awmack *et al.* 2010) deposits.

Based on the positive spessartine response obtained from the gravel, a systematic indicator mineral survey was conducted in 2012 across much of the Blackwater property. Most of the samples collected were of till rather than gravel because till is unsorted and its matrix, though silt–biased, also contains sand grains of all sizes. Therefore samples collected within the mineral dispersal trains of any Blackwater- or Capoose-type mineralized zones on the property would be expected to contain both fine gold and coarse spessartine grains. The program was very successful, with large, strong gold-spessartine dispersal anomalies identified at both deposits along with other indicator mineral anomalies.

The Blackwater and Capoose deposits have only thin till cover but the till in some parts of the property is thick, potentially compromising the effectiveness of surface sampling. Therefore, in 2013, the till in these thickly covered areas was sampled from top to bottom by reverse circulation drilling. As well, four test holes were drilled on the Blackwater gold-spessartine dispersal train to investigate its subsurface mineralogy, geochemistry, and continuity.

The results obtained from the drilling and sampling programs would normally be confidential for an extended period but in recognition of their scientific importance and geochemical significance New Gold has authorized their early publication. Therefore, in this paper, the signature of the Blackwater dispersal train is described in more detail. In particular, it is shown that the mineralogy and geochemistry of the anomalous till samples are dependent to a significant degree on whether the samples were collected at surface or from the drillholes, i.e., whether the sampled till was oxidized or unoxidized.

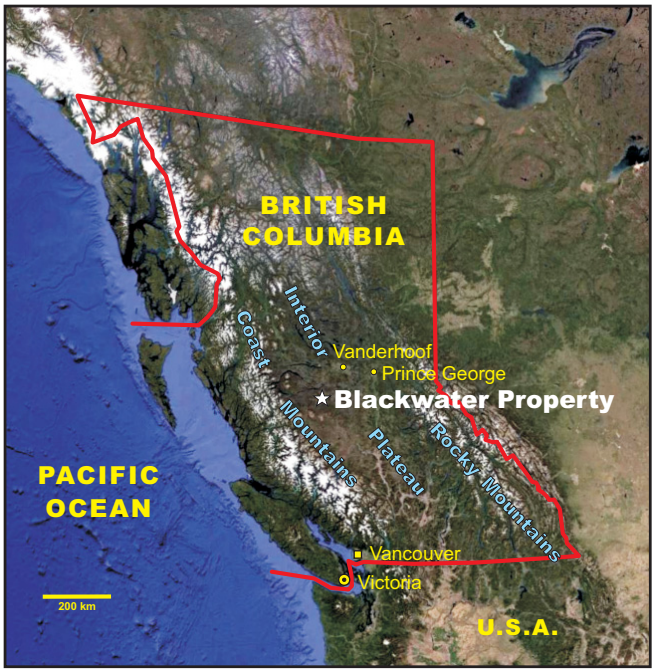

Fig. 1. Location of the Blackwater property.

PHYSIOGRAPHY AND QUATERNARY GEOLOGY

New Gold's Blackwater property is ~110 km southwest of the town of Vanderhoof (Fig. 1) on Highway 16, the northern Trans-Canada route, from which it is accessed by forest service roads. Physiographically it is located in the hilly terrain of the Nechako Plateau (Fig. 2). This plateau is part of the larger Interior Plateau of the Canadian Cordillera, which lies between the Rocky Mountains to the east and the Coast Mountains to the West (Fig. 1).

The Blackwater Au-Ag deposit lies on the northern slope of Mount Davidson, one of two peaks of the Fawnie Range on the property (Fig. 2). The Capoose deposit lies atop the other peak, Fawnie Nose. The base of Mount Davidson is ~1500 m above sea level. Its peak is at 1800 m and the Blackwater deposit is at 1600 m, well down the slope.

In the Late Pleistocene, the Blackwater area was glaciated repeatedly by the Cordilleran Ice Sheet, which migrated northeastward from the high mountains of the Coast Range. The last glacial event was the Fraser Glaciation from ca. 25,000 to 10,000 years ago (Fig. 3; Clague 1989) during which the ice sheet reached its most easterly limit. The direction of ice flow was

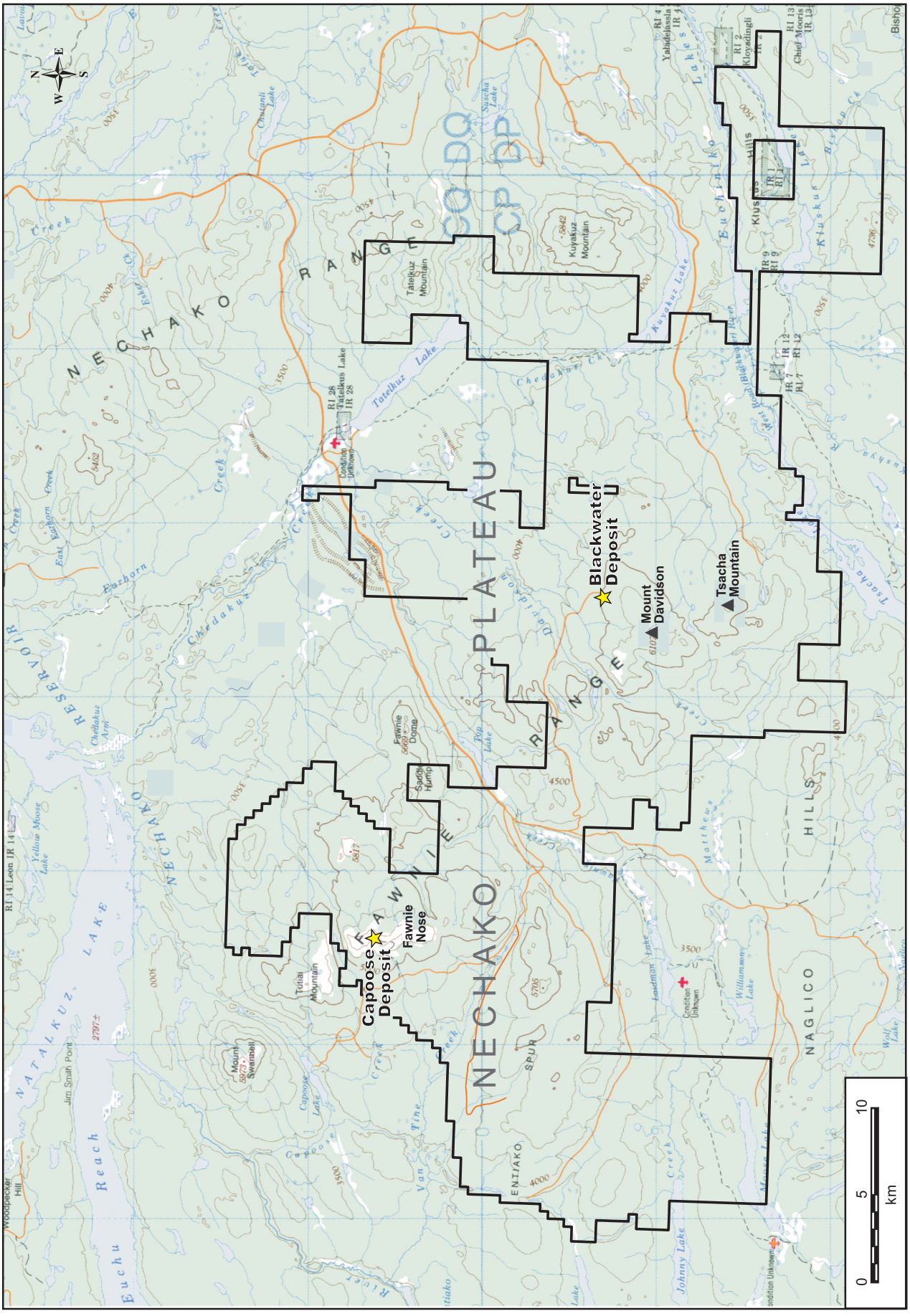

Fig. 2. Topography and physiography of the Blackwater property.

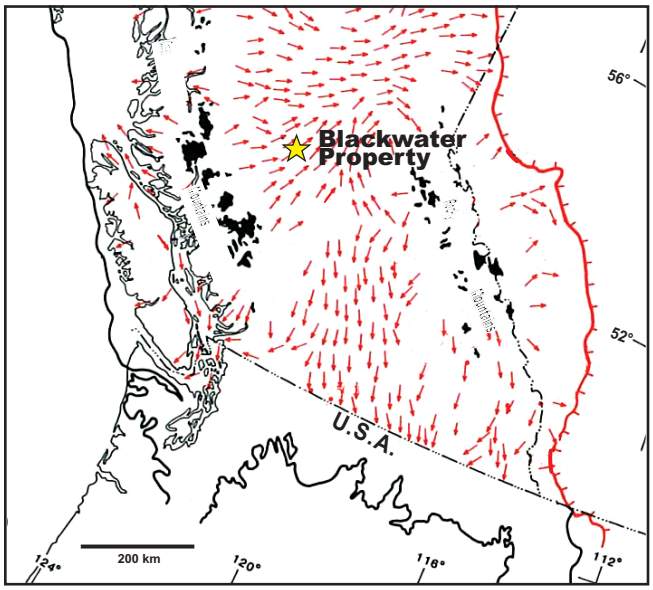

Fig. 3. Maximum extent and final flow directions in the Cordilleran Ice Sheet in south-central British Columbia. Modified from Clague (1989).

060°, which is recorded in the orientations of numerous drumlins, particularly in the lee of the mountains (Plouffe *et al.* 2004). Most of the till in the area is related to the Fraser Glaciation but a possibly older till horizon has been identified to the north (Plouffe & Levson 2001). The till is only 2 to 30 m thick over most of the Blackwater deposit (Fig. 4) but thickens rapidly downslope (i.e. glacially down-ice) to as much as 100 m (Fig. 5).

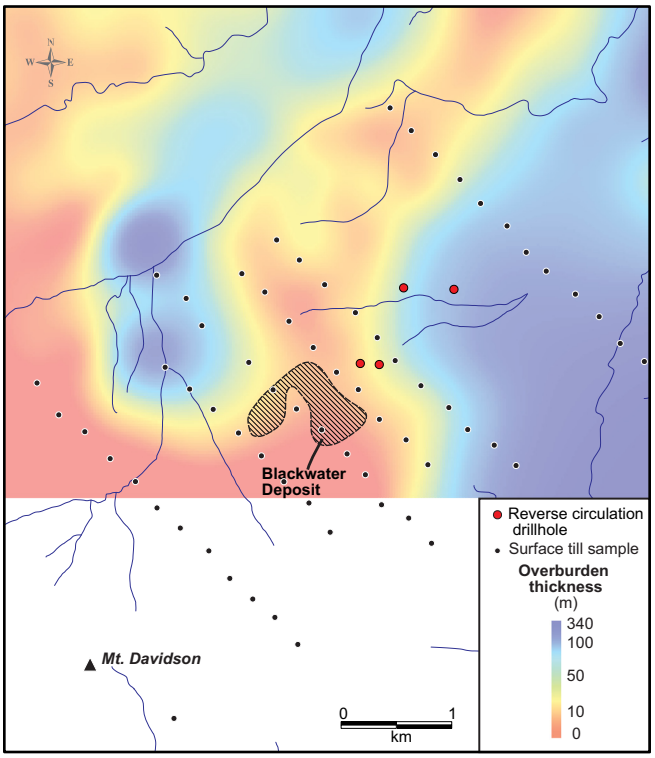

Fig. 5. Overburden thicknesses in the vicinity of the Blackwater deposit. Overburden thickness was determined from vertical condemnation holes drilled by New Gold. The locations of the 68 relevant surface till samples and four investigative reverse circulation drillholes are also shown.

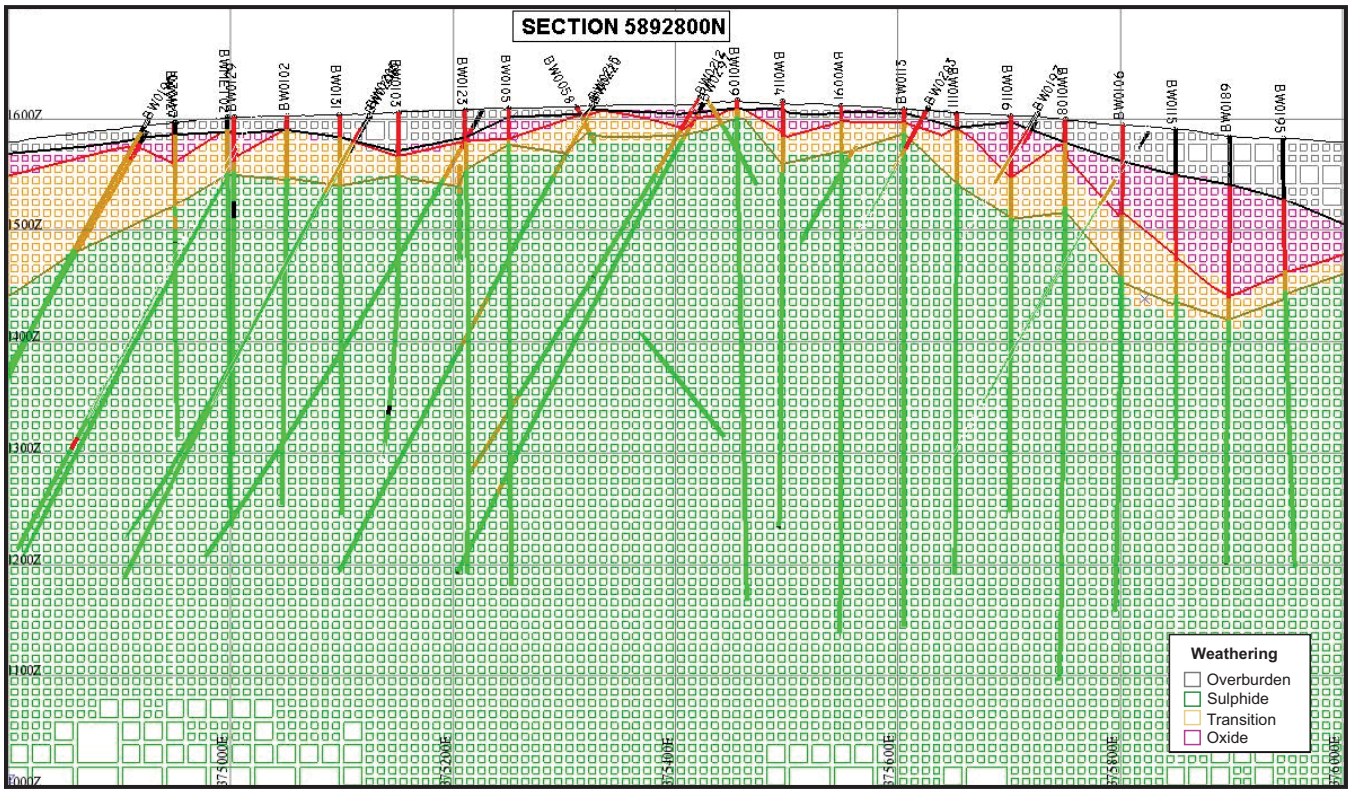

Fig. 4. East-west vertical longitudinal section through the Blackwater deposit showing the thickness of glacial till cover and depth of preglacial supergene alteration. Source: Simpson *et al.* (2012).

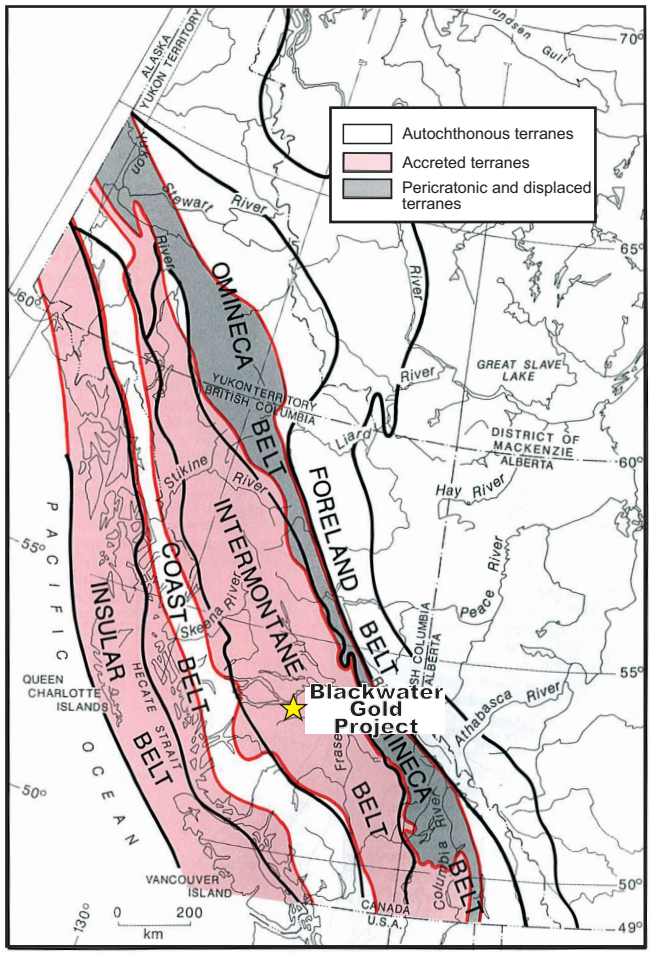

Fig. 6. Morphogeological belts and terranes of the Canadian Cordillera. Source: Gabrielse *et al.* (1991).

GEOLOGICAL SETTING

The Blackwater property is located centrally within the Intermontane Belt of the Western Cordillera (Fig. 6). It covers part of a structurally raised block or horst, the Nechako uplift. Within this uplifted block allochthonous, mainly submarine volcanic rocks of the Middle Jurassic and granitoid plutons of the Late Cretaceous are exposed in windows within a regionally extensive cover of autochthonous, terrestrial, Eocene and Miocene volcanic rocks (Diakow *et al.* 1997).

The Early to Middle Jurassic volcanic rocks were accreted tectonically from the ancestral Pacific Ocean onto the North American protocontinent in the Middle Jurassic (Monger & Price 2002) during construction of the Cordillera (Fig. 6). Diakow *et al.* (1997) assigned them to the bimodal Hazelton Group, which consists of typical island arc rhyolite flows and volcaniclastic sedimentary rocks of the Entiako Formation overlain by submarine basalt flows of the Naglico Formation. The northeastern slope of Mount Davidson, as far west as the Blackwater deposit, is underlain by the Entiako Formation (Fig. 7). On both the western slope and foot of the mountain, these older rocks are largely covered by Eocene andesitic to rhyolitic flows and tuffs of the Ootsa Lake Group.

The Blackwater deposit does not crop out; its geology is known only from drilling. The deposit occurs within and is hosted by an isolated, 2 km wide zone of rhyolitic to andesitic volcanic and volcaniclastic rocks of the Late Cretaceous Kasalka Group (Fig. 7). The Capoose deposit occurs in a similar setting. Regionally, the Kasalka Group is restricted to isolated volcanic centres, mostly at high elevations as at Blackwater and Capoose.

The Kasalka succession at the Blackwater deposit is much disrupted by faulting but primarly consists of massive to brecciated porphyritic andesite overlain successively by massive to laminated rhyodacitic tuff and heterolithic volcaniclastic breccia (Petersen *et al.* 2013). Gold mineralization is present in all lithologies but occurs mainly in the tuff and volcaniclastic breccia in association with sericite-silica alteration and 1–5% pyrite ± sphalerite. The sulphides occur mainly as disseminated grains but locally with quartz in stockwork veins (Looby *et al.* 2013; Petersen *et al.* 2013). The sericitic alteration appears to be superimposed on an earlier potassic hornfels that, in the outboard andesite, is recorded as replacement of primary hornblende phenocrysts by biotite + spessartine garnet ± pyrrhotite (Looby *et al.* 2013). Spessartine, however, also occurs in the sericitic alteration zone (Petersen *et al.* 2013), where it has been observed in quartz-garnet-pyrite veinlets and appears to envelop pyrite grains that contain micron-scale gold inclusions (Looby *et al.* 2013), suggesting a late rather than early paragenesis.

Gold at Blackwater occurs mainly as micron-sized native grains and silver as argentite; visible gold is rare and restricted to quartz-pyrite veins (Petersen 2013). The mineralization has been determined to be epithermal and of the Zn-rich intermediate sulphidation variety (Petersen 2013; Looby *et al.* 2013; Petersen *et al.* 2013) although it is rather atypical of this style of alteration (Looby *et al.* 2013) due to the presence of spessartine garnet, a paucity of As, and the apparent absence of adularia. Recent work by New Gold has established a continuum between the Blackwater mineralization and porphyry-style mineralization on Tsacha Mountain, south of Mount Davidson (Fig. 2; M.A. Petersen, pers. comm. 2015).

FOOTPRINT OF THE BLACKWATER DEPOSIT

The Blackwater deposit is large with a NI43-101 compliant proven and probable mineral reserve of 8.17 Moz gold and 60.8 Moz silver in 344 Mt grading 0.74 g/t Au and 5.5 g/t Ag (Christie *et al.* 2014). Its subcrop beneath the till, i.e., the area exposed to glaciation, measures ~300 x 1000 m based on a 0.3 g/t Au cut-off (Figs. 5, 7). Therefore, despite its relatively low grade, the deposit and its alteration zone would be expected to be well reflected in the till, both mineralogically and geochemically. Both primary and secondary indicator minerals could be present because 10 to 100 m of the former (preglacial) supergene oxide cap remains over most of the deposit (Fig. 4).

METHODS

Sample collection

In the surface sampling program in 2012, samples of till were collected at 300 m intervals on lines oriented northwest-southeast, orthogonal to the northeast ice-flow direction. The locations of the 68 samples collected closest to and/or glacially in line with the Blackwater deposit are shown in Figure 7. The line spacing for these samples varied from 1500 m for the most distal sample sites to 500 m over the deposit, providing coverage at a density of ~2 to 6 samples per km^2.

ODM, with assistance from New Gold, collected samples from hand-dug pits at a depth 0.5 to 1 m within the C-horizon

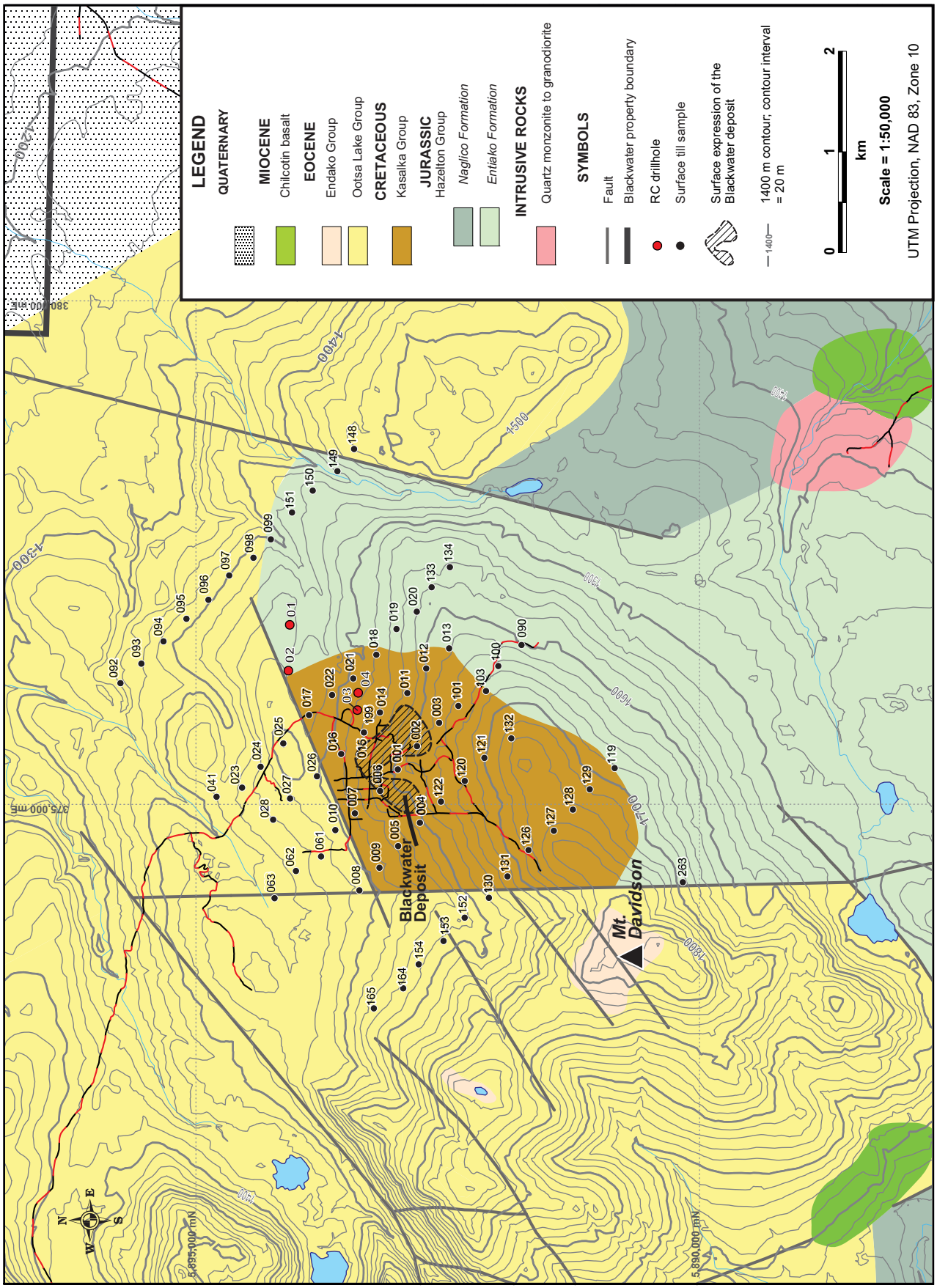

Fig. 7. Locations of the surface till samples and reverse circulation drillholes in relation to the underlying rock formations. Bedrock geology modified from Massey *et al.* (2005) and Simpson *et al.* (2012).

Figure 8. Typical till sample pit. The sample is normally collected at a depth of 0.5 to 1 m from the C-horizon of the soil profile which is less oxidized than the overlying B-horizon but still depleted of sulphide minerals as illustrated by the extracted heavy mineral concentrate. At this site, which is not on the Blackwater property, duplicate 10 kg samples of sieved till matrix were taken for quality control. Source: ODM archives.

of the soil profile (Fig. 8). The till in the C-horizon is less oxidized than that in the B-horizon but the only sulphide mineral that survives to any degree is chalcopyrite (Averill 2001, 2013a), increasing the dependence of indicator mineral surveys on gold grains and chemically resistant oxide and silicate minerals. The samples were rubbed through an 8 mm sieve to obtain 12 to 13 kg of -8 mm material, sufficient to yield ~10 kg of -2 mm till matrix for indicator mineral processing at the laboratory.

The RC drilling program in 2013 used a rig that was purpose-built for efficient, continuous sampling of unconsolidated surficial sediments of any consistency and bedrock of any hardness. All holes were logged and sampled by ODM. In till sections, 10 kg samples of wet-screened -2 mm material, which includes fine drill cuttings from the till clasts in addition to the matrix of the till, were collected over intervals ranging from 1 m in thin sections to 2 to 3 m in sections over 20 m thick. The till below a depth of 2 to 3 m was found to be unoxidized and thus not depleted in sulphide mineral grains. Seventy-one till samples were obtained from the four holes drilled down-ice from the Blackwater deposit, with Hole 01 abandoned at a depth of 43.5 m without reaching bedrock.

Sample processing

In ODM's mineral extraction laboratory, the oxidized surface samples were processed to extract (a) the specific gravity (SG) >3.2 heavy mineral fraction for indicator mineral study; and (b) a large, ~30 g subsample of the -0.063 mm silt + clay fraction for geochemical analysis. The heavy mineral concentrates (HMCs) were not analyzed because, with the till being oxidized and depleted of sulphides, they would contain negligible base metals and gold only in the form of liberated grains, most of which were observed during processing and physically measured to determine their Au value.

A second, lower density concentrate of SG 2.8 to 3.2 had been prepared from the 12 gravel samples collected in 2012 to check for possible jarosite dispersal from the supergene zone of the Blackwater deposit because jarosite is a key indicator mineral at the glaciated Pebble porphyry Cu-Au deposit in Alaska (Kelley *et al.* 2011). Only a few jarosite grains were found; therefore, preparation of the low-density concentrates was discontinued.

SG >3.2 HMCs were also prepared from the odd-numbered and bottom samples collected from the drillholes. Since the till at depth was unoxidized and sulphide-bearing, the HMCs rather than the -0.063 mm till fines were analyzed geochemically. Only the -0.25 mm fraction of the concentrates was analyzed; the coarser, 0.25 to 2 mm fraction was reserved for indicator mineral determination.

The HMCs were extracted from the till samples using a well established process involving successive separations by tabling, heavy liquids, magnetism, paramagnetism, and sieving to produce 0.25–0.5 mm, 0.5–1 mm, and 1–2 mm nonferromagnetic heavy mineral fractions with the finest, 0.25–0.5 mm fraction further separated into four subfractions of varying paramagnetic susceptibility to facilitate indicator mineral identification. The gold grains were counted after the first separation (i.e. tabling), then returned to the table concentrate. The gold-grain counts were not normalized because the sample weights were relatively constant.

Indicator mineral identification

All six nonferromagnetic heavy mineral fractions were thoroughly examined for indicator mineral grains by experienced mineralogists using a binocular microscope with scanning electron microscope (SEM) support to resolve any questionable grains. The number of grains of each indicator mineral in each of the three particle size ranges was either counted or estimated, depending on the number of grains present. For key minerals, either all of the grains or representative populations were put in vials to form an organized grain library. The overall mineralogy of each concentrate was also recorded systematically, mainly to identify any major changes in till provenance that might suggest the presence of more than one till horizon.

Sample analysis

All geochemical analyses were performed by Actlabs Limited in Ancaster, Ontario. The same analytical methods were used to analyze the -0.063 mm fines from the surface samples and the -0.25 mm HMCs from the drillhole samples. Au and As were determined by instrumental neutron activation (INA) analysis using a large split of the available sample material to ensure that most or all of the gold grains were represented. No pulverizing was required; therefore the gold grains remained intact. Base metals and other potential indicator elements were determined on a small split by inductively coupled plasma (ICP) analysis following aqua regia digestion.

RESULTS

Indicator mineralogy of the surface till samples

The surface sampling identified and outlined a strong indicator mineral dispersal train down-ice from the Blackwater deposit (Fig. 9). This dispersal train, hereinafter called the Blackwater train, is defined equally well by gold (Fig. 9A) and spessartine (Fig. 9B) grains although the margins of the spessartine train are more diffuse. The trend of the train is 060°, matching the azimuth of ice flow at the end of the Fraser Glaciation (Fig. 3). The train is ribbon-shaped and ~1300 m wide, or 300 m wider than the 1000 m footprint of the deposit at a 0.3 g/t Au cut-off grade. This suggests that the train reflects both the eco-

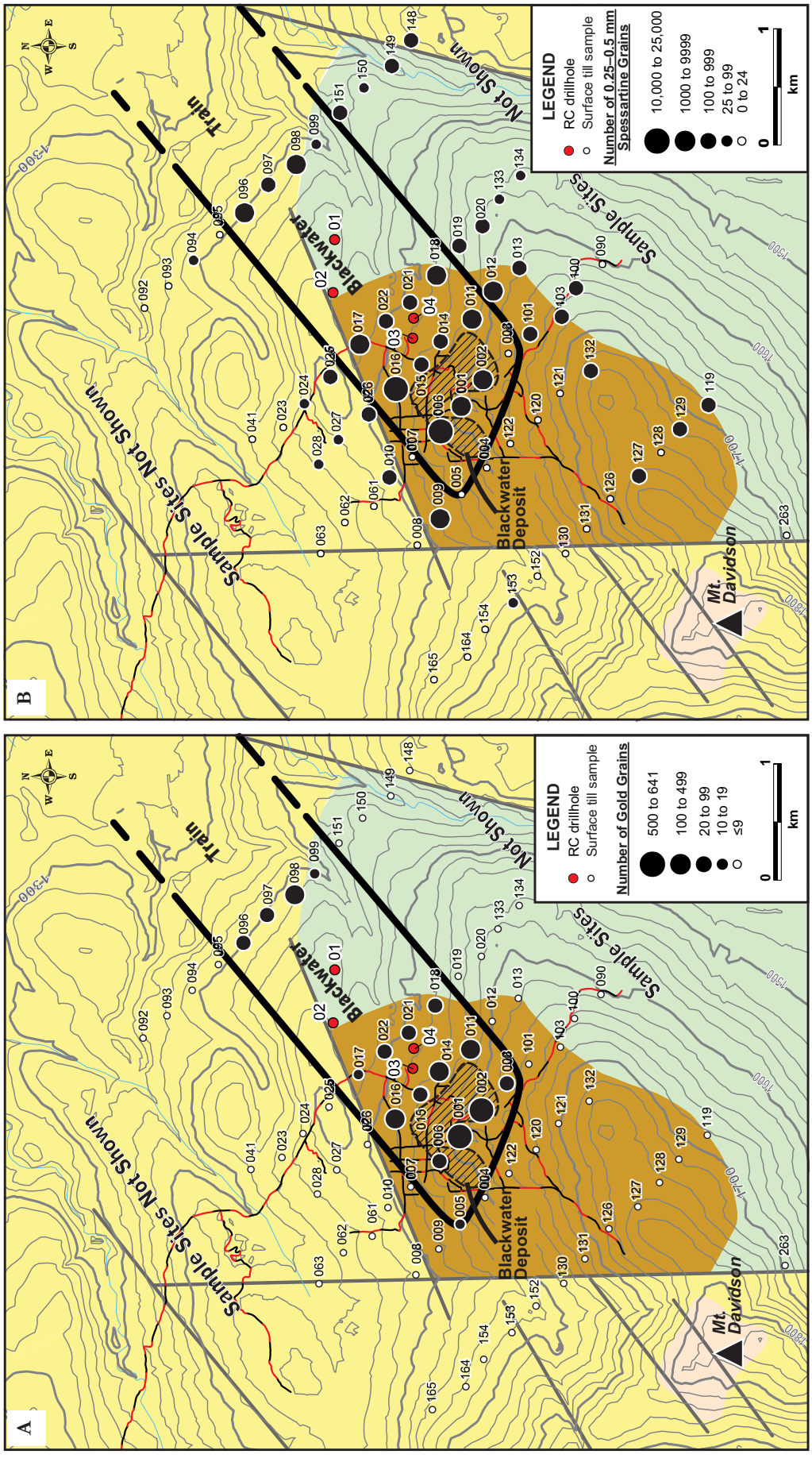

Fig. 9. Concentrations of **(A)** gold and **(B)** 0.25–0.5 mm spessartine grains in the surface till samples. See Figure 7 for bedrock lithologies.

Table 1. Indicator mineralogy and -0.063 mm geochemistry of the surface till samples collected along the Blackwater train. Only the four central samples on each line across and up-ice from the train are shown.

Distance Down-Ice from Centre of Deposit (m)	Sample No.	No. of Gold Grains				% Pristine or Modified	No. of Spessartine Grains (0.25–0.5 mm)	Geochemistry of -0.063 mm Fraction								
								ppb	ppm							%
		Total	Pristine	Modified	Reshaped			Au	Ag	As	Cu	Zn	Pb	Cd	Mo	Mn	S
-1500	152	1	0	0	1	0	15	< 2	< 0.2	7	8	50	11	< 0.5	3	317	0.02
	130	4	0	3	1	75	9	< 2	< 0.2	15.5	13	62	14	< 0.5	4	427	0.01
	131	1	0	0	1	0	8	< 2	< 0.2	47.1	13	61	9	< 0.5	3	372	0.05
	126	1	0	0	1	0	6	< 2	< 0.2	19.6	24	78	9	< 0.5	2	676	0.03
-500	005	10	2	6	2	80	16	< 2	< 0.2	7.7	6	52	13	< 0.5	< 2	234	0.01
	004	5	3	1	1	80	5	< 2	< 0.2	18	20	91	18	0.6	< 2	768	0.01
	122	1	0	0	1	0	0	8	0.8	12	18	207	31	1	4	393	0.02
	120	3	0	0	3	0	13	< 2	< 0.2	10.5	13	56	7	< 0.5	3	474	0.01
0	006	62	20	41	1	98	25,000	37	< 0.2	32	39	1620	49	8.5	< 2	1210	0.01
	001	641	180	446	15	98	2000	74	< 0.2	26.1	25	266	71	1.4	< 2	676	0.01
	002	561	287	257	17	97	1000	42	< 0.2	31.4	18	118	47	1	< 2	506	0.01
	003	23	3	17	3	87	3	11	< 0.2	21.6	11	95	10	0.6	< 2	547	0.01
+500	016	119	29	78	12	90	12,000	34	1.5	57.8	7	761	70	0.9	< 2	612	0.01
	015	26	8	18	0	100	800	< 2	< 0.2	12.8	24	125	17	0.6	< 2	1140	0
	014	151	68	78	5	97	500	19	< 0.2	11.7	10	120	26	0.6	< 2	475	0.01
	011	214	148	66	0	100	2500	14	< 0.2	24.9	18	208	66	2.7	< 2	1020	0
+1000	017	11	6	5	0	100	1500	< 2	0.6	9.5	5	158	79	0.5	2	195	0.01
	022	23	6	17	0	100	250	15	0.7	14.3	8	123	32	< 0.5	< 2	395	0.02
	021	44	17	25	2	95	400	13	0.2	8.8	9	133	20	0.6	< 2	326	0.01
	018	58	21	35	2	97	1200	36	0.3	7.5	8	101	45	0.6	< 2	325	0.01
+2500	096	32	0	16	16	50	2500	< 2	0.3	9.4	12	70	21	< 0.5	< 2	266	0.01
	097	28	0	12	16	43	800	7	0.3	9	12	115	25	< 0.5	3	270	0.01
	098	162	19	82	61	62	2000	9	0.3	6.8	12	100	45	< 0.5	2	300	0.01
	099	14	0	2	12	14	18	7	0.4	5.6	18	72	8	0.5	3	373	0.01

nomic core and lower grade margins of the deposit.

Sixteen samples were collected within the main part of the Blackwater train, four on each of four lines across the train (Fig. 9A). Of these, twelve were collected from 0 to 1000 m down-ice from the centre of the mineralized zone and the other four were collected 2500 m down-ice. All sixteen yielded significantly anomalous levels of gold grains, with the counts ranging from 10 to 641 grains per sample (Fig. 9A, Table 1). In contrast, the samples collected alongside and up-ice from the train consistently yielded <10 and mostly 0 to 5 grains, with the exception of sample No. 005 which was collected on the alteration envelope 500 m up-ice from the centre of the mineralized zone and yielded 10 gold grains. The four most distal samples on the dispersal train, on the line 2500 m down-ice from the deposit, still yielded from 14 to 162 grains (Table 1), suggesting that the total detectable length of the train is at least 3 km.

Approximately 90% of the recovered grains were silt-sized (Fig. 10) as expected because (a) most gold grains crystallize at this size in bedrock; and (b) the grains retain their sizes during glacial transport due to their malleability; i.e., they are deformed, not comminuted during transport (Averill 2001, 2013b). This is readily seen in Figure 10 where the gold grains in the most distal gold-rich sample, No. 098, which was collected 2500 km down-ice, have the same particle-size distribution as two gold-rich samples collected close to (sample No. 011) or directly over (sample No. 001) the deposit.

In the twelve samples collected within 1000 m of the deposit, 95 to 100% of the gold grains are either pristine or only partly modified (Table 1). In contrast, only 14 to 62% of the gold grains in the four distal samples, which were collected 2500 m down-ice, are of these morphologies. The rest are fully reshaped, reflecting the progressive grain modification that occurs with increasing transport distance (Averill 2001).

Three of the seventeen auriferous samples that define the Blackwater train (Fig. 9A), samples 003 and 005, which are beyond the economic limits of the mineralized zone, and sample No. 099, collected on the distal line, 2500 m down-ice, were not significantly anomalous in spessartine (Fig. 9B), yielding only 3 to 25 grains of 0.25–0.5 mm size (Table 1), which is only marginally above the regional spessartine background of 0 grains. The other fourteen samples yielded from 250 to 25,000 grains, with the highest counts being closest to the deposit. Due to the much higher concentration of spessartine grains than gold grains in the Blackwater train, the train should be detectable for a considerably greater distance using spessartine, possibly as far as 10 km down-ice from the Blackwater deposit.

While the highest spessartine concentrations occur within the limits of the gold dispersal train, significantly anomalous responses were obtained up to 1 km outboard on either side of the gold train and 1.5 km further up-ice on the southeastern side (Fig. 9B). The distribution of the outlying anomalous sam-

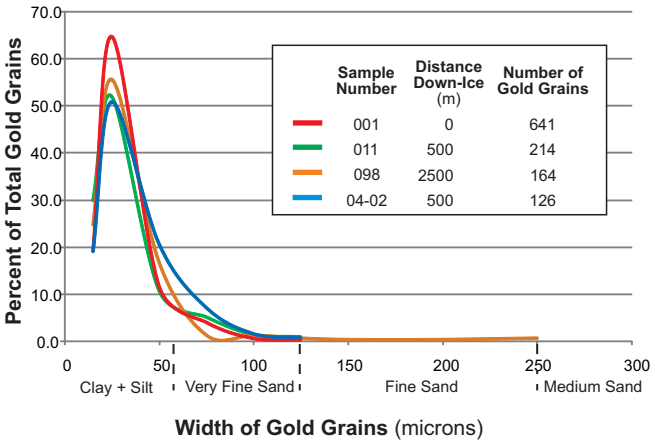

Fig. 10. Gold particle-size distribution in three oxidized, gold-rich surface till samples and in an unoxidized till sample from reverse circulation drillhole No. 04.

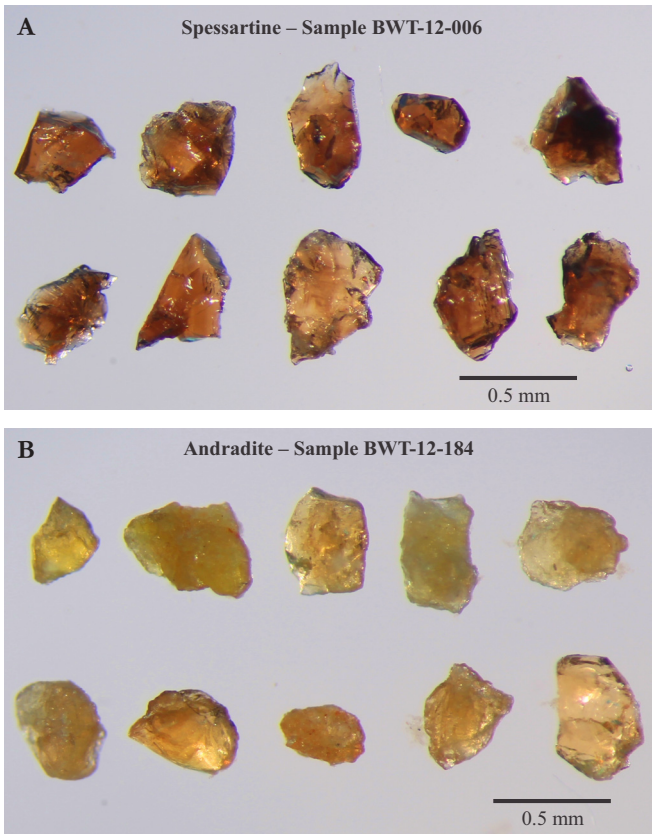

Fig. 11. Binocular microscope photographs of representative **(A)** spessartine and **(B)** andradite garnet grains from selected till samples.

ples relative to the Kasalka Group volcanic rocks suggests that all of the spessartine is derived from these rocks and thus that additional zones of spessartine alteration occur beyond the immediate alteration envelope of the Blackwater deposit.

The spessartine occurs as rather bland orange-brown grains (Fig. 11A) rather than as euhedral crystals, reflecting the relatively low temperatures and pressures of the near-surface environment in which it crystallized. Despite their blandness, the spessartine grains are readily recognizable in most of the HMCs due to an absence of almandine garnet, which reflects the essentially unmetamorphosed condition of even the oldest, Early Jurassic volcanic rocks in the Blackwater district. On some parts of the property, however, another variety of garnet, andradite, is very abundant in the till. This andradite is also a key indicator mineral, being derived from either skarns (Dawson & Kirkham 1996) or the propylitic alteration zones of porphyry Cu deposits (Averill 2011). Therefore it is critical that the spessartine and andradite grains in the till be differentiated. The only significant difference is that the andradite grains are of a slightly paler yellow-brown colour (Fig. 11B). Andradite occurs at much lower concentrations than spessartine in the study area, impeding its recognition, and it is probable that some grains were misclassified as spessartine.

Geochemistry of the -0.063 mm fraction of the surface till samples

The Au, Ag, As, Cu, Zn, Pb, Cd, Mo, Mn, and S analyses obtained from the -0.063 mm fines of the 24 surface till samples collected within and directly up-ice from the gold grain dispersal train (Fig. 9A) are presented in Table 1. The Blackwater deposit contains three main metals, of which two, Au and Zn, are the most strongly anomalous elements in the dispersal train. They were detected in all samples collected within 1000 m of the deposit. The third metal, Ag, is not anomalous in the till, probably because in the mineralized zone it occurs mainly as argentite (Petersen *et al.* 2013), a sulphide mineral (Ag_2S), and the sampled till was oxidized and sulphide minerals were depleted. The oxidation is also reflected in very low-S analyses of 0–0.05%. The till samples that were collected no more than 1000 m down-ice from the centre of the deposit are also weakly anomalous in Pb, and those collected within 500 m are weakly anomalous in As, Cd, and Mn but not in Cu or Mo. The elevated Mn probably reflects the high concentration of spessartine garnet in the till.

The Au and Zn geochemical anomalies are shown in Figure 12A and 12B, respectively. Although both elements are anomalous for 1000 m down-ice from the centre of the Blackwater deposit, the highest Au response — directly over the deposit — is just 74 ppb, and the highest Zn response — also directly over mineralization — is 1620 ppm. The frequency of gold grains in the anomalous samples is sufficient (Fig. 9A, Table 1) for one or more grains to be present in the ~30 g aliquot of -0.063 mm fines that was analyzed, especially as most of the grains were also finer than 0.063 mm (Fig. 10). Therefore most and probably all of the Au anomalies were caused by this particulate gold rather than by Au chemically adsorbed by clay minerals or limonite. However, an outlying, 39 ppb Au anomaly obtained from sample 154, collected west of the Blackwater deposit, may be due to adsorbed Au because no gold grains were observed in this sample.

Till stratigraphy of the reverse circulation drillholes

Two RC drill holes were originally planned along the axis of the Blackwater train to investigate the train at depth: a proximal hole ~600 m down-ice from the centre of the gold deposit and a more distal hole ~1700 m down-ice. However, the original distal hole, Hole 01, was abandoned in till at 43.5 m due to drilling issues and a 70.4 m replacement hole, Hole 02, was drilled further west off the axis of the train. In addition the planned proximal hole, Hole 03, encountered only 1.6 m of till and was replaced by a 40 m hole to the east, Hole 04.

A longitudinal section of the Blackwater train from the gold deposit northeastward through Hole 04 to Hole 02 is shown in Figure 13. The overburden forms a distinct wedge; its thickness increases rapidly downslope to the northeast along the Blackwater train, from <5 m thick over the Blackwater deposit to 70.4 m at Hole 02, ~1300 m down-ice. Nevertheless it consists entirely of till and this till is of a relatively uniform texture and composition, suggesting that it was all deposited during the Fraser Glaciation.

The depth of oxidation in the three deep drillholes varies from 1.8 to 5.0 m. Below this depth the till is as fresh as when it was deposited ~10,000 years ago, although it contains some highly oxidized clasts derived from preglacially saprolitized bedrock. It typically consists of 20 to 40% pebble- to boulder-size clasts in a matrix dominated by silty to sandy rock flour but locally by clay. This clay is grey-brown and is probably derived from organic-rich glaciolacustrine sediments of the same colour that were intersected within the till on the western part of the property. The clast lithologies indicate a mostly local provenance; 90 to 100% are volcanic and <10% are granitoid,

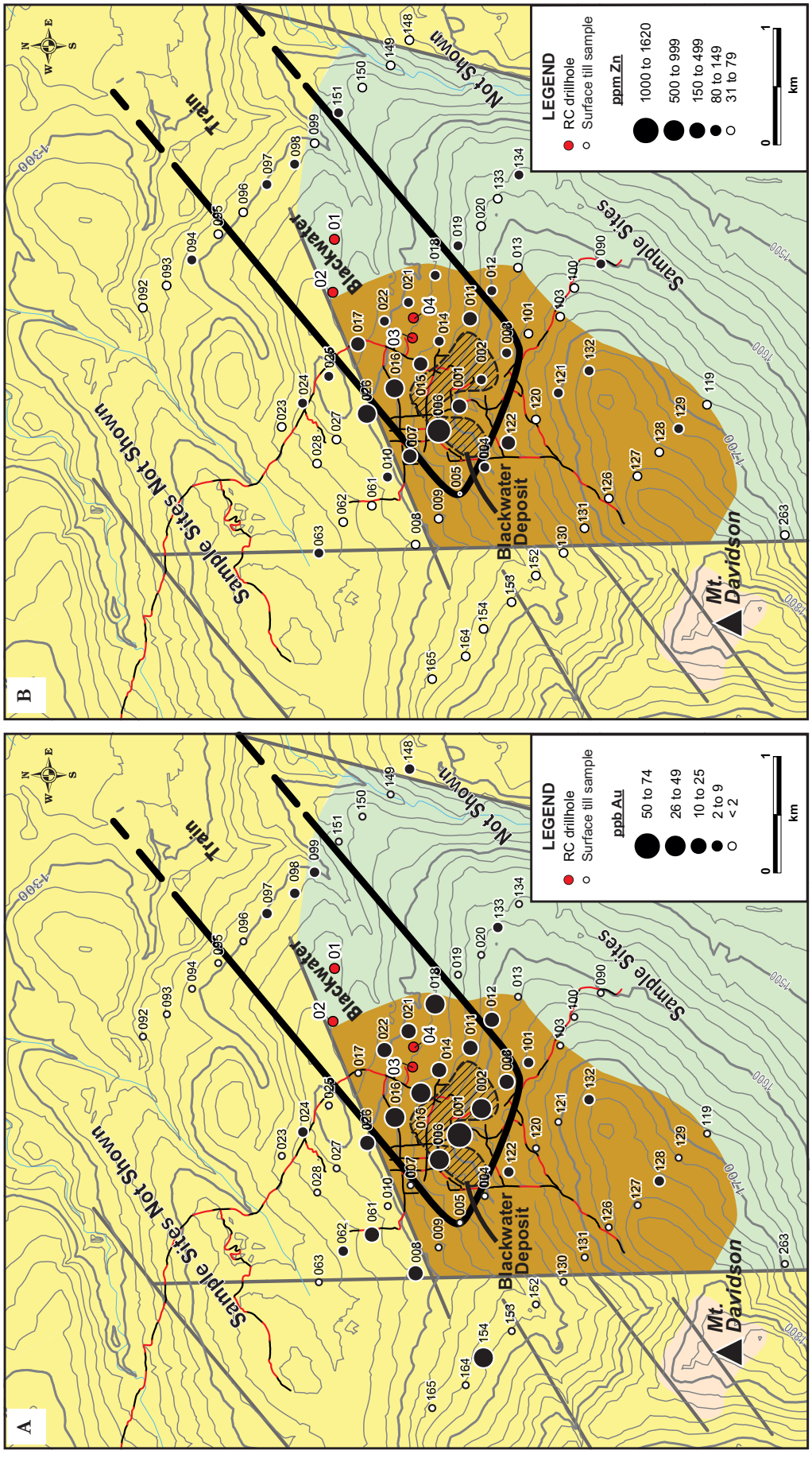

Fig. 12. (A) Au and **(B)** Zn analyses for the -0.063 mm fraction of surface till samples. See Figure 7 for bedrock lithologies.

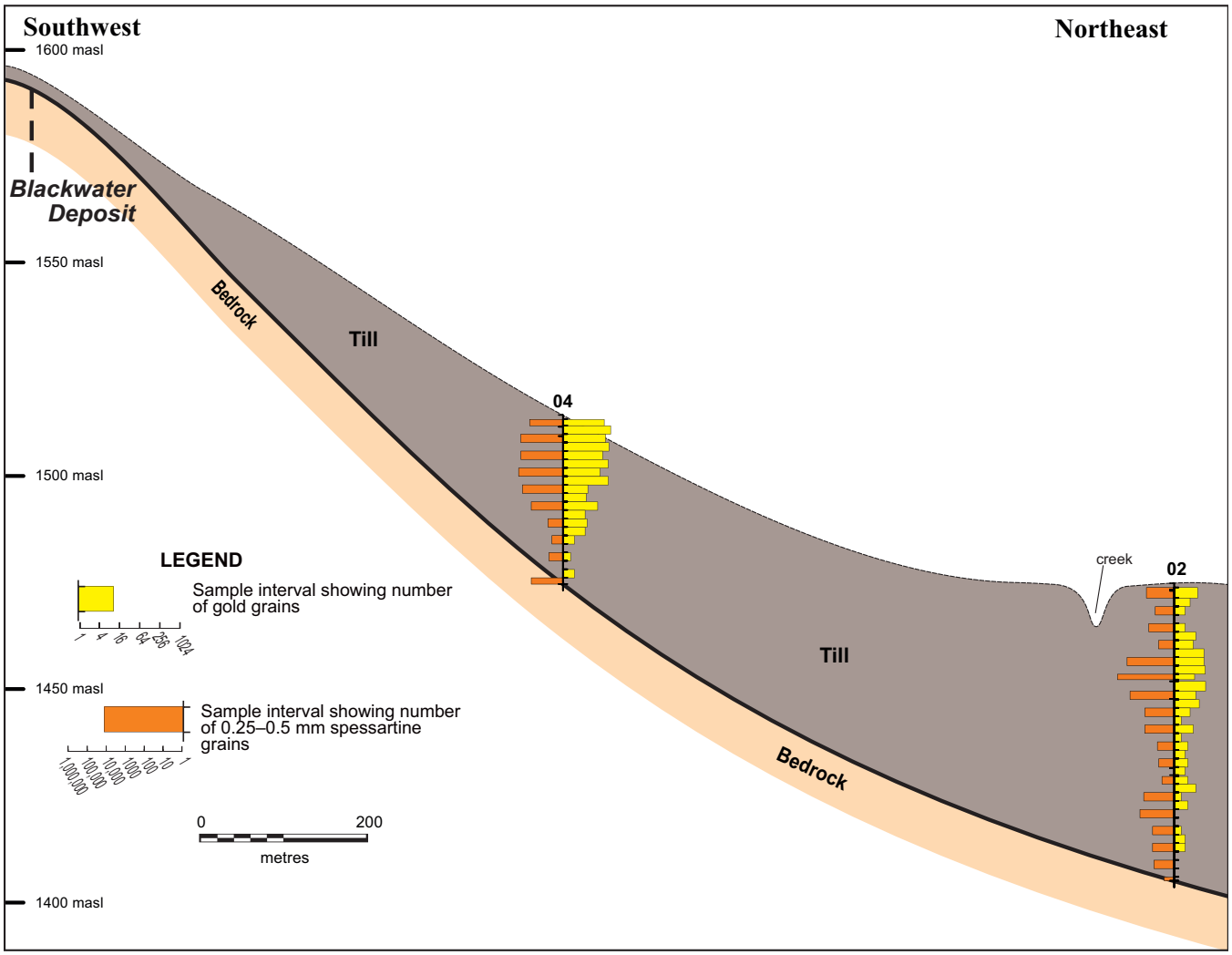

Fig. 13. Longitudinal section of the Blackwater train through reverse circulation drillholes No. 04 and 02.

even though a large pluton, the Laidman Batholith, is present just 10 km up-ice.

Indicator mineralogy of the till sections

Twenty samples were collected from the 40 m thick till section in the deposit-proximal drillhole, Hole 04. The top eleven samples, spanning 22.5 m, were all found to be anomalous, yielding from 10 to 126 gold grains, with an average of 68 grains (Fig. 13, Table 2). The next three samples, spanning 6 m, yielded nearly anomalous to weakly anomalous levels of 9 to 11 grains per sample, giving the gold dispersal train a remarkable total thickness of 28.5 m. The last six samples, spanning 11.5 m between the dispersal train and bedrock, yielded only background levels of 0 to 3 grains per sample. In neighbouring Hole 01, the single till sample obtained from the thin, 1.6 m till section yielded 32 gold grains.

Thirty-five samples were collected from the 70.4 m thick till section in Hole 02. The gold grain results obtained from this hole (Fig. 13) are similar to but weaker than those from Hole 04 because Hole 02 was drilled ~800 m further down-ice and off the axis of the dispersal train. As well, the nearest surface samples, Nos. 017 and 022 (Fig. 9A), yielded just 11 and 23 gold grains (Table 1).

In the drillhole, the main part of the gold dispersal train occurs in a 12 m interval between 17.5 and 29.5 m although the top sample in the hole, between 1.0 and 3.5 m, yielded 11 gold grains, supporting the weak surface anomaly (Fig. 9A). In the main anomalous zone (Fig. 13), seven successive samples yielded from 8 to 25 gold grains, averaging 17 grains. As in Hole 04, the anomalous zone is followed by a zone of elevated but sub-anomalous gold grain concentrations, then a thick zone directly above bedrock — in this case 14.9 m — of only background levels of 0 to 3 grains per sample. The gold grain response obtained from neighbouring Hole 01 was similar; it is not shown in Figure 13 because the hole was not completed to bedrock.

In the thick, unoxidized portion of the Blackwater train at depth, as in the thin, oxidized zone at surface, ~90% of the gold grains are silt sized (Fig. 10). Also as in the surface samples (Table 1), the proportion of pristine to modified grains is high in the proximal part of the train (Table 2) and lower in the distal part. Interestingly, however, the proportion of pristine to modified grains appears to decrease in the upper part of the train. In the top four anomalous samples collected from the train in Hole 04, for example, only 69 to 85% of the gold grains are pristine to modified, compared to 86 to 100% (mostly >90%) in the bottom seven samples (Table 2). This

Table 2. Indicator mineralogy and HMC geochemistry of the till samples from reverse cirvulation drillhole No. 04 proximal to the Blackwater deposit. Only the odd-numbered and bottom samples from the hole were tested for indicator minerals.

Sample No.	End Depth (m)	No. of Gold Grains				% Pristine or Modified	No. of 0.25–0.5 mm Mineral Grains			Geochemistry of the HMCs									
										ppb	ppm								%
		Total	Pristine	Modified	Reshaped		Spessartine	Pyrolusite	Pyrite	Au	Ag	As	Cu	Zn	Pb	Cd	Mo	Mn	S
04-01	2.5	65	23	22	20	69	400	0	0	2350	2.6	152	34	128	212	3	1.4	896	0.02
04-02	4.5	126	49	48	29	77				11300	11.1	328	45	493	1150	4	5.5	12000	0.05
04-03	6.5	75	28	35	12	84	2,000	1,500	0	1870	19.4	863	119	3530	2280	6	17.3	14200	0.19
04-04	8.5	106	45	45	16	85				725	17.2	856	122	1650	1980	9	15.5	20000	0.05
04-05	10.5	55	28	23	4	93	2,000	1,500	0	364	9.9	297	44	620	717	5	5.1	9940	0.01
04-06	12.5	97	56	35	6	94				1330	40.7	418	86	915	2200	8	11.9	19500	0.02
04-07	14.5	42	24	16	2	95	3,000	6,000	30	420	19.1	614	74	1110	1350	7	17.1	18700	0.1
04-08	16.5	99	41	44	14	86				613	17.7	311	51	879	863	5	11.9	13700	0.01
04-09	18.5	12	7	5	0	100	1,500	2,000	0	84	3.7	140	31	448	262	3	2.1	7640	0.14
04-10	20.5	10	3	6	1	90				207	69.5	536	120	2260	1810	12	13.6	34500	0.01
04-11	22.5	33	25	7	1	97	300	60,000	15	1040	56	668	92	1920	1720	7	11.4	32000	0.02
04-12	24.5	9	4	4	1	89				221	8.5	126	56	408	949	4	2.8	12400	<0.01
04-13	26.5	11	5	4	2	82	15	5,000	20	288	16.9	119	67	985	974	5	7.3	18200	0.03
04-14	28.5	9	2	3	4	56				495	10.4	92	43	427	494	6	3.4	10500	<0.01
04-15	30.5	3	1	2	0	100	7	800	1	90	2.7	98	55	197	303	9	1.6	6000	<0.01
04-16	32.5	1	1	0	0	100				<5	0.5	53	55	140	121	7	1.3	4580	<0.01
04-17	34.5	2	1	1	0	100	12	300	0	105	1.4	83	82	147	247	9	1.7	12300	<0.01
04-18	36.5	1	1	0	0	100				478	2.9	125	102	197	285	11	2.5	20000	0.06
04-19	38.5	3	1	2	0	100	1	40	0	56	3.7	72	61	180	112	5	1	10900	<0.01
04-20	40.0	0	0	0	0	0	300	1,500	0	144	6.1	114	67	306	326	7	3.8	12400	<0.01

suggests that the till in the upper part of the dispersal train has a longer transport history, i.e., it was transported the same horizontal distance as the till in the lower part of the train but a greater vertical distance and in a longer period of time with the result that the gold grains are physically more mature. Another interesting feature is that in the thick, underlying zone, which has only background levels of 0 to 3 gold grains, 100% of the grains are pristine to modified rather than reshaped, suggesting that they too are related to the Blackwater deposit rather than to distal gold sources.

As previously noted, the concentration of spessartine and other potential indicator minerals other than gold was determined only for the odd-numbered and bottom samples collected from the till section in each drillhole. Spessartine levels in the unoxidized zone of the gold dispersal train at depth (Fig. 13, Table 2) mirror those of the oxidized zone at surface (Fig. 9B, Table 1). Most of the anomalous samples yielded >1000 grains of 0.25 to 0.5 mm size versus a background to slightly elevated concentration of 0 to 20 grains. The strongest response was 30,000 grains, mirroring the 25,000-grain peak in the surface samples. Spessartine levels in the train are not only much higher than gold grain levels, but also appear to decrease more slowly down-ice (Fig. 13). Therefore, in the subsurface as at surface, the Blackwater train should be detectable much further down-ice with spessartine grains than with gold grains.

While the Blackwater train in the subsurface is hosted by unoxidized till and the gold grains in this till are clearly derived from the Blackwater deposit, where the gold is closely associated with pyrite (Petersen 2013, Petersen *et al.* 2013, Looby *et al.* 2013), the till contains negligible pyrite. No sample from the 22.5 m thick section of the gold dispersal train in Hole 04 (Fig. 13) yielded more than 30 pyrite grains of 0.25 to 0.5 mm size and most samples yielded no pyrite (Table 2).

The paucity of pyrite in the unoxidized till is evidently due to preglacial oxidation of most of the hypogene sulphides in the supergene zone that caps the deposit because the till is anomalous not only in gold and spessartine but also in pyrolusite (Table 2), a supergene Mn-oxide mineral (MnO_2). In Hole 04, the top till sample was from the oxidized zone and, like all of the surface samples along the train (Fig. 9, Table 1), yielded no pyrolusite grains, whereas the next ten samples were from the unoxidized zone and yielded from 1500 to 60,000 grains between 0.25 and 0.5 mm, a response similar to that for spessartine. Moreover, many larger grains of pyrolusite, which is a coarse-biased mineral, were found in the 0.5–1 mm and 1–2 mm fraction of the HMCs. The indicated presence of pyrolusite in the oxidized cap of the Blackwater deposit contrasts with its absence in oxidized till and suggests that the preglacial climate was more arid.

Geochemistry of the heavy mineral concentratess from the till sections

As previously mentioned, the -0.25 mm HMCs of the drilled till samples were analyzed instead of the -0.063 mm till fines because the unoxidized till at depth retains any heavy sulphide mineral grains that were dispersed during glaciation.

The Au, Ag, As, Cu, Zn, Pb, Cd, Mo, Mn, and S analyses obtained from the HMCs of the 20 samples collected from the 40 m thick till section in Hole 04 are shown in Table 2. The highest Au analyses, ranging up to 11,300 ppm, were obtained in the top half of the till section from the eleven samples having anomalous concentrations of gold grains. However, the observed gold grains were expected to collectively produce Au analyses only one tenth to one-fifth as high as the reported values, due to the very small average size of the grains (Fig. 10). Such a large discrepancy between the expected and actual Au analyses normally indicates that another auriferous mineral is present in the HMCs. Most commonly this mineral is pyrite, as in the dispersal train of New Gold's large Rainy River gold deposit in Ontario, where 90% of the Au occurs within pyrite grains and pyrite is so plentiful in the till that the HMCs are oversized (Averill 2013a).

As previously noted and reinforced by very low-S analyses of <0.01 to 0.19% for the HMCs from Hole 04 (Table 2), pyrite is rare in the Blackwater train but pyrolusite, a secondary mineral apparently derived from the supergene cap of the Blackwater deposit and a known scavenger of metals, is abundant and results in HMC Mn analyses of up to 34,500 ppm or 3.45%. To check the metal content of the pyrolusite, a hand-picked separate of the largest grains from the most pyrolusite-

Table 3. Geochemical analyses for pyrolusite grains separated from Sample 11 in Hole 04.

Sample Number	Ag ppm	As ppm	Cu ppm	Zn ppm	Pb ppm	Cd ppm	Mo ppm	Ni ppm	Mn ppm	S %
04-11	264	781	133	8660	2010	58.9	18	66	90400	0.04

rich sample in Hole 04, sample No. 11, was submitted for geochemical analysis (Table 3). This separate was too small for gold analysis but was found to be extremely anomalous in both Ag (264 ppm or 7.5 ounces per ton) and Zn (8660 ppm) and also, in the same manner as the -0.063 mm fines from the oxidized surface samples, significantly anomalous in As (781 ppm), Pb (2010 ppm) and Cd (58.9 ppm) but not in Cu (only 133 ppm) or Mo (18 ppm). These results strongly suggest that the unseen Au in the HMCs resides in the pyrolusite.

Pure pyrolusite contains ~60% or 600,000 ppm Mn, but the Mn analysis obtained from the pyrolusite separate was only 90,400 ppm (Table 3), indicating that the grains are very impure. Analysis of the HMC before the pyrolusite grains were removed yielded 32,000 ppm Mn, which suggests a pyrolusite content of ~35%. The HMC also returned 56 ppm Ag, 668 ppm As, 1920 ppm Zn, 1720 ppm Pb, and 7 ppm Cd, each of which is fully accounted for by the high pyrolusite content of the HMC.

CONCLUSIONS

The till sampling performed near the Blackwater Au-Ag deposit successfully delineated a large, previously unknown indicator mineral dispersal train — the Blackwater train — directly down-ice from the deposit (Fig. 9). The sampling program was unusually comprehensive as it established not only the indicator mineralogy but also the geochemistry of the dispersal train, both at surface where the till is oxidized and in the subsurface where it is unoxidized.

The oxidized zone of the till was sampled for 2.5 km down-ice from the Blackwater deposit at a density varying from 2 to 6 samples per km^2. At this sample spacing, the Blackwater train was faithfully detected mineralogically for more than 2.5 km from source using either gold (Fig. 9A) or spessartine (Fig. 9B) grains; whereas it is was detected for only 1 km geochemically in the -0.063 mm silt + clay fraction of the till (Fig. 12). Moreover the Mn in the spessartine was detected only in the samples that were collected within 500 m of the Blackwater deposit; these proximal samples contained thousands of spessartine grains.

Gold grains are the best indicator of the Blackwater deposit because they reflect the actual mineralization; the spessartine grains reflect only its alteration envelope. Moreover, the gold grains are malleable and their morphologies change systematically along the train from pristine to reshaped (Table 1), providing a measure of their transport distance. In 10 kg samples, background levels of both gold and spessartine grains are near zero. At an anomaly threshold of 10 gold grains per sample, the dispersal train is probably detectable for at least 3 km down-ice. With spessartine its detectable length may be as much as 10 km because spessartine grains are much more abundant than gold grains within the train.

Gold grains (Fig. 9A) define a train that is ~1.3 km wide — similar to the width of the Blackwater deposit — and ribbon-shaped with straight, sharp, lateral boundaries and a clear cut-off at the deposit. Using spessartine (Fig. 9B), the axis of the train is unchanged but the lateral margins are diffuse and the width doubles. The spessartine train appears to originate entirely from the Late Cretaceous Kasalka volcanic rocks that host the Blackwater deposit, with its core reflecting the known spessartine-bearing alteration envelope of the deposit and the lower grade margins suggesting that the outlying Kasalka volcanic rocks contain other, similar alteration zones.

In the subsurface, the Blackwater train is up to 22.5 m thick and is elevated well above the bedrock surface (Fig. 13). Gold grain and spessartine levels are similar to those at surface (Fig. 9), suggesting that the train is detectable for the same distance down-ice in the subsurface. Although the till that hosts the gold and spessartine grains is unoxidized, and the Blackwater deposit, from which these grains are derived, contains ~1 to 5% pyrite (Petersen *et al.* 2013, Christie *et al.* 2014), the till contains negligible pyrite. This appears to be due to the presence of an oxidized, preglacial supergene cap on the primary pyritic mineralization (Fig. 4). Instead of pyrite, the unoxidized till contains pyrolusite, a heavy, supergene Mn-oxide mineral that is apparently derived from the oxidized cap of the Blackwater deposit. Except at the surface of the Blackwater train where any glacially dispersed pyrolusite grains in the till were consumed by post-glacial oxidation, pyrolusite is as abundant as spessartine (Table 2), constituting up to 35% of some HMCs.

The pyrolusite grains are remarkably enriched in scavenged Ag (256 ppm or 7.5 oz/ton), As (781 ppm), Zn (8660 ppm), Pb (2010 ppm), and Cd (58.9 ppm) (Table 3). The HMC analyses for these elements are roughly proportional to the percentage of pyrolusite in the HMCs. The pyrolusite was not analyzed for Au but apparently it is as enriched in this element as in Ag because the HMC Au analyses are five to ten times higher than expected from the recovered gold grains, 90% of which are silt-sized (Fig. 10) and thus make only a small contribution to the Au analyses.

Possibly the most unusual feature of the gold grain dispersal train is its rapid separation from bedrock in the down-ice direction (Fig. 13). In Hole 04, ~600 m down-ice from the centre of the Blackwater deposit, the base of the dispersal train, excluding the underlying zone of elevated but subanomalous levels of gold grains, is 17.5 m above bedrock and in Hole 02, ~800 m further down-ice, it is 50.9 m above bedrock. While this could suggest the presence at depth of an older, barren till horizon deposited by ice that flowed in a more easterly or northerly direction, only one till appears to be present because (a) macroscopically the till section is very homogeneous; (b) both the barren and auriferous till contain spessartine (Table 2, Fig. 13); and (c) while the barren till in Hole 04 contains only sparse gold grains, all of the grains are pristine (Table 2) and thus are probably derived from the Blackwater deposit.

The progressive separation of the gold-spessartine-pyrolusite dispersal train from bedrock with increasing distance from the Blackwater deposit is probably due to the englacial thrusting process described by Clayton & Moran (1974), which is also responsible for elevating mineralized boulders to surface down-ice from ore deposits. This upthrusting may have been accelerated by the steep drop-off in the bedrock surface down-ice from the Blackwater deposit (Figs. 5, 13). Similarly perched indicator mineral dispersal trains have been identified by RC drilling at Matagami and a few other mineral deposits that occur on bedrock-highs directly up-ice from deep bedrock valleys in the Abitibi Greenstone Belt of Eastern Canada (Averill 2003). None of these perched trains would have been recognized if only the bottom of the till section, commonly referred

to as "basal" till, had been sampled. As demonstrated by the Blackwater program, the top till samples from a drillhole can be more important than the bottom samples and the entire till section must be sampled to determine the limits and significance of a dispersal train.

ACKNOWLEDGEMENTS

A number of geologists were key to the success of the Blackwater till sampling program. Robin Whiteaker, New Gold's Senior Project Geologist and Manager, worked closely with ODM, both in planning the program and assisting with field logistics. Three of the author's colleagues led specific aspects of the program. Don Holmes organized and supervised the field work, Remy Huneault supervised the laboratory sample processing, and Kenzie MacNeil led the indicator mineral identification team. The illustrations and data tables in the paper were prepared by David Hozjan and Michael D. J. Michaud.

The author particularly thanks Mark Petersen, New Gold's Vice-President Exploration, for reviewing the paper and authorizing the early publication of proprietary but scientifically significant data, even though exploration of the Blackwater property is ongoing. It is hoped that others will recognize the major benefits that this practice brings to the science of mineral exploration.

REFERENCES

Andrew, K.P.E. 1988. Capoose precious and base metal prospect, *In: Geological Fieldwork 1986*. British Columbia Ministry of Energy, Mines and Petroleum Resources Paper 1987-1, p. 53–56.

Averill, S.A. 2001. The application of heavy indicator mineralogy in mineral exploration with emphasis on base metal indicators in glaciated metamorphic and plutonic terrains, *In:* McClenaghan, M.B., Bobrowsky, P.T., Hall, G.E.M. & Cook, S.J. (eds) Drift Exploration in Glaciated Terrains. Geological Society, London, Special Publications, 185, 69–81.

Averill, S.A. 2003. Indicator mineralogy: a tool for reviving mineral discoveries in the Abitibi. *In: Résumés des Conférences et des Photoprésentations, Québec Exploration 2003*. Association de L'Éxploration Minière du Québec, Oral Presentation.

Averill, S.A. 2011. Viable indicator minerals in surficial sediments for two major base metal deposit types: Ni-Cu-PGE and porphyry Cu. *Geochemistry: Exploration, Environment, Analysis*, **11**, 279–292.

Averill, S.A. 2013a. Indicator mineral fingerprints in surficial sediments near Cu-Au deposits of the porphyry-epithermal-volcanogenic suite, *In: Application of Indicator Methods to Mineral Exploration*. The Association of Applied Geochemists, 26th International Applied Geochemistry Symposium, Workshop SC07, New Zealand.

Averill, S.A. 2013b. Discovery and delineation of the Rainy River gold deposit using glacially dispersed gold grains sampled by deep overburden drilling: A 20 year odyssey, *In: New Frontiers for Exploration in Glaciated Terrain*. Prospectors and Developers Association of Canada, Workshop, Toronto.

Awmack, H.J., Armitage, A., Campbell, J. & Pawliuk, D. 2010. 2010 technical report on the Capoose project, Nechako Plateau, Omenica Mining Division. Unpublished report prepared for Silver Quest Resources Ltd.

Christie, G., Lipiec, I., Simpson, R.G., Horton, J. & Borntraeger, B. 2014. *NI 43-101 Technical report on feasibility study, Blackwater Gold project, British Columbia*. Retrieved from http://www.marketline.com.

Clague, J.J. 1989. Quaternary geology of the Canadian Cordillera, *In:* Fulton, R.J. (ed.) *Quaternary Geology of Canada and Greenland*. Geological Survey of Canada, Geology of Canada, No. 1, 17–137.

Clayton, L. & Moran, S.R. 1974. A glacial process-form model, *In:* Coates, D.R. (ed) *Glacial Geomorphology*. State University of New York, Binghamton, 89–119.

Dawson, K.M. & Kirkham, R.V. 1996. Skarn copper, *In:* Eckstrand, O.R., Sinclair, W.D. & Thorpe, R.I. (eds) *Geology of Canadian Mineral Deposit Types*. Geological Survey of Canada, Geology of Canada, No. 8, 460–476.

Diakow, L.J., Webster, I.C.L., Richards, T.A. & Tipper, H.W. 1997. Geology of the Fawnie and Nechako Ranges, southern Nechako Plateau, *In:* Newell, J.M. & Diakow, L.J. (eds) *Interior Plateau Geoscience Project Summary of Geological, Geochemical and Geophysical Studies*. British Columbia Ministry of Energy, Mines and Petroleum Resources Paper 1997-2, 7–30.

Gabrielese, H., Monger, J.W.H., Wheeler, J.O. & Yorath, C.J. 1991. Part A. Morphogeological belts, tectonic assemblages and terranes. *In:* Gabrielese, H. & Yorath, C.J. (eds) *Geology of the Cordilleran Orogen in Canada*. Geological Survey of Canada, Geology of Canada, 4, 15-28.

Kelley, K.D., Eppinger, R.G., Lang, J., Smith, S.M. & Fey, D.L. 2011. Porphyry Cu indicator minerals in till as an exploration tool: example from the giant Pebble porphyry Cu-Au-Mo deposit Alaska, USA. *Geochemistry: Exploration, Environment, Analysis*, **11**, 321–334.

Looby, E., Gregory, M., Hart, C., Petersen, M. & Lipske, J. 2013. *The geology of the Blackwater epithermal Au-Ag deposit*. Society of Economic Geology 2013 Annual Meeting, Whistler B.C., Poster Session.

Massey, N.W., MacIntyre, D.G., Desjardins, P.J. and Cooney, R.T. 2005. *Digital geology map of British Columbia: Tile NN10 Central B.C.* British Columbia Ministry of Energy and Mines, Geofile 2005-6.

Monger, J & Price, R. 2002. The Canadian Cordillera: Geology and tectonic evolution. *CSEG Recorder*, **27**, No. 2.

Petersen, M.A. 2013. *Geology and exploration of the Blackwater gold-silver deposit, British Columbia, Canada*. Society of Economic Geology 2013 Annual Meeting, Whistler British Columbia, Oral Presentation Abstract.

Petersen, M.A., Della Libera, M., Lipske, J. & Templeman-Kluit, D. 2013. Blackwater: Discovery and development of an emerging multi-million ounce gold-silver district in the Nechako Plateau, British Columbia, Canada, *In: NewGenGold: Conference Proceedings: Case Histories of Discover.* 77–93.

Plouffe, A. & Levson, V.M. 2001. Late Quaternary glacial and interglacial environments of the Nechako River – Cheslatta Lake area, central British Columbia. *Canadian Journal of Earth Sciences*, **38**, 719–731.

Plouffe, A., Levson, V.M. & Mate, D.J. 2004. *Surficial geology, Nechako River, British Columbia*. Geological Survey of Canada, Map 2067A.

Simpson, R.G., Welhener, H.E., Borntraeger, B., Lipiec, I. & Reyes, R.M. 2012. *NI 43-101 technical report on preliminary economic assessment, Blackwater project, British Columbia*. Unpublished report prepared for New Gold Inc.

A review of scheelite chemistry and its use an a discriminator in ore-deposit settings, use as an indicator mineral and monitor of ore-forming processes

D.J. Kontak[1]*, R.S. Poulin[1], A.M. McDonald, and B.M. McClenaghan[2]

[1]Department of Earth Sciences, Laurentian University, 935 Ramsey Lake Road, Sudbury, Ontario, Canada P3E 2C6

[2]Geological Survey of Canada, 601 Booth Street, Ottawa, Ontario Canada K1A 0E8

**Corresponding author's e-mail: dkontak@laurentian.ca*

Scheelite ($CaWO_4$) is an important accessory mineral in a variety of magmatic-hydrothermal ore deposit settings, including Cu-Mo porphyry, skarn and vein Sn-W, volcanogenic massive sulphide, orogenic Au, and epithermal. Due to its physical (e.g. H=4.5–5, D=6) and chemical properties, scheelite is relatively impervious to physical and chemical degradation and can be concentrated in surficial environments. Scheelite, therefore, has the potential to be used as a powerful indicator mineral in exploration; however, this application is limited owing to the fact that no comprehensive chemical database (trace elements, stable isotopes, cathodoluminescence character, etc.) exists for the mineral. Here we present the results of a crystal-chemical study of scheelite from a large range and number of ore-deposit settings to assess its application as a pathfinder mineral. In this study scheelite from 32 ore deposits was examined using a variety of analytical methods to fully characterize and assess the features that may prove most useful as discriminators. The following methods have been integrated into this study: (1) SEM-EDS to assess minor element chemistry and document zoning; (2) cathodoluminescence (CL) to characterize zoning; (3) point analyses and elemental mapping using the LA-ICP-MS for minor and trace elements; (4) stable isotopes (^{18}O) to identify source reservoirs (e.g. magmatic versus metamorphic); and (5) the presence of both mineral and fluid inclusions. The results of this work indicate that scheelite is a chemically complicated mineral that exhibits a large range in the parameters investigated, including (1) zonation, which varies from absent to normal, oscillatory, and discordant; (2) minor-element composition, in particular for As and Mo, which varies greatly; (3) trace-element chemistry, specifically the REEs that vary in terms of ∑REEs (10^4 range in chondrite-normalized values), degree and type of fractionation patterns (flat, convex, concave), and type (+, -) and amount of Eu anomalies (<0.1 to >20–30); (4) stable isotope chemistry, specifically $\delta^{18}O$ that ranges from -4.6 to +9.1‰; and (5) whereas mineral inclusions are rare, fluid inclusions may be present with a range of fluid types (e.g. HvO versus H_2O-CO_2).This dataset, the most comprehensive for scheelite, are presently being evaluated to assess the discriminating potential of scheelite and its use an indicator mineral. These new data also provide, in addition, insight into the fluid chemical evolution of a large range of ore deposit types not previously appreciated (e.g. cryptic paragenesis) and will serve as a basis for further applied crystal-chemical studies of this mineral phase.

Indicator mineral signatures of the Mount Pleasant Sn-W-Mo-Bi-In deposit, New Brunswick, Canada

M.B. McClenaghan[1*], M.A. Parkhill[2] & A.G. Pronk[3]

[1]Geological Survey of Canada, 601 Booth Street, Ottawa, Ontario Canada K1A 0E8
[2]New Brunswick Department of Energy and Mines, Geological Surveys Branch, P.O. Box 50, Bathurst, New Brunswick, Canada E2A 3Z1
[3]New Brunswick Department of Energy and Mines, Geological Surveys Branch, P.O. Box 6000, Fredericton, New Brunswick, Canada E3B 5H1
**Corresponding author's e-mail: bethmcclenaghan@nrcan-rncan.gc.ca*

The use of indicator minerals to explore for Sn-W mineralization is well documented for stream sediments, but much less so for glacial sediments. To address this knowledge gap, the Geological Survey of Canada (GSC) conducted a case study at the Mount Pleasant Sn-W-Mo-Bi-In deposit in eastern Canada to test and demonstrate modern indicator mineral exploration methods for intrusion-hosted S-W deposits. The study was funded by the GSC's Targeted Geoscience Initiative 4, a collaborative federal geoscience program with a mandate to provide industry with the next generation of geoscience knowledge and innovative techniques for more effective targeting of buried mineral deposits. It was a collaborative effort between the GSC and the New Brunswick Department of Energy and Mines (NBDEM). These short course notes provide an overview of published literature on the use of indicator minerals for Sn-W exploration, with specific reference to the Mount Pleasant deposit.

Overviews of cassiterite, scheelite, wolframite, fluorite, and topaz are provided below as background information because their physical characteristics and recovery from, and abundance in, till is not well known.

CASSITERITE

Cassiterite (SnO_2) has a long history as an indicator mineral starting with its recovery from placer stream deposits in southwest England as far back as the Bronze age (Camm & Groot 1994). It is considered the best indicator mineral of Sn deposits (Stendal & Theobald 1994) because it is Sn-rich, dense (specific gravity (SG) 6.8–7), and chemically and physically robust (H = 6–7) and thus survives fluvial or glacial transport. Its colour varies from deep red to reddish brown (Fig. 1A) to black. Cassiterite is identified in heavy mineral concentrates (HMC) by its adamantine luster, prismatic habit (Fig. 1A), and that it is often still attached to quartz in till samples (Fig. 1B).

Cassiterite has been recovered in stream sediments surveys around the world, including Spain (Zantop & Nespereira 1979; Fernández-Turiel & Durán-Barrachina 1989), and Australia (Towsey & Patterson 1984), as well as from placer deposits such as those in Indonesia (Aleva 1985), Great Britain (e.g. Dunlop & Meyer 1978; Camm & Hosking 1985; Camm & Groot 1994), Russia (e.g. Patyk-Kara 1999), the USA (e.g. Johnson 1910; Theobald & Thompson 1960; Chapman *et al.* 1963), and Canada (e.g. Thompson 1945; Gleeson & Boyle 1980; Ballantyne & Ellwood, 1988). The presence of cassiterite in till has been reported in a few studies (e.g. Brundin & Bergstrom 1977; Mattila & Peurnaiemi 1980; Toverud 1982; Peuraniemi & Heinänen 1985; Ryan *et al.* 1988; Turner & Stea 1990; Averill 2001) but only in a few till samples that were first determined to have high Sn contents.

SCHEELITE

Scheelite ($CaWO_4$) is an important indicator of W mineralization. It is moderately hard (H = 4–5) and dense (SG 5.9–6.1). It is relatively insoluble in the natural pH range of surface water, but survives only moderate distances of glacial or fluvial transport because it is brittle (Horsnail 1979; Hosking 1982; Ottensen & Theobald 1994). It is identified in HMC by its pale yellow colour (Fig. 1C), distinctive cleavage, and its bright blue-white-yellow fluorescence under short-wave ultraviolet (UV) light, which can vary due to Mo content (i.e. powellite substitution). Pure scheelite fluoresces strong whitish blue and with increasing Mo content, this colour changes to white (0.5–1.0 wt% Mo), yellow (>1 wt% Mo), and deep orange-yellow (>4 wt% Mo) (Hosking 1982).

Mainly because of its fluorescence, scheelite is easy to visually identify, and thus is one of the most commonly used indicator minerals in stream sediment surveys for W, Sn, and Au exploration globally (e.g. Zeschke 1961), including Turkey (e.g. Özcan & Çağatay 1989), Spain (e.g. Zantop & Nespereira 1979; Fernández-Turiel *et al.* 1992), Pakistan (e.g. Zeschke 1961; Asrarullah 1982), Malaysia (e.g. Rajah 1982), Somalia (Frizzo & Hassan 1983); USA (e.g. Theobald & Thompson 1960), and India (e.g. de Smeth *et al.* 1985). It has also been recovered from stream sediments in glaciated terrain, including Norway (e.g. Stendal 1978), Greenland (e.g. Hallenstein *et al.* 1981; Steenfelt 1987) and Canada (e.g. Maurice 1986; Allen *et al.* 1999). In some areas, scheelite content in stream sediments is sufficient for the sediments to be characterized as placer W deposits (e.g. Hess 1917; Wildon & Hotz 1955). In some parts of the world, scheelite is recovered from soils in support of mineral exploration (e.g. Petersen & Stendal 1987; Özcan & Çağatay 1989; Surya Prakash Rao *et al.* 1989).

Recovery of scheelite grains from till has been reported for several studies (e.g. Nikkarinen & Bjorklund 1976; Brundin & Bergström 1977; Lindmark 1977; Steiger 1977; Stea & O'Reilly 1982; Toverud 1984; Johansson *et al.* 1986; Salminen & Hartikainen 1986; Petersen & Stendal 1987; Snow & Coker 1987; Peuraniemi 1992; Averill 2001) but only in a few till samples in each study that were first determined to have high W contents. It was often noted that the scheelite in till formed

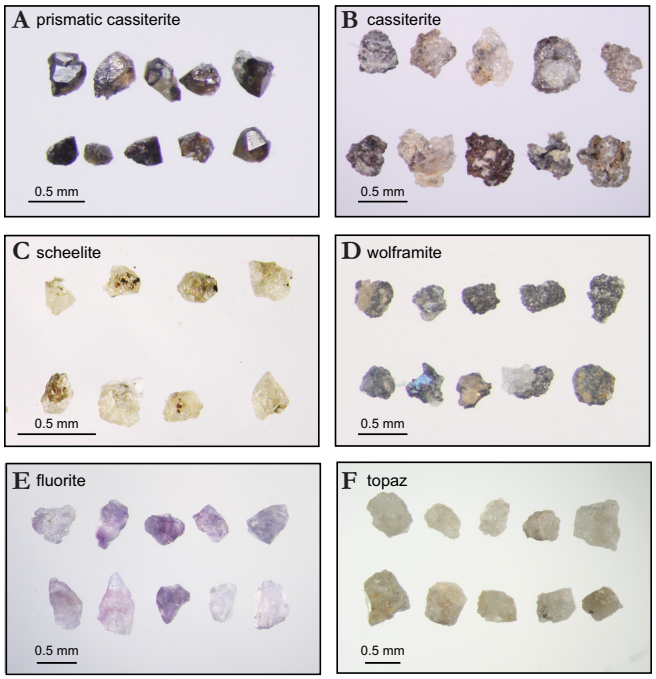

Fig. 1. Colour photographs of indicator minerals from the Mount Pleasant Sn-W-Mo-Bi-In deposit: **A)** prismatic brown cassiterite grains; **B)** brown irregular cassiterite grains with adhering quartz; **C)** scheelite; **D)** black wolframite; **E)** purple fluorite; and **F)** translucent white topaz (modified from McClenaghan *et al.* in press b).

larger anomalies than those outlined using W content. Recently, scheelite has been reported in till and stream sediments down-ice and downstream of the Sisson W-Mo deposit in eastern Canada (McClenaghan *et al.* 2014a, in press a).

WOLFRAMITE

The other common W-bearing indicator mineral is wolframite ($(Fe,Mn)WO_4$). It is relatively insoluble in the natural pH range of surface water (Horsnail 1979) and is dense (SG 7.1–7.5). It is identified in HMC by its black colour (Fig. 1D), prismatic crystal form, moderate hardness (H= 4.5, can be scratched with a needle), reddish brown streak, and lack of fluorescence under UV light. When rounded, it can be difficult to distinguish from other visually similar black heavy minerals (e.g. hornblende, tourmaline, ilmenite) that can be abundant in stream sediments and till. Because of its brittle nature and perfect cleavage, it breaks apart more readily than scheelite and thus tends to be rarer. When present, it is usually is found in the finest fraction of stream sediments within 2 to 3 km downstream of its bedrock source (ESCAP Secretariat 1982; Hosking 1982; Meizhong 1982).

Wolframite has been recovered in stream sediment surveys around the world (Zeschke 1961), including Spain (Zantop & Nespereira 1979; Fernández-Turiel & Durán-Barrachina 1989; Fernández-Turiel *et al.* 1992), and USA (e.g. Johnson 1910; Theobald & Thompson 1960) and from W placer deposits (Hess 1917), such as those in Thailand (e.g. Pungrassami 1986) and Burma (e.g. ESCAP Secretariat 1982). Recovery of wolframite from glacial sediments has been occasionally noted when it occurred in association with scheelite (e.g. Brundin & Bergström 1977; Averill 2001). More recently, wolframite has been reported in till and stream sediments down-ice and downstream of the Sisson W-Mo deposit (McClenaghan *et al.* 2014a, in press a).

FLUORITE

Fluorite (CaF_2) occurs in carbonatite, peralkaline intrusions, Mississippi Valley-Type deposits, fluorite ± barite veins in igneous, sedimentary, and metamorphic rocks, and Climax-type Mo deposits (Stendal & Theobald 1994; Makin *et al.* 2014). It is easily identified in HMC by its purple (Fig. 1E) to green colour, or colourless nature, octahedral or cubic crystal form, low to moderate hardness (H=4, can be scratched with a needle), and its white-blue fluorescence under short and long-wave ultraviolet light. Its SG spans a range from 3.01 to 3.2, thus only some of the fluorite will be captured in a HMC (>3.2 or >3.3 SG). To optimize recovery of fluorite, the mid-density (3.0–3.2 SG) mineral fraction in addition to the heavy mineral fraction should be examined. Its presence has been reported in stream sediments (e.g. Zeschke 1961; Tripp *et al.* 1978; Watts & Hassemer 1980) and glacial sediments (e.g. Szabo *et al.* 1975; Brundin & Bergstrom 1977; Mattila & Peuraniemi 1980; Peuraniemi & Heinänen 1985; Peuraniemi & Gehör 2000; Averill 2001).

TOPAZ

Topaz ($Al_2SiO_4(F,OH)_2$) is commonly found in felsic igneous rocks and some hydrothermal veins, and surrounding hydrothermally altered rocks (Stendal & Theobald 1994). Because it is dense (SG 3.5–3.6) and physically and chemically robust (H = 8), it is relatively resistant to weathering and stream abrasion, making it a useful indicator mineral of topaz-bearing rocks. It is sometimes recovered by Sn or W placer mining. Topaz may be recognized in HMC by its transparent to translucent (Fig. 1F) white colour and extreme hardness. It fluoresces golden yellow under short-wave UV light and cream colour under long-wave UV light. Its presence has been reported in stream sediments (e.g. Zeschke 1961; Tripp *et al.* 1978) and glacial sediments (e.g. Szabo *et al.* 1975; Brundin & Bergstrom 1977; Friske *et al.* 2001; Averill 2001).

MOUNT PLEASANT Sn-W-Mo-Bi-In DEPOSIT CASE STUDY

The bedrock geology of the Mount Pleasant area is summarized below from Hosking (1963), Petruk (1972, 1973), Kooiman *et al.* (1986), Invemo & Hutchinson (2004), Sinclair *et al.* (2006), McCutcheon *et al.* (2010), and McCutcheon *et al.* (2013). The deposit occurs within two subvolcanic intrusions in the Late Devonian Mount Pleasant Caldera Complex along the north flank of the Saint George Batholith. The McDougall Brook granitic suite is related to the early stages of caldera development, and the Mount Pleasant granitic suite is related to the late stages of caldera development. The deposit consists of Sn, W, and Mo mineralization that is genetically related to highly evolved granitic rocks of the Mount Pleasant Granitic Suite (Granites I,II,III) that are enriched in incompatible elements F, Li, Rb, Cs, U, Th, and Nb. Granite I and related breccia host W-Mo-Bi mineralization and Granite II hosts Sn-In mineralization (Figs. 2, 3). Two mineralized zones subcrop and were glacially eroded during the last 2 million years: the North Zone and the Fire Tower Zone (Fig. 4).

The North Zone consists of older W-Mo mineralization and younger Sn-In mineralization, some of which is at or near surface. The Sn-In zones contain cassiterite, arsenopyrite,

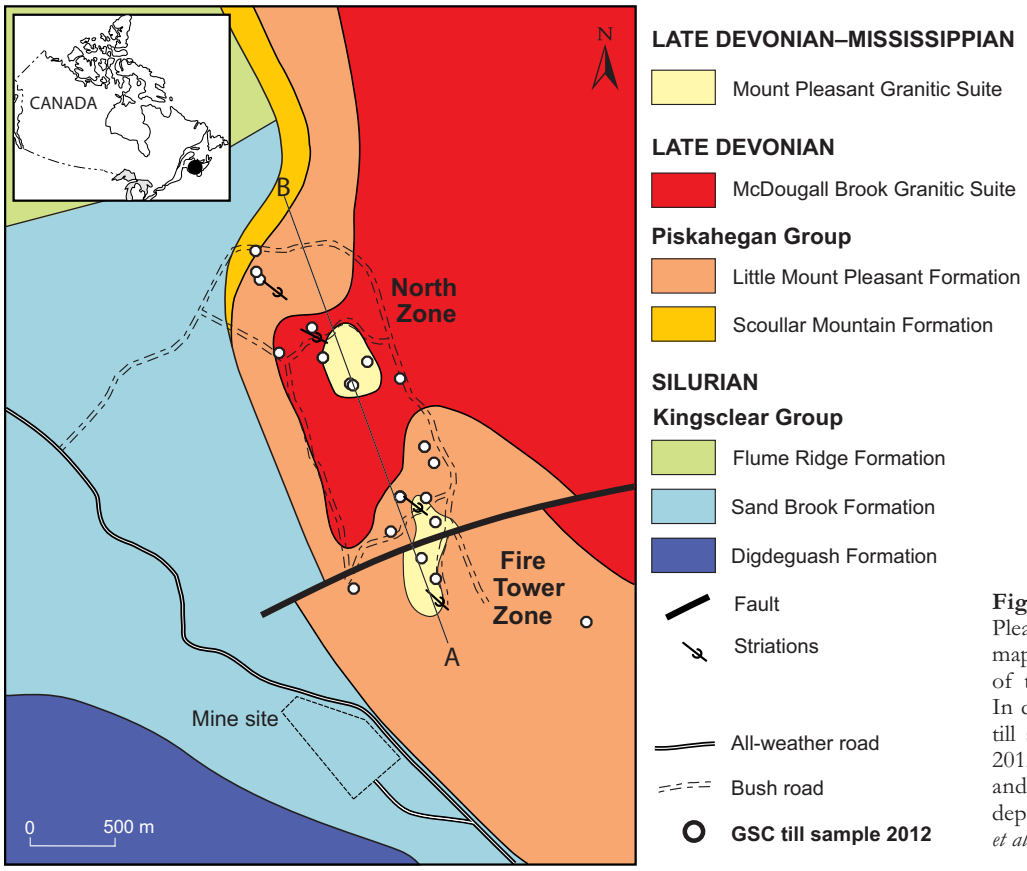

Fig. 2. Location of the Mount Pleasant area in eastern Canada (inset map) and local bedrock geology map of the Mount Pleasant Sn-W-Mo-Bi-In deposit area and location of GSC till samples (white dots) collected in 2012 up-ice (northwest), overlying, and down-ice (southeast) of the deposit (modified from McCutcheon *et al.* 1997; Fyffe & Thorne 2010).

loellingite, sphalerite, and chalcopyrite as well as the other sulphide minerals listed in Table 1. The Fire Tower Zone, 1200 m to the south, contains predominantly large, low-grade W-Mo deposits with some small In-bearing Sn-base metal resources. The main ore minerals in the Fire Tower Zone are wolframite and molybdenite and minor native bismuth and bismuthinite. Gangue minerals include cassiterite, arsenopyrite, and loellingite, quartz, topaz, and fluorite. The Fire Tower Zone also contains small In-bearing Sn-base metal zones in irregular veins and breccias consisting mainly of cassiterite and wolframite along with the sulphide minerals listed in Table 1. Indium in the Mount Pleasant deposit occurs mainly as a solid solution between sphalerite and roquesite, but also in chalcopyrite and stannite (Petruk 1972, 1973; Sinclair *et al.* 2006). In places, the ore minerals are so fine-grained that they cannot be seen in hand specimen (Petruk 1972). The NI 43-101 resource esti-

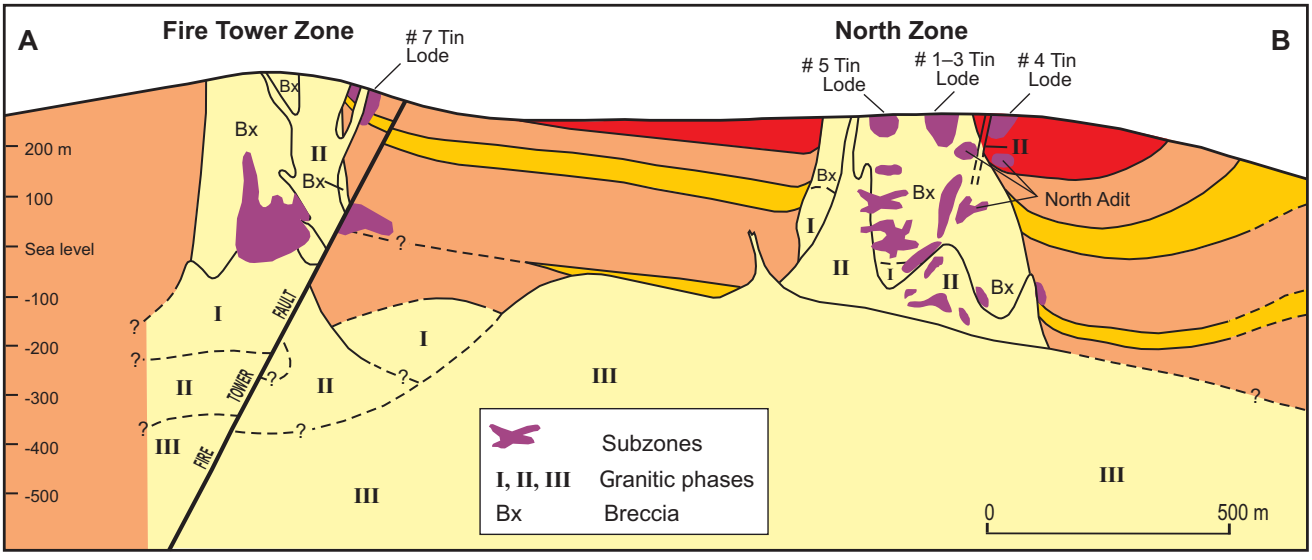

Fig. 3. Cross-section A-B (location shown in from Fig. 2) through the North and Fire Tower zones at Mount Pleasant, showing the ore subzones (purple). Note subzones at the North Zone subcrop. Bedrock geology units same as those in Figure 2 (modified from McCutcheon *et al.* 1997; Fyffe & Thorne 2010).

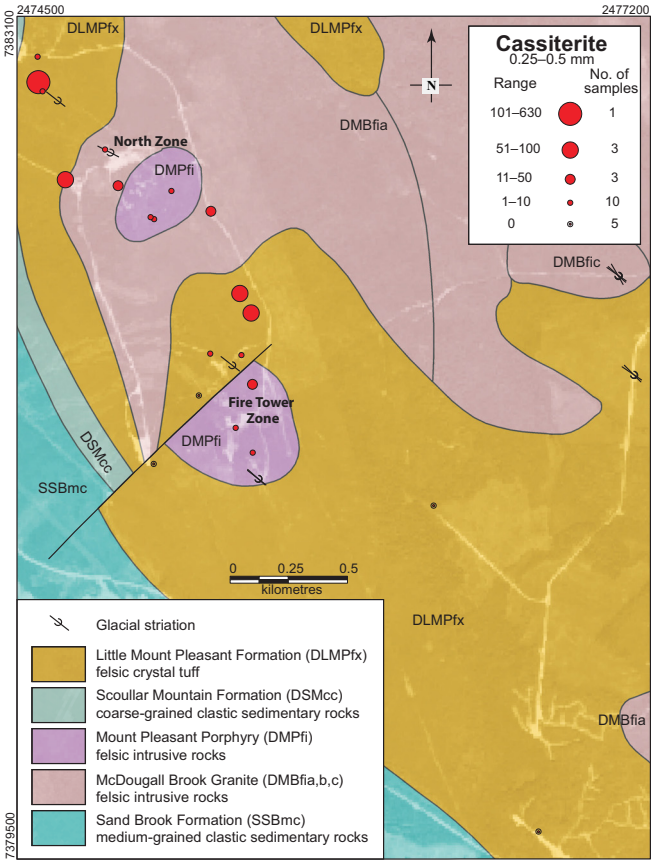

Fig. 4. Distribution of cassiterite grains in the 0.25–0.5 mm heavy mineral fraction of till normalized to 10 kg plotted on the local bedrock geology of the deposit area. Glacial dispersal train outline down-ice (southeast) of the deposit was first identified by Szabo *et al.* (1975). Bedrock geology from McLeod *et al.* (2005). Modified from McClenaghan *et al.* (in press b).

mate for the Fire Tower Zone consists of an indicated resource of 13.489 million tonnes at 0.33% WO_3 and 0.21% MoS_2, 0.57% As, and 0.06% Bi, as well as an inferred resource of 0.8417 million tonnes at 0.26% WO_3, 0.20% MoS_2, 0.21% As, and 0.04% Bi (McCutcheon *et al.* 2013). The NI 43-101 mineral resource estimate for the North Zone includes an indicated resource of 12.4 million tonnes averaging 0.38% Sn, 0.86% Zn, and 64 ppm In, as well as an inferred resource of 2.8 million tonnes averaging 0.30% Sn, 1.13% Zn, and 70 ppm In (McCutcheon *et al.* 2013).

Mount Pleasant is a striking topographic feature that rises approximately 220 m above the surrounding landscape and is covered by a till veneer <1 m thick. The surrounding lower lying areas are covered by a till blanket 1 to 5 m thick. Till in the area was deposited by southeast- to south-southeast-flowing ice during the Caledonia Phase (Early to Middle Wisconsin) (Szabo *et al.* 1975; Allard 2011; Stea *et al.* 2011). Szabo *et al.* (1975) defined a glacial dispersal train extending more than 16 km southeast of the deposit using Sn, As, Cu, Pb, and Zn content of the 0.5–2.0 mm heavy mineral fraction (SG >2.95) of till.

Methods

Bedrock samples and large (~15 kg) surface till samples were collected up-ice, overlying, and up to 2 km down-ice (southeast) of the Mount Pleasant deposit to document its indicator mineral signature. Sampling was focused within Szabo *et al.*'s (1975) glacial dispersal train to maximize the chance of collecting metal-rich till for indicator minerals studies. Small bags of till were tested in the field for their Sn, W, Mo, Bi, and In content using a portable bench-top XRF to help guide till sampling on a daily basis. A few mineralized bedrock samples were collected to determine the minerals indicative of the Mount Pleasant deposit. Bedrock and till samples were processed at the commercial lab Overburden Drilling Management Ltd., Ottawa, using a combination of shaking table, panning, and heavy liquid methods to produce heavy mineral concentrates (HMC) (>3.2 SG) and mid-density concentrates (3.0–3.2 SG) for picking. Pan concentrates, as well as the 0.25–0.5, 0.5–1.0, and 1.0–2.0 mm non-ferromagnetic HMC fractions were examined and potential indicator minerals of Sn-W-Mo-Bi-In mineralization were counted. Detailed descriptions of sample processing methods as well as indicator mineral abundance data for bedrock and till samples are reported in McClenaghan *et al.* (2014b, 2015a, in press b).

Indicator mineral species

Ore minerals recovered from both bedrock and till samples from the Mount Pleasant deposit include cassiterite scheelite, wolframite (Fig. 1), and molybdenite. Other indicator minerals recovered from bedrock and glacial sediments include chalcopyrite, galena, sphalerite, arsenopyrite, loellingite, and pyrite (Table 1), as well as fluorite and topaz. Indicator minerals recovered from till also include secondary Pb sulphate minerals beudantite ($PbFe_3(AsO_4)(SO_4)(OH)_6$) and anglesite ($Pb(SO_4)$), and the Pb phosphate mineral plumbogummite ($PbAl_3(PO_4)_2(OH)_5H_2O$), which formed from the oxidation and weathering of galena.

Selected indicator mineral abundances in till are reported in Table 2 according to distance down-ice of known mineralization. The most abundant indicator minerals in till down-ice of the deposit are cassiterite, wolframite, and topaz. Cassiterite content of the till varies from zero grains in background samples to a maximum of 630 grains. Wolframite content varies from zero grains in background samples to a maximum of 35 grains immediately down-ice of known mineralization. Topaz content ranges from 0 to 1 grain in background samples to ~32,000 grains overlying mineralization. Sulphide indicator minerals are present in far fewer till samples and in much less abundance (e.g. molybdenite, pyrite, arsenopyrite, loellingite), or absent (chalcopyrite, sphalerite) (Table 2).

Table 2 reports fluorite abundance in both the heavy (>3.2 SG) and mid-density (3.0–3.2 SG) fractions of 10 kg till samples from the intrusion-hosted Mount Pleasant deposit (McClenaghan *et al.* in press b). Fluorite abundance is far greater in the 3.0–3.2 SG mid-density fraction of till, indicating that this density fraction is optimal for recovery and determining the abundance of fluorite in till.

All indicator minerals recovered from till are most abundant in the 0.25 to 0.5 mm fraction of till. Coarser (0.5–2.0 mm) grains of cassiterite, wolframite, and topaz were also recovered from till samples overlying or just down-ice (up to 1 km southeast) of the North Zone. This pattern indicates that the presence of coarse indicator minerals in till is a strong indicator of proximity to the mineralization.

COMPARISON OF INDICATOR MINERALS AND TILL GEOCHEMISTRY

Indicator elements in till for the Mount Pleasant deposit

Table 1. Indicator minerals in the Mount Pleasant deposit (Petruk 1972, 1973; Parrish 1977; Kooiman *et al.*1986; Sinclair *et al.* 2006) and those found in bedrock polished thin sections (PTS), bedrock heavy mineral concentrates (HMC), and till heavy mineral concentrates (HMC) from this study.

Mineral	Formula	Hardness	Specific Gravity	Presence Reported by Other Authors	Identified in Bedrock PTS in this Study	Identified in Bedrock HMC in this Study	Identified in Till HMC in this Study
Tin minerals							
cassiterite	SnO_2	6-7	6.8-7	Petruk (1972)	no	yes	yes
stannite	Cu_2FeSnS_4	3.5-4	4.3-4.5	Petruk (1972)	no	no	no
këstерite	$Cu_2(Zn,Fe)SnS_4$	4.5	4.54-4.59	Petruk (1972)	no	no	no
ferrokësterite	$Cu_2(Fe,Zn)SnS_4$	4.0	4.5	Parrish (1977)	no	no	no
stannoidite	$Cu_8Fe_3Sn_2S_{12}$	4	4.29	Petruk (1972)	no	no	no
mawsonite	$Cu_6Fe_2SnS_8$	3.5-4	4.66	Petruk (1972)	no	no	no
Tungsten minerals							
scheelite	$CaWO_4$	4-5	5.9-6.12	Parrish (1977)	no	no	yes
wolframite	$(Fe,Mn)WO_4$	4.5	7.1-7.5	Petruk (1972)	no	no	yes
Sulphide and arsenide minerals							
molybdenite	MoS_2	1	5.5	Petruk (1972)	no	no	yes
pyrite	FeS_2	5-5.02	6.5	Petruk (1972)	yes	yes	yes
marcasite	FeS_2	6.0-6.5	4.89	Petruk (1972)	no	no	no
sphalerite	(Zn,Fe)S	3.5-4	3.9-4.2	Petruk (1972)	yes	yes	no
pyrrhotite	$Fe_{(1-x)}S$ (x=0-0.17)	3.5-4	4.58-4.65	Petruk (1972)	no	no	no
arsenopyrite	FeAsS	5	6.07	Petruk (1972)	no	yes	yes
loellingite	$FeAs_2$	5.0	7.1-7.7	Petruk (1972)	no	no	yes
ferrimolybdite	$Fe_2(MoO_4)3•8(H_2O)$	2.5-3	4-4.5	Parrish (1977)	no	no	no
scorodite	$Fe(AsO_4)•2(H_2O)$	3.5-4	3.1-3.3	Parrish (1977)	no	no	no
Bismuth minerals							
bismuthinite	Bi_2S_3	2	6.8-7.2	Petruk (1972)	no	no	no
native bismuth	Bi	2-2.5	9.7-9.8	Petruk (1972)	no	no	no
arsenobismite	$Bi_2(AsO_4)(OH)_3$	3	5.7	Parrish (1977)	no	no	no
zairite	$Bi(Fe,Al)_3[(OH)_6(PO_4)_2])$	4.5	4.37	no	no	no	yes
Copper minerals							
chalcopyrite	$CuFeS_2$	3.5	4.1-4.3	Petruk (1972)	no	yes	no
covellite	CuS	1.5-2.0	4.6-4.76	Petruk (1972)	no	no	no
tennantite	$(Cu,Fe)_{12}As_4S_{13}$	3.5-4	4.6-4.7	Petruk (1972)	no	no	no
bornite	Cu_5FeS_4	3.0	4.9-5.3	Petruk (1972)	no	no	no
chalcocite	Cu_2S	2.5-3	5.5-5.8	Parrish (1977)	no	no	no
roquesite	$CuInS_2$	3.5-4	not reported	Petruk (1973)	no	no	no
digenite	Cu_9S_5	2.5-3	5.6	Parrish (1977)	no	no	no
famatinite	Cu_3SbS_4	3-4	4.57	Parrish (1977)	no	no	no
Lead minerals							
galena	PbS	2.5	7.2-7.6	Petruk (1972)	yes	yes	yes
wittichenite	Cu_3BiS_3	2.5	6.3-6.7	Petruk (1973)	no	no	no
galenobismutite	$PbBi_2S_4$	2.5-3	6.9-7.1	Petruk (1972)	no	no	no
aikinite	$PbCuBiS_3$	2-2.5	6.1-6.8	Petruk (1972)	no	no	no
cosalite	$Pb_2Bi_2S_5$	2.5-3	6.4-6.8	Petruk (1972)	no	no	no
krupkaite	$PbCuBi_3S_6$	4	6.98	Petruk (1972)	no	no	no
beudantite	$PbFe_3(AsO_4)(SO_4)(OH)_6$	4.0	4.1-4.3	no	no	no	yes
anglesite	$Pb(SO_4)$	2.5-3	6.3	no	no	no	yes
plumbogummite	$PbAl_3(PO_4)_2(OH)_5•HO_2$	4-5	4-5	no	no	no	yes
Au and Ag minerals							
freibergite	$(Ag,Cu,Fe)_{12}(Sb,As)_4S_{13}$	3.5-4	4.85-5	Petruk (1973)	no	no	no
pyrargyrite	Ag_3SbS_3	2.5	5.85	Petruk (1973)	no	no	no
native silver	Ag	2.5-3	10-11	Petruk (1972)	no	no	no
gold	Au	2.5-3	16-19.3	Parrish (1977)	no	no	yes
Alteration minerals							
topaz	$Al_2SiO_4(F,OH)_2$	8	3.5-3.6	Petruk (1972)	yes	yes	yes
fluorite	CaF_2	4	3.01-3.25	Petruk (1972)	yes	yes	yes
tourmaline (black)	$NaAl_3Al_6(BO_3)_3(Si_6O_{18})(O,OH)_4$	7	3.01	Petruk (1972)	no	no	yes
columbite	$(Fe,Mn)(Nb,Ta)_2O_6$	6.0	5.3-7.3	Petruk (1972)	no	no	no

Table 2. Abundance of indicator minerals in 0.25–0.5 mm heavy (>3.2 SG) mineral fraction or mid-density (3.0–3.2 SG) (highlighted in red) fractions of till normalized to 10 kg at varying distances up ice, overlying, and down ice of the Mount Pleasant deposit (data from McClenaghan *et al.* 2013).

Sample Number	Location relative to mineralized bedrock	Distance from North Zone (km)	Distance from Fire Tower Zone (km)	Cassiterite			Wolframite			Topaz			Beudantite	Anglesite	Pyrite	Fluorite		Tourmaline	Scheelite	Arsenopyrite
				0.25–0.5 mm	0.5–1.0 mm	1.0–2.0 mm	0.25–0.5 mm	0.5–1.0 mm	1.0–2.0 mm	0.25–0.5 mm	0.5–1.0 mm	1.0–2.0 mm	0.25–0.5 mm	0.25–0.5 mm	0.25–0.5 mm	0.25–0.5 mm SG 3.0–3.2	0.25–0.5 mm	0.25–0.5 mm SG 3.0–3.2	0.25–0.5 mm	0.25–0.5 mm
12-MPB-1024	background	-13 NW		0	0	0	0	0	1	1	1	0	0	0	0	0	0	51	1	0
12-MPB-1013	up-ice	-0.6 NW		2	0	0	0	0	0	40	2	0	1	0	12	0	1	4	0	59
12-MPB-1020	up-ice	-0.5 NW		630	24	2	3	1	0	787	31	8	0	1181	0	0	0	31	0	0
12-MPB-1019	up-ice	-0.45 NW		7	3	0	0	0	0	14	2	0	1	1	0	0	0	68	0	0
12-MPB-1014	up-ice	-0.2 NW		2	0	0	0	0	0	1	0	0	0	0	0	13	0	35	1	0
12-MPB-1012	up-ice	-0.2 W		89	36	0	14	1	0	268	15	0	0	0	45	0	0	45	0	0
12-MPB-1007	overlying	0.0		8	1	0	2	0	0	500	42	4	0	1	0	4	1	83	0	0
12-MPB-1008	overlying	0.0		6	3	0	0	0	0	72	4	0	0	0	4	72	9	11	0	0
12-MPB-1009	overlying	0.0		10	0	0	0	0	0	1266	14	0	0	0	0	0	0	6	0	0
12-MPB-1010	overlying	0.0		37	3	0	8	2	0	2222	74	4	0	0	0	0	0	30	0	0
12-MPB-1015	down-ice	0.3 SE		44	11	1	11	4	1	5556	222	12	0	0	0	0	0	20	0	0
12-MPB-1006	down-ice	0.5 SE		53	10	0	35	19	2	4425	88	1	2	18	0	106	0	35	0	0
12-MPB-1001	down-ice	0.6 SE		63	10	1	32	6	3	1190	40	0	0	3	1	0	0	32	0	0
12-MPB-1018	up-ice		-0.1 N	1	0	0	0	0	0	44	9	0	0	0	1	0	0	10	0	0
12-MPB-1002	overlying		0.0	5	0	0	2	2	0	317	32	2	1587	2	0	0	0	5	0	0
12-MPB-1003	overlying		0.0	2	0	0	0	0	0	870	43	0	0	0	0	0	0	54	0	0
12-MPB-1004	overlying		0.0	12	0	0	32	13	0	31746	952	0	0	11905	0	12	0	32	0	0
12-MPB-1005	overlying		0.0	9	0	0	9	0	0	214	15	0	0	43	0	0	0	36	0	0
12-MPB-1017	overlying		0.0	0	0	0	0	0	0	0	0	0	0	0	0	0	0	43	1	0
12-MPB-1016	background		0.3 SW	0	0	0	0	0	0	0	0	0	0	0	0	0	0	38	0	0
12-MPB-1022	down-ice		0.7 SSE	0	0	0	0	0	0	661	25	0	0	0	0	0	0	41	0	0
12-MPB-1023	down-ice		2.2 SE	0	0	0	0	0	0	561	37	0	0	0	0	0	0	37	0	0

include the main ore elements Sn, W, Mo, Bi and In. Pathfinder elements include Ag, As, Cd, Cu, Pd, Re, Te, Tl, and Zn (McClenaghan *et al.* 2015b). The Mount Pleasant deposit is a significant source of In and this study is one of the first to report the glacial dispersal of In in till. Overlying and just down-ice of the deposit the till contains between 1 and 13 ppm In, which are some of the highest In values ever reported for till. Indicator mineral abundance in the 0.25–0.5 mm HMC fraction of till is compared to till geochemistry of the <0.063 mm fraction in Table 3. Tin values in till range from 2 ppm in background samples to a maximum of 349 ppm overlying mineralization. Not all till samples that contain cassiterite have corresponding high Sn values. Wolframite is present in 10 of the 16 till samples, however, no high W values are reported in till samples. These patterns suggest that indicator minerals are more useful than till geochemistry for identifying the presence of Sn- and W-rich debris in till.

Copper, Pb, Zn, Ag, As, and In values are high for many of the till samples, however, ore-associated sulphide mineral (e.g. galena, sphalerite, chalcopyrite, arsenopyrite) abundance in the same till samples is low to zero. Pb-bearing secondary minerals beudantite, anglesite, and plumbogummite are present in some of these same till samples. These patterns indicate that sulphide minerals were either destroyed during pre- or post-glacial oxidation, or both. As a result, till geochemistry and the presence of secondary sulphate or phosphate minerals are useful for identifying the presence of polymetallic (Cu, Pb, Zn, Ag, As, and In) metal-rich debris glacially eroded from the deposit.

Table 3. Comparison of the normalized (10 kg) abundance of cassiterite, wolframite, and topaz in the 0.25–0.5 mm fraction and trace elements in the <0.063 mm fraction of till samples from the Mount Pleasant deposit (data from McClenaghan *et al.* 2014a, b).

Sample Number	Location relative to mineralized bedrock	Distance from North Zone (km)	Distance from Fire Tower Zone (km)	Cassiterite 0.25–0.5 mm	Wolframite 0.25–0.5 mm	Topaz 0.25–0.5 mm	Sn ppm (fusion)	W ppm (fusion)	Mo ppm (aqua regia)	Cu ppm (aqua regia)	Pb ppm (aqua regia)	Zn ppm (aqua regia)	Ag ppb (aqua regia)	As ppm (aqua regia)	Bi ppm (aqua regia)	In ppm (aqua regia)
12-MPB-1024	background	-13 NW		0	0	1	2	2	1	25	15	53	54	13	1	<0.02
12-MPB-1013	up ice	-0.6 NW		2	0	40	5	2	1	38	27	2989	21	166	1	0.1
12-MPB-1020	up ice	-0.5 NW		630	3	787	166	3	9	110	292	1149	228	384	10	2.8
12-MPB-1019	up ice	-0.45 NW		7	0	14	59	4	8	144	254	1241	877	302	12	2.2
12-MPB-1014	up ice	-0.2 NW		2	0	1	5	2	11	125	17	2214	17	145	2	0.3
12-MPB-1012	up ice	-0.2 W		89	14	268	52	5	13	123	59	1487	36	541	9	2.2
12-MPB-1007	overlying	0.0		8	2	500	85	6	9	103	327	986	124	426	14	4.7
12-MPB-1008	overlying	0.0		6	0	72	10	2	15	165	168	2060	42	312	4	1.1
12-MPB-1009	overlying	0.0		10	0	1266	70	11	14	44	273	563	640	198	46	1.5
12-MPB-1010	overlying	0.0		37	8	2222	59	8	4	82	41	397	47	195	8	1.3
12-MPB-1015	down ice	0.3 SE		44	11	5556	143	8	45	115	214	671	94	520	69	2.7
12-MPB-1006	down ice	0.5 SE		53	35	4425	142	25	18	165	270	462	503	937	41	4.1
12-MPB-1001	down ice	0.6 SE		63	32	1190	75	19	16	167	179	455	66	477	43	2.3
12-MPB-1018	up ice		-0.1 N	1	0	44	6	4	1	41	40	882	28	44	2	0.1
12-MPB-1002	overlying		0.0	5	2	317	263	35	386	82	1799	440	165	800	192	4.7
12-MPB-1003	overlying		0.0	2	0	870	7	25	5	40	45	138	514	2392	77	0.5
12-MPB-1004	overlying		0.0	12	32	31746	349	23	305	227	2479	562	1666	1347	208	13.1
12-MPB-1005	overlying		0.0	9	9	214	35	3	3	164	200	999	160	93	4	0.7
12-MPB-1017	overlying		0.0	0	0	0	6	2	14	151	219	887	607	125	12	1.4
12-MPB-1016	background		0.3 SW	0	0	0	29	5	11	374	203	1156	596	197	29	1.6
12-MPB-1022	down ice		0.7 SSE	0	0	661	19	4	24	479	359	851	571	374	12	1.1
12-MPB-1023	down ice		2.2 SE	0	0	561	13	4	3	76	64	166	496	99	6	0.6

CONCLUSIONS

The Mount Pleasant case study is the first detailed indicator mineral study around a major Sn deposit in glaciated terrain using modern and commercially available indicator mineral recovery methods. Indicator minerals for the Mount Pleasant deposit include the main ore minerals, cassiterite, wolframite, and molybdenite, as well as topaz, chalcopyrite, galena, sphalerite, arsenopyrite, pyrite, and loellingite in the 0.25–0.5 mm >3.2 SG fraction of till, and fluorite in the 3.0–3.2 SG fraction. Secondary minerals beudantite, anglesite, and plumbogummite, which formed from the oxidation of galena, may also be useful indicator minerals. Collectively, the indicator minerals identified in till in this study reflect the presence of Sn-W mineralization as well as the polymetallic nature of the deposit. The presence of coarse (0.5–2.0 mm) indicator minerals in till around the Mount Pleasant deposit indicates proximity (<1 km) to the mineralized source. Indicator minerals methods are optimal for identifying the presence of Sn and W mineralization because these minerals are physically and chemically robust and survive post-glacial weathering. Pre- or post-glacial weathering of sulphides combined with the glacial crushing of sulphides, or their weathering products, has resulted in high metal contents in the fine fraction of till around Mount Pleasant. As a result, geochemistry of the <0.063 mm fraction of till is therefore useful for detecting the Cu, Pb, Zn, Ag, As, and In signature of the deposit.

ACKNOWLEDGMENTS

The Mount Pleasant case study was conducted as part of the Geological Survey of Canada's Targeted Geoscience Initiative 4 (TGI-4) (2010–2015) and was a collaborative effort between the Geological Survey of Canada and the New Brunswick Department of Energy and Mines. Adex Mining Inc., in particular Gustaaf Kooiman, is thanked for providing access to the Mount Pleasant property. Kathleen Thorne, New Brunswick Department of Energy and Mines, is thanked for her discussions of the bedrock geology. John Chapman (Geological Survey of Canada) and Dave Sinclair (retired, Geological Survey of Canada) are thanked for sharing bedrock samples from the deposit. Rod Smith (Geological Survey of Canada) is thanked for his review of this manuscript.

REFERENCES

Aleva, G.J.J. 1985. Indonesian fluvial cassiterite placers and their genetic environment. Journal of the Geological Society of London, 142, 815–836.

Allen, T.L., Hart, C.J.R. & Marsh, E.E. 1999. Placer gold and associated heavy minerals of the Clear Creek drainage, central Yukon: past to present. *In:* Roots, C.F & Emonds, D.S. (eds) *Yukon Exploration and Geology 1998*. Yukon Indian and Northern Affairs, Exploration and Geological Services Division, 197–214.

Allard, S. 2011. *Surficial geology of the McDougall Lake area (NTS 21 G/07), Charlotte County, New Brunswick*. New Brunswick Department of Natural Resources, Lands, Minerals, and Petroleum Division, MP 2011-11, Scale: 1:50,000.

Asrarullah, 1982. Investigations for tungsten in Pakistan, *In:* Hepworth, J.V. (ed.) Symposium on Tungsten Geology, Jiangxi, China. ESCAP/RMRDC Bandung, Indonesia and Geological Publishing House, Bejing, China, 9–13.

Averill, S.A. 2001. The application of heavy indicator mineralogy in mineral exploration with emphasis on base metal indicators in glaciated metamorphic and plutonic terrains. *In:* McClenaghan, M.B., Bobrowsky, P.T., Hall, G.E.M. & Cook, S.J. (eds) *Drift Exploration in Glaciated Terrain*. Geological Society of London, Special Publication 185, 69–81.

Ballantyne, S.B. & Ellwood, D.J. 1988. An evaluation of reconnaissance and follow-up geochemical surveys to delineate favourable areas for tin mineralization in the northern Canadian Cordillera. *In:* Hutchinson, C.S. (ed.) *Geology of Tin Deposits in Asia and the Pacific*, Selected Papers from the International Symposium on the Geology of Tin Deposits held in Nanning, China, October 26–30, 1984. Springer, Berlin-Heidelberg, 127–162.

Brundin, N.H. & Bergström, J. 1977. Regional prospecting for ores based on heavy minerals in glacial till. *Journal of Geochemical Exploration*, **7,** 1–19.

Camm, G.S. & Groot, D.G. 1994. Quaternary placer cassiterite deposits in Cornwall: the role of periglacial processes in their development, *In: Proceedings of the Ussher Society 1994*, Volume 8, Part 3, Notes, ISSN 0566-3954, 328–330.

Camm, G.S. & Hosking, K.F.G. 1985. Stanniferous placer development on an evolving landsurface with special reference to placers near St Austell, Cornwall. *Journal of the Geological Society of London*, **142**, 803–813.

Chapman, R.M., Coats, R.R. & Payne, T.G. 1963. *Placer tin deposits central Alaska*. US Geological Survey, Open-File Report 63–15.

de Smeth, J.B., Rao, K.S. & Schuling, R.D. 1985. Gold-scheelite mineralization in the Veligallu schist belt, Andhra Pradesh, India. *Economic Geology*, **80**, 1996–2000.

Dunlop, A.C. & Meyer, W.T. 1978. Detrital tin patterns in stream sediments and soils in mid-Cornwall. *Journal of Geochemical Exploration*, **10**, 259–276.

ESCAP Secretariat, 1982. Note on tungsten occurrences in Burma. *In:* Hepworth, J.V. (ed.) *Symposium on Tungsten Geology*, Jiangxi, China. ESCAP/RMRDC Bandung, Indonesia and Geological Publishing House, Bejing, China, 45–48.

Fernández-Turiel, J.L. & Durán-Barrachina, M.E. 1989. A contribution to regional tin exploration in the Iberian Massif. *Journal of Geochemical Exploration*, **31**, 295–305.

Fernández-Turiel, J.L., Durán, M.E., Querol, X. & López-Soler, A. 1992. Comparison between analytical and mineralometric methods in regional scheelite exploration. *Journal of Geochemical Exploration*, **43**, 205–211.

Friske, P.W.B., McCurdy, M.W., Day, S.J.A. & McNeil, R.J. 2001. Evaluation of total, partial and selective leach data from humus, B horizon and till: a case study form the Clarence Stream gold property, southern New Brunswick. *In:* Carroll, B.M.W. (ed.) *Current Research 2000*. New Brunswick Department of Natural Resources and Energy, Minerals and Energy Division, Mineral Resources Report 2001-4, 25–45.

Frizzo, P. & Hassan, A.H. 1983. Scheelite in stream sediments in the crystalline basement of northern Somalia (area NNE of Hargheisa). *Bollettino della Societa Geologica Italiana*, **102**, 385–390.

Fyffe, L.R. & Thorne, K.G. 2010. *Polymetallic deposits of Sisson Brook and Mount Pleasant, New Brunswick, Canada*. New Brunswick Department of Natural Resources, Field Guide No. 3.

Gleeson, C.F. & Boyle, R.W. 1980. *Minor and trace element distribution in the heavy minerals of the rivers and streams of the Keno Hill District, Yukon Territory*. Geological Survey of Canada, Paper 76-31.

Hallenstein, C.P., Pedersen, J.L. & Stendal, H. 1981. Exploration for scheelite in East Greenland- a case study. *Journal of Geochemical Exploration*, **15**, 381–392.

Hess, F.L. 1917. *Tungsten minerals and deposits*. United States Geological Survey, Bulletin 652.

Horsnail, R.F. 1979. The geology of tungsten. *In: Proceedings of the First Tungsten Symposium*, Stockholm, September 5–7, 1979, Mining Journal Books Limited, 18–31.

Hosking, H.K.F. 1963. Geology, mineralogy, and paragenesis of the Mount Pleasant tin deposits. *Canadian Mining Journal*, **84**, 95–102.

Hosking, K.F.G. 1982. A general review of the occurrence of tungsten in the world. *In:* Hepworth, J.V. (ed.) *Symposium on Tungsten Geology*, Jiangxi, China. ESCAP/RMRDC Bandung, Indonesia and Geological Publishing House, Bejing, China, 59–86.

Invemo, C.M.C. & Hutchinson, R.W. 2004. The endogranitic tin zone, Mount Pleasant, New Brunswick, Canada, and its metallogenesis. *Institution of Mining and Metallurgy Transactions, Section B-Applied Earth Science*, **113**, B261–B288.

Johansson, K., Keinänen, V. & Lehmuspelto, P. 1986. Geochemical exploration of tungsten in glaciogenic deposits in Soretiapulju, Western Finnish Lapland. *In: Prospecting in Areas of Glaciated Terrain*. Institute of Mining and Metallurgy, 61–68.

Johnson, B.L. 1910. *Occurrence of wolframite and cassiterite in the gold placers of Deadwood Creek, Birch Creek district (Alaska)*. United States Geological Survey, Bulletin 442, 246–250.

Kooiman, G.J.A., McLeod, M.J. & Sinclair, W.D. 1986. Porphyry tungsten-molybdenum orebodies, polymetallic veins and replacement bodies and tin-bearing greisen zones in the Fire Tower Zone, Mount Pleasant, New Brunswick. *Economic Geology*, **81**, 1356–1373.

Lindmark, B. 1977. Till-sampling methods used in exploration for scheelite in Kaustinen, Finland. *In: Prospecting in Areas of Glaciated Terrain 1977*. Institute of Mining and Metallurgy, 46–48.

Makin, S.A., Simandl, G.J. & Marshall, D. 2014. Fluorite as an indicator mineral for carbonatite-related rare earth element deposits. *In: Geological Fieldwork 2013*. British Columbia Geological Survey, Paper 2014-1, 207–212.

Mattila, E. & Peuraniemi, V. 1980. On geochemical prospecting for tin in southern Finland. *In: Methods of the Geochemical Mapping and Boulder Prospecting in the Eastern Part of the Baltic Shield*. Geological Survey of Finland, 133–159.

Maurice, Y.T. 1986. Interpretation of a reconnaissance geochemical heavy mineral survey in the Eastern Townships of Quebec. *In: Current Research, Part A*. Geological Survey of Canada, Paper 86-1A, 307–317.

McClenaghan, M.B., Parkhill, M.A., Averill, S.A., Pronk, A.G., Seaman, A.A., Boldon, R., McCurdy, M.W. & Rice, J.M. 2013. *Indicator mineral abundance data for bedrock, till, and stream sediment samples from the Sisson W-Mo deposit, New Brunswick*. Geological Survey of Canada, Open File 7387, 18 p. doi:10.4095/293858

McClenaghan, M.B., Parkhill, M.A., Seaman, A.A., Pronk, A.G., Pyne, M., Rice, R.M. & Pyne, M. 2014a. *Indicator mineral signatures of the Sisson W-Mo deposit, New Brunswick: Part 2 till*. Geological Survey of Canada, Open File 7467. doi:10.4095/293349

McClenaghan, M.B., Parkhill, M.A., Averill, S.A., Pronk, A.G., Boldon, R., Chapman, J. & Rice, J.M. 2014b. *Indicator mineral abundance data for bedrock and till from the Mount Pleasant Sn-W-Mo-Bi-In deposit, New Brunswick*. Geological Survey of Canada, Open File 7573. doi:10.4095/293927

McClenaghan, M.B., Parkhill, M.A., Chapman, J.B. & Sinclair, W.D. 2015a. *Indicator mineral content of bedrock from the Mount Pleasant Sn-W-Mo-Bi-In deposit, New Brunswick*. Geological Survey of Canada, Open File 7721.

McClenaghan, M.B., Parkhill, M.A., Pronk, A.G., Boldon, G.R., Pyne, R.M. & Rice, J.M., 2015b. *Till geochemical signatures of the Mount Pleasant Sn-W-Mo-Bi-In deposit, New Brunswick*. Geological Survey of Canada, Open File 7722.

McClenaghan, M. B., Parkhill, M.A., Pronk, A.G., McCurdy, M.W., Boldon, R., Leybourne, M.I., Pyne, M. & Rice, J.M. In press a. *Geochemical and indicator mineral data for stream sediments and waters around the Sisson W-Mo deposit, New Brunswick (NTS 21J/06, 21J/07)*. Geological Survey of Canada, Open File 7756.

McClenaghan, M.B., Parkhill, M.A., Pronk, A.G., Boldon, R., Pyne, M. & Rice, J.M. in press b. *Indicator mineral content of till from the Mount Pleasant Sn-W-Mo-Bi-In deposit, New Brunswick*. Geological Survey of Canada, Open File 7804.

McCutcheon, S.R., Anderson, H.E. & Robinson, P.T. 1997. Stratigraphy and eruptive of the Late Devonian Mount Pleasant caldera complex, Canadian Appalachians. *Geological Magazine*, **134**, 17–36.

McCutcheon, S.R., Reddick, J., McKeen, T., El-Rassi, D. & Kociumbas, M. 2013. *Amended technical report of the Mount Pleasant property, including mineral resource estimates, southwestern New Brunswick* for Adex Mining Inc. 43-101 Technical Report, Watts, Griffs and McQuat, SEDAR website, http://www.sedar.com/

McCutcheon, S.R., Sinclair, W.D., McCleod, M.J., Boyd, T. & Kooiman, G.J.A. 2010. Part 2: Mount Pleasant Sn-W-Mo-Bi-In deposit. *In:* Fyffe, L.R. & Thorne, K. (comp) *Polymetallic Deposits of Sisson Brook and Mount Pleasant, New Brunswick, Canada*. New Brunswick Department of Natural Resources, Field Guide No. 3, 37–68.

McCleod, M.J., Fyffe, L.R. & McCutcheon, S.R. 2005. *Bedrock geology of the McDougall Lake area (NTS 21 G/07), Charlotte County, New Brunswick*. New Brunswick Department of Natural Resources, Map Plate MP 2005-30.

Meizhong, Y. 1982. Basic theory and chief methods applied in tungsten prospecting in Jiangxi Province, *In:* Hepworth, J.V. (ed.) *Symposium on Tungsten Geology*, Jiangxi, China. ESCAP/RMRDC Bandung, Indonesia and Geological Publishing House, Bejing, China, 489–502.

Nikkarinen, M. & Björklund, A. 1976. Kaustinen: The use of till in tungsten prospecting. *Journal of Geochemical Exploration*, **21**, 247–248.

Ottensen, R.T. & Theobald, P.K. 1994. Stream sediments in mineral exploration, Chapter 5 *In:* Hale, M. & Plant, J.A. (eds), *Drainage Geochemistry*. Handbook of Exploration Geochemistry, **6**, 147–185.

Özcan, A. & Çağatay, M.N. 1989. Tungsten exploration in semiarid environment: Central Anatolian massif, Turkey. *Journal of Geochemical Exploration*, **31**, 185–199.

Parrish, I.S. 1977. Mineral catalog for the Mount Pleasant deposit of Brunswick Tin Mines Ltd. *The Canadian Mineralogist*, **15**, 121–126.

Patyk-Kara, N.G. 1999. Cenozoic placer deposits and fluvial channel systems on the Arctic Shelf of Siberia. *Economic Geology*, **94**, 707–720.

Petersen, L.R. & Stendal, H. 1987. Tungsten exploration in the Valnesfjord region, Nordland, northern Norway. *Journal of Geochemical Exploration*, **29**, 151–163.

Petruk, W. 1972. *The W-Bi-Mo deposit of the Brunswick Tin Mines Limited: its mode of occurrence, mineralogy, and amenability to mineral beneficiation*. Department of Energy, Mines and Resources, Mineral Sciences Division, Report MS PP 72-3.

Petruk, W. 1973. Tin sulphides from the deposit of Brunswick Tin Mines Limited. *Canadian Mineralogist*, **12**, 46–54.

Peuraniemi, V. 1992. Hieronmaki: W, Sn, Cu and Zn concentrations of till near a scheelite mineralization in hilly region. *In:* Kauranne, K., Salminen, R. & Salonen, V-P. (eds) *Handbook of Exploration Geochemistry: Regolith Exploration Geochemistry in Arctic and Temperate Terrains*. Elsevier, Espoo, Finland, 277–282.

Peuraniemi, V. & Gehör, S.A. 2000. Mineralogy and mineral chemistry of Sn-Nb-Ta anomalous heavy mineral till samples from the Hämeenlinna area, southern Finland. *In:* Rammlmair, D., Mederer, J., Oberthür, T.H., Heimann, R.B. & Pentinghaus, H. (eds) *Applied Mineralogy in Research, Technology, Ecology, and Culture*, Proceedings of the Sixth International Congress on Applied Mineralogy. A.A. Balkema, Rotterdam, 391–394.

Peuraniemi, V. & Heinänen, K. 1985. Mineralogical investigations in the interpretation of heavy-mineral geochemical results. *Journal of Geochemical Exploration*, **23**, 315–328.

Pungrassami, T. 1986. Cassiterite and wolframite deposits in and around the Hat Yai Basin, Songkhla Province, Thailand. *In:* Thiramongkol, N. (ed.) *Proceedings of the Workshop on Economic Geology, Tectonics, Sedimentary Processes and Environment of the Quaternary in Southeast Asia*, 3-7 February, 1986, Haad Yai, Thailand, 135–155.

Rajah, S.S. 1982. Tungsten mineralization in Peninsular Malaysia, *In:* Hepworth, J.V. (ed.) *Symposium on Tungsten Geology*, Jiangxi, China. ESCAP/RMRDC Bandung, Indonesia and Geological Publishing House, Bejing, China, 179–195.

Ryan, R.J., Turner, R.R., Stea, R.R. & Rogers, P.J. 1988. Heavy minerals and sediment dispersal trends as exploration tools for potential tin and gold paleoplacers in Carboniferous rocks, Nova Scotia, *In: Prospecting in Areas of Glaciated Terrain-1988*. Canadian Institute of Mining and Metallurgy, 41–56.

Salminen, R. & Hartikainen, A. 1986. Tracing gold, molybdenum and tungsten mineralization by use of a step by step geochemical study in Ilomantsi, eastern Finland, *In: Prospecting in Areas of Glaciated Terrain-1986*. Institution of Mining and Metallurgy, London. 201–209.

Sinclair, W.D., Kooiman, G.J.A., Martin, D.A. & Kjarsgaard, I.M. 2006. Geology, geochemistry and mineralogy of indium resources at Mount Pleasant, New Brunswick, Canada. *Ore Geology Reviews*, **28**, 123–145.

Snow, R.J. & Coker, W.B. 1987. Overburden geochemistry related to W-Cu-Mo mineralization at Sisson Brook, New Brunswick, Canada: an example of short- and long-distance glacial dispersal, *In:* Garrett, R.G. (ed) *Geochemical Exploration 1985*. *Journal of Geochemical Exploration*, **28**, 353–368.

Stea, R.R. & O'Reilly, G.A. 1982. Till geochemistry of the Meguma Terrane in Nova Scotia and its metallogenic implications. *In: Prospecting in Areas of Glaciated Terrain-1982*. Institute of Mining and Metallurgy, 82–104.

Stea, R.R., Seaman, A.A., Pronk, T., Parkhill, M.A., Allard, S. & Utting, D. 2011. The Appalachian Glacier Complex in Maritime Canada, Chapter 48 *In:* Ehlers, J., Gibbard, P.L. & Hughes, P.D. (eds) *Quaternary Glaciations - Extent and Chronology – a closer look*. Elsevier, Developments in Quaternary Science, 15, 631–659.

Steenfelt, A. 1987. Geochemical mapping and prospecting in Greenland- a review of results and experience. *Journal of Geochemical Exploration*, **29**, 183–205.

Steiger, R. 1977. Prospecting for lithium and tungsten in Ireland, *In: Prospecting in Areas of Glaciated Terrain-1977*. Institute of Mining and Metallurgy, 14–24.

Stendal, H. 1978. Heavy minerals in stream sediments, southwest Norway. *Journal of Geochemical Exploration*, **10**, 91–102.

Stendal, H. & Theobald, P.K. 1994. Heavy-mineral concentrates in geochemical exploration, *In:* Hale, M. & Plant, J.A. (eds) *Drainage Geochemistry, Handbook of Exploration Geochemistry*, Volume 6, 185–225.

Surya Prakash Rao, K., Sastry, R.S.N. & Raju, S.V. 1989. Scheelite as a prospecting tool in the Ramagiri greenstone belt, Andhra Pradesh, India. *Journal of Geochemical Exploration*, **31**, 307–317.

Szabo, N.L., Govett, G.J.S. & Lajtai, E.Z. 1975. Dispersion trends of elements and indicator pebbles in glacial till around Mt. Pleasant, New Brunswick, Canada. *Canadian Journal of Earth Sciences*, **12**, 1534–1556.

Theobald, P.K. & Thompson, C.E. 1960. *Geochemical prospecting with heavy-mineral concentrates used to locate a tungsten deposit*. United States Geological Survey, Circular 411.

Thompson, R.M. 1945. An occurrence of cassiterite at Dublin Gulch, Yukon Territory. *Economic Geology*, **40**, 142–147.

Toverud, Ö. 1982. Geochemical prospecting for tin in upper central Sweden using heavy mineral concentrate of glacial till. *In:* Davenport, P.H. (ed) *Prospecting in Areas of Glaciated Terrain 1982*. Canadian Institute of Mining and Metallurgy, 204–212.

TOVERUD, Ö. 1984. Dispersal of tungsten in glacial drift and humus in Bergslagen, south central Sweden. *Journal of Geochemical Exploration*, **21**, 261–272.

TOWSEY, C.A.J. & PATTERSON, D.J. 1984. Tin exploration at Mount Isa - a case history. *Journal of Geochemical Exploratio*n, **22**, 71–82.

TRIPP, R.B., KARLSON, R.C., & CURTIN, G.C. 1978. *Maps showing mineralogical data for nonmagnetic heavy-mineral concentrates in the Talkeetna quadrangle, Alaska*. United States Geological Survey, Miscellaneous Field Studies Map MF-870-I.

TURNER, R.G. & STEA, R.R. 1990. Interpretation of till geochemical data in Nova Scotia, Canada: using mapped till units, multi-element anomaly patterns and the relationship of till clast geology to matrix geochemistry. *Journal of Geochemical Exploration*, **37**, 225–254.

WATTS, K.C. & HASSEMER, J.R. 1980. *Distribution and abundance of fluorite in stream-sediment concentrates, Silver City 1 degree by 2 degrees Quadrangle, Arizona and New Mexico*. United States Geological Survey, Miscellaneous Field Studies, Map 1183-C.

WILDON, R. & HOTZ, P.E. 1955. A gold-scheelite-cinnabar placer in Humboldt County, Nevada. *Economic Geology*, **50**, 661–668.

ZANTOP, H. & NESPEREIR, J. 1979. Heavy-mineral panning techniques in the exploration for tin and tungsten in NW Spain. *In:* WATTERSON, J.R. & THEOBALD, P.K. (eds) *Geochemical Exploration 1978*. Association of Exploration Geochemists, 329–336.

ZESCHKE, G. 1961. Prospecting for ore deposits by panning heavy minerals from river sands. *Economic Geology,* **56**, 1250–1257.